Universal Journal of Carbon Research
https://ojs.wiserpub.com/index.php/UJCR/

Review

Correlating Heat Treatment Conditions with the Physicochemical Properties of Thermally Reduced Graphene Oxide-Based Materials: A Comprehensive Review

Hamdane Akbi[1*], Souleymen Rafai[1], Ahmed Mekki[1*], Sabri Touidjine[2], Mohamed Abderrahim Hamouche[2]

[1]UER Physicochimie des Matériaux, Ecole Militaire Polytechnique, EMP, BP 17 Bordj-El-Bahri, 16046, Algiers, Algeria
[2]UER Procédés Energétiques, Ecole Militaire Polytechnique, EMP, BP 17 Bordj-El-Bahri, 16046, Algiers, Algeria
E-mail: akbibeniamrane@gmail.com; mekki_ahmedkarim@yahoo.fr

Received: 30 April 2024; **Revised:** 2 June 2024; **Accepted:** 4 June 2024

Abstract: The straightforward, cost-efficient, and scalable route of preparing graphene oxide-based materials (GOBMs) from graphite and transforming them into thermally reduced graphene oxide-based materials (T-RGOBMs) through heat treatment offers unparalleled versatility in customizing and refining the physicochemical properties of T-RGOBMs for various applications. To fully exploit the potential of this route, it is essential to determine the correlation between the physicochemical properties of the resulting T-RGOBMs and the preparation and heat treatment conditions of GOBMs. This article intends to provide a comprehensive discussion of the use of heat treatment routes to prepare T-RGOBMs with finely tuned physicochemical properties for specific applications. The review will focus on the key factors that can affect the end-product features, including the method of preparation of graphite oxide, the physical form of the ensuing GOBMs, and the parameters of the heat treatment process, such as temperature, heating rate, duration, atmosphere, and pressure. Furthermore, it will concentrate on the thermal transformations that take place during heat treatment, delve into the mechanisms and kinetics governing thermal decomposition, evaluate the potential risks associated with reducing GOBMs through heat treatment, and outline strategies to ensure a safe reduction process. The review will also explore recent advancements in the application of T-RGOBMs, providing examples of heat treatment strategies employed across various fields, including supercapacitors, gas sensing, and interference shielding. It serves as a useful guide for researchers and practitioners looking to appropriately prepare GOBMs and safely utilize the heat treatment to fine-tune their properties toward specific applications.

***Keywords*:** thermally reduced graphene oxide-based materials; heat treatment conditions; graphene oxide-based materials; physicochemical properties; applications

1. Introduction

Reduced graphene oxide-based materials (RGOBMs), including, reduced graphene oxide sheets (RGOS), reduced graphene oxide film (RGOF), and reduced graphene oxide aerogel (RGOA) are receiving particular attention in recent years because they are structurally similar to pristine graphene and possess excellent physicochemical properties, making them ideal for a wide range of potential uses [1,2], including supercapacitors [3,4], batteries [5], sensors [6–8], membranes [9], energetic materials [10,11], electromagnetic shielding [12],

DOI: https://doi.org/10.37256/2220244853

solar cell [13], hydrogen storage [14], drug delivery [15], and among others [16,17]. RGOBMs are typically produced from their corresponding graphene oxide-based materials (GOBMs) through a reduction process [18,19].

Up to now, a broad spectrum of techniques, including chemical, laser [20,21], microwave irradiation [22–24], and heat treatments [25–27], are readily available for reducing GOBMs. Heat treatment is the most economical, simplest, cleanest, and controllable strategy for producing high-quality Thermally made RGOBMs (T-RGOBMs) among the existing reduction strategies [28]. More importantly, heat treatment is regarded as the most convenient route for scaling up the production of T-RGOBMs from GOBMs to be employed in a wide range of exciting applications.

Despite these impressive attributes, there is still a requirement to thoroughly determine the correlation between the physicochemical properties of the resulting T-RGOBMs and the preparation and heat treatment conditions of GOBMs [29]. The quality of graphite oxide (GO) can be affected by factors such as the source of the parent graphite, the granular size, and the oxidation methods used [30]. These factors can have an impact on the sheet size, the defect concentration, and, most notably, the content and variety of attached oxygen groups (AOGs). Heat treatment of GOBMs can lead to a range of structural transformations, such as elimination of water and AOGs, recovery of Sp2 domains, the introduction of defects, and heteroatoms doping, and morphological changes such as shrinkage, agglomeration, interlayer distance expansion, sheet corrugation, sheet exfoliation, and porosity formation. Gaining an understanding of the impact of the quality of the starting GO, the physical form of the ensuing GOBMs, and annealing conditions on the structural and morphological transformations of the resulting T-RGOBMs is crucial for effectively tailoring T-RGOBMs for specific applications.

The primary objective of this review is to provide a clear guideline for the appropriate preparation of GOBMs and utilization of the heat treatment to fine-tune the physicochemical properties of T-RGOBMs toward specific applications. These properties include, but are not limited to, thermal and electrical conductivity, flexibility, porosity, hydrophilicity, reactivity, absorption, and electrochemical properties. The review covers key factors that affect the end-product features, including the quality of GO and the physical form of GOBMs, heat treatment temperature, time, pressure, and atmosphere. To the best of our knowledge, there is currently no comprehensive review that encompasses the crucial aspects of heat treatment for fine-tuning the physicochemical properties of T-RGOBMs.

2. Pathways for Reducing GOBMs

The production of RGOBMs can be achieved through multiple pathways, including chemical, hydrothermal, electrochemical, laser, and microwave irradiation methods. Particularly for large-scale industrial applications, simplicity, cost-effectiveness, low energy consumption, brief processing periods, and non-toxicity have been primary considerations in the pursuit of RGOBMs production [31,32].

Chemical reduction of GOBMs can be readily accomplished at lower temperatures, but it involves the use of hazardous and toxic chemicals like hydrazine and sodium borohydride; moreover, chemical approaches may introduce impurities into the RGOBMs' structure, potentially affecting their physicochemical properties [32,33]. For instance, the use of hydrazine introduces nitrogen impurities into the RGOBMs [34]. Importantly, It is critical to emphasize that the majority of chemical-reducing agents cannot be utilized to reduce films and aerogels as they tend to compromise their structural integrity [35]. Hydrothermal processes are carried out within an autoclave, allowing the solvent to reach temperatures significantly higher than its boiling point due to increased pressure from heating. In this method, supercritical water, heated beyond its boiling point, serves as a reducing agent, providing an environmentally friendly alternative to organic solvents [36]. Furthermore, the physicochemical properties of the resulting RGOBMs can be finely adjusted by varying both pressure and temperature [37]. However, it's worth noting that this approach tends to have a relatively extended processing time. Electrochemical reduction is a green and non-destructive method that preserves the structural integrity of basal planes. It allows for precise control of the reduction process by adjusting the electrical potential and buffer electrolyte [38]. Microwave reduction utilizes heat generated from microwave irradiation, a form of electromagnetic radiation with frequencies between 300 MHz and 300 GHz [32]. It serves as an alternative thermal method for the rapid reduction of GOBMs. One of the key benefits of microwave irradiation in comparison to traditional heating techniques is its capacity to promptly and uniformly heat substances. At room temperature and in a commercial microwave oven, RGOBMs can be readily produced from GOBMs in as little as one minute [39]. Laser irradiation is another method that induces local heating to trigger the deoxidation reaction of GOBMs. The degree of reduction can be precisely controlled by adjusting various irradiation parameters, such as wavelength, power density, scanning speed, beam energy profile, focusing, and processing conditions. Theoretical models have demonstrated that laser irradiation can induce localized annealing, briefly reaching temperatures of up to 1000°C for just a few

nanoseconds. This temperature increase leads to the decomposition of AOGs found in GOBMs, thereby enabling the synthesis of RGOBMs [40]. However, it's important to note that electrochemical, laser, and microwave irradiation methods require complex and high-cost instruments [32].

Interestingly, Heat treatment offers a versatile approach to tailor T-RGOBMs for specific applications. This customization is achievable through the manipulation of various annealing parameters, including temperature, atmosphere, pressure, time, and heating rate. Remarkably, it can be conducted at relatively low temperatures, such as 120°C, using straightforward equipment, and within a short timeframe [41]. Utilizing heat treatment can result in a high degree of reduction and a significant extent of exfoliation, ultimately leading to the development of distinctive physicochemical properties such as excellent electrical and thermal conductivities [42]. Furthermore, this method is environmentally friendly, and it stands out as a nondestructive technique that preserves the structural integrity of GOBMs, including films and aerogels [19].

3. Protocols for tuning properties of T-RGOBMs

The protocol for preparing T-RGOBMs depends extensively on their intended application. This is due to the unique physicochemical properties required for each application, which are, in turn, influenced by a specific approach to GOBMs preparation and their corresponding heat treatment conditions. in the existing literature, several protocols have been explored to develop T-RGOBMs tailored for specific applications. One particularly effective method is heat treatment, which allows for simultaneous exfoliation and reduction of GO through the decomposition of AOGs. The gases produced during AOG decomposition increase the inter-sheet pressure, and when this pressure surpasses the van der Waals forces that bind the sheets together, exfoliation occurs [43]. This approach yields T-RGOBMs with extensive exfoliation and an exceptional specific surface area, making them appealing candidates for various applications, including supercapacitors, sensors, and fillers in composite materials [44]. In addition, heat treatment at varying temperatures is one of the most commonly used protocols for customizing GOBMs. Lower temperatures (e.g., 200°C) can be employed to restore graphitic characteristics to their structure. On the other hand, higher temperatures (e.g., 2000°C) can yield highly crystalline T-RGOBMs with minimal defects [45]. Heat treatment has also been employed to produce flexible, highly aligned films through the thermal annealing of GOBMs within confined spaces. This approach results in films with exceptional thermal and electrical conductivity, rendering them promising candidates for electronic, optoelectronic, electromagnetic shielding, and energy storage applications [46,47]. Additionally, doping T-RGOBMs to enhance their physicochemical properties can be achieved during heat treatment within a specific environment containing the dopant substances. Furthermore, heat treatment can be synergistically combined with other methods, such as joule heating and hydrothermal synthesis, to further boost the physicochemical properties of the resulting T-RGOBMs [48]. In the upcoming section, a comprehensive exploration will be conducted to elucidate how operating conditions influence the preparation of T-RGOBMs when employing various protocols, with the aim of fine-tuning their physicochemical properties to meet the specific requirements of their intended applications.

4. Influence of preparation variables of GOBMs on their thermal behavior and the physicochemical properties of resulting T-RGOBMs

The quality of GO may greatly vary depending on the parent graphite source, granular size, and oxidation protocols used. These factors can impact the size of the sheets, defect density, and most importantly, the content and type of AOGs. Moreover, It is verified that the more GO's attached oxygen group content, the greater its water storage capacity [49]. These variations greatly affect the mechanisms of thermal decomposition upon heat treatment, ultimately determining the physicochemical properties of the resulting T-RGOBMs [50]. Furthermore, the physical form of the ensuing GOBMs has a tremendous impact on the thermal decomposition behavior of GOBMs and the resulting T-RGOBMs ' physicochemical properties. [51].

4.1 *Effect of GO quality*

The elaboration step of GO, which is the starting material for the preparation of all GOMBs, has a significant impact on their structure. Consequently, optimizing the graphite oxidation process is a vital approach for tailoring the GO's quality [52–54]. GOMBs quality is frequently correlated with the degree of oxidation (carbon-to-oxygen ratio), which in turn influences such specifications as, the ratio of Sp2 to Sp3 carbon atoms, the type and distribution of AOGs, hydrophilicity, the level of exfoliation (number of layers per sheets), GO sheets (GOS) size,

and defects density. Optimization of GO's quality may be achieved by selecting the appropriate size and purity of the graphite powder, utilizing the suitable protocol of oxidation (such as Staudenmeier [55], Brodie [56], Hummers [57], and improved ones [58,59]), and adjusting operational conditions such as the composition and amount of reactive species, the temperature, and the period of oxidation, purification, and sonication[60,61].

To gain a complete understanding of how to optimize the quality of GO, it is essential to thoroughly review recent studies that have examined the influence of various factors on its quality. In this vein, to demonstrate the effect of the oxidation protocol, Botas et al. derived GO from the same graphite using the Brodie and Hummers methods. The Brodie oxidation yielded fewer AOGs but created highly thermally stable epoxy and hydroxyl groups. In contrast, the Hummers oxidation produced more AOGs, but led to weaker intensity of epoxy and hydroxyl groups, making it easier to be reduced into T-RGOBMs with fewer defects[62].

Furthermore, the influence of graphite powder supply and particle size has been extensively studied [63–65]. Botas et al. investigated the synthesis of GO using graphite crystals of varying sizes (**Fig. 1a**). They found that when smaller crystals were oxidized, smaller GOS with acid carboxylic groups confined to the edges were obtained. However, when larger graphite crystals were used, larger GOS decorated with a higher proportion of epoxy groups were produced [63].

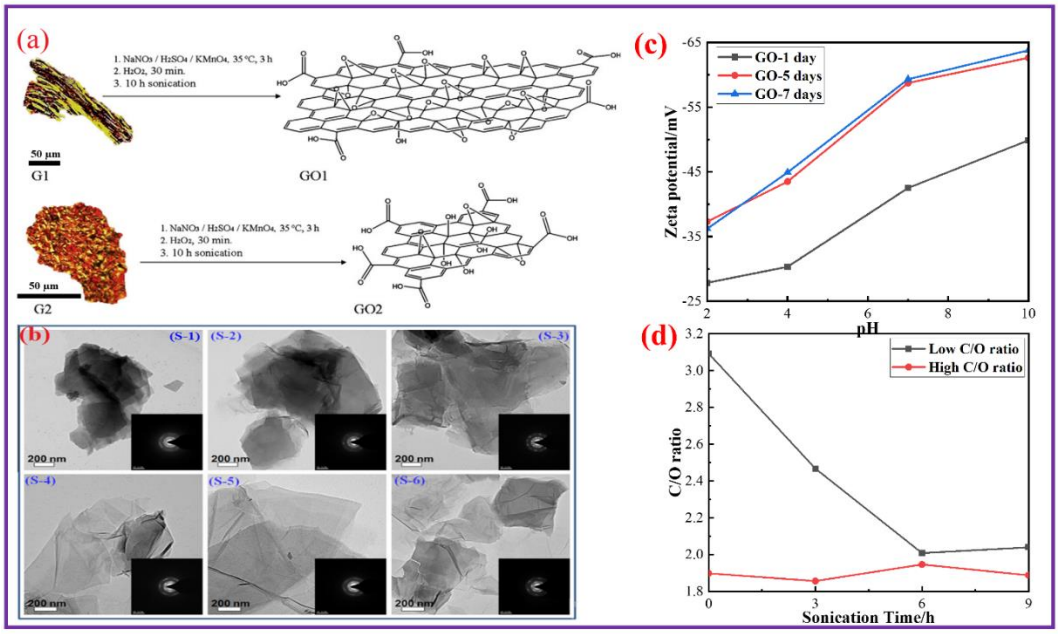

Figure 1. **(a)** Effect of parent graphite crystal size on the quality and morphology of GO (presentation of graphites G1 and 2 with their corresponding GOS structures) [63]. **(b)** Transmission electron microscopy (TEM) images show the effect of the oxidation degree on the thickness of the GOS. (S-1, 2, 3, 4, 5, and 6, are samples of GO made by using different masses of $KMnO_4$, 1, 2, 3, 4, 5, and 6 g, respectively) [66]. **(c)** Effect of oxidation time on the zeta potential of the resulting GO [67]. **(d)** Effect of sonication time on the C/O ratio of the resulting GO [68]

Krishnamoorthy et al. synthesized graphene oxide samples with varying levels of oxidation. Their findings suggest that the number of AOGs and the degree of exfoliation can be regulated by adjusting the amount of oxidizing agent used. The analysis revealed that increasing the degree of oxidation leads to a decrease in the graphitic domains of the resulting GO. Additionally, it was observed that at lower oxidation degrees, the formation of hydroxyl and carbonyl groups is favored, whereas, at higher oxidation degrees, these groups are converted into epoxides. The lower AOGs content minimizes the exfoliation of GO into a few layered GOS (as shown in **Fig. 1b**), according to TEM ivestigation [66].

The number of AOGs in GO structure can be adjusted by carefully controlling the oxidation period [67]. Increasing the oxidation period leads to a higher intensity of AOGs, with the majority of carboxylic groups forming after a longer oxidation period. Additionally, epoxide and hydroxyl groups are mainly present throughout the structure of GO between 1 and 5 days. The GO that was synthesized within a week had the most negative value (**Fig. 1c**), but there were no significant differences when compared to the GO that was synthesized in 5 days. The great stability of GO can be attributed to the negatively charged AOGs located at the edges of the GO sheets, which create electrostatic repulsion and prevent the graphitic sheets from aggregating during oxidation, resulting in electrostatic stabilization. Overall, the study suggests that a 5-day oxidation duration is optimal for increasing the number of AOGs on both the basal planes and edges of GO without damaging the carbon structure.

Regulating the sonication time can be consistently used as an effective technique to exfoliate GO and manage its size. Studies revealed that longer ultrasonication periods result in smaller and thinner GOS [68,69]. The process of separating GO into GOS occurs through the creation of a compressive stress wave resulting from the collapse of cavitation bubbles. This force acts on the surface of the GO stack, penetrating through the top layer and being reflected back by the GO flat body. As a result, a tensile stress wave is formed, propagating away from the stack and causing GOS to separate. Additionally, the micro-jets exerting force on the surface of GO created during the sonication process break larger GOS into smaller ones. Furthermore, ultrasonic treatment can enhance the level of oxidation in GOS, particularly when the initial C/O ratio is low (**Fig. 1d**) [68]. Ultrasonication possesses the potential to produce highly concentrated bursts of energy, which in turn can generate intense reaction conditions such as high pressure and temperatures. These conditions can effectively facilitate the oxidation process of GOS.

To fully understand how the quality of the starting GO affects the structure and physicochemical properties of the resulting T-RGOBMs, it is crucial to review recent studies that have investigated the impact of GO quality on the structure of the derived T-RGOBMs. Bagri et al. have highlighted the primary barrier that hinders the performance of T-RGOBMs devices, which is the nature of the AOGs that remain in T-RGOBMs after intense thermal annealing. They have determined that the initial oxygen content and the OH/O ratio of the starting GO are important factors that affect the physicochemical properties of the ensuing T-RGOBMs. The simulation results indicate that while hydroxyl groups can decompose at relatively low temperatures without causing significant damage to the basal plane, epoxy groups are more resistant to decomposition. Moreover, the desorption of epoxy groups has a detrimental effect on the integrity of the T-RGOBMs skeleton. Additionally, it has been revealed that carbon removal from the T-RGOBMs plane is more likely to take place when hydroxyl and epoxy groups are bonded adjacently. Furthermore, the arrangement of two neighboring AOGs after heat treatment yields thermally very stable carbonyl and ether groups [70]. Antidormi et al. demonstrated that the initial C/O ratio affects the efficiency of the reduction process. Specifically, when the C/O ratio is greater than 0.35, thermal reduction fails to produce a substantial improvement in the crystallinity of the T-RGOBMs structure. Instead, the primary reactions triggered by thermal energy in these cases are the removal of carbon atoms from the plane, which leads to the formation of defects. This causes a significant rearrangement of the atomic configuration and distortion of the basal plane, resulting in a loss of regularity. Furthermore, it has been revealed that the crystallinity of T-RGOBMs may be improved by carefully controlling the parameters of the heat treatment and the starting GOBMs structure. Specifically, by identifying the optimal temperature for a given distribution of AOGs on GOBMs structure, it is possible to achieve a minimal distortion of the T-RGOBMs structure and a significant recovery of Sp2 carbon character [71].

Furthermore, a wealth of research exists on the correlation between the quality of GOBMs and the resultant physicochemical properties of T-RGOBMs [72]. **Table 1** summarizes some studies that have investigated the impact of oxidation and annealing conditions on the specifications and properties of the resulting T-RGOBMs. Poh et al. conducted a study highlighting the substantial impact of the GO preparation method on the electrochemical properties of resulting T-RGOBMs. They explored three distinct protocols for GO synthesis: the Hummers method, utilizing potassium permanganate and sodium nitrate as oxidizing agents, and the Hofmann and Staudenmaier methods, employing potassium chlorate as the oxidizing agent. Notably, Hummers' T-RGOBM exhibited lower overpotential and superior heterogeneous electron transfer when compared to T-RGOBMs obtained from Hofmann's and Staudenmaier's methods of GO synthesis. The enhanced electrochemical performance seen in Hummers' T-RGOBM may be ascribed to the introduction of nitrogen into the structure of the Hummers' GO during the oxidation process, which is assisted by the presence of sodium nitrate as a reactant (**Fig. 2f**) [61]. Dao et al. examined how the size of graphite particles influences the physicochemical properties of the synthesized GO and the derived T-RGOBMs. Using smaller raw graphite particles led to an increase in the C/O ratio of the GO, resulting in smaller graphene particles but with a higher exfoliation degree. Additionally, the size of the starting graphite affects the chemical structure of the resulting GO, including the types and the amount of AOGs. These changes in GO properties then affect the reduction degree, the graphitic structure, and the electrical conductivity of the resulting T-RGOBMs. Moreover, it has been found that using graphite particles with a size of around 50 micrometers is crucial for achieving better T-RGOBMs structure with low oxygen content, expanded SSA, and improved conductivity (**Fig. 2g**) [65]. The study by Chee et al. investigated the relationship between the size of graphite materials and the structural properties of T-RGOBMs. They discovered that the size of the raw graphite particles had minimal impact on the defect density, the number of AOGs, and the rate of heterogeneous electron transfer for T-RGOBMs. Most importantly, they found that the size of the graphite materials had no effect on the electrochemical performance of the T-RGOBMs [64].

The Specific Surface Area (SSA) of the resulting T-RGOBMs is directly related to the initial amount of AOGs in GOBMs. Upon heat treatment, they decompose into gaseous products, which generate high pressure in the interlayer space and lead to the exfoliation of graphite oxide. The greater the amount of AOGs, the higher the

pressure of the gaseous products, resulting in improved exfoliation. Jankovsky et al. highlighted the crucial role that the starting GO composition and type of AOGs play in determining the structure and SSA of T-RGOBMs. The team meticulously analyzed the chemical composition of GOs produced through various oxidation methods (Brodie (BR), Hofman (HO), Hummers (HU), Staudenmaier (ST), and TOUR (TO)) before and after thermal annealing and SSA of the resulting T-RGOBMs. Results shown in **Fig. 2a** indicate that the highest C/O ratio was observed in T-RGOBM-HU and T-RGOBM-TO made from highly oxidized GOs, produced using potassium permanganate as the oxidizing agent. This is because the high level of oxidation resulted in a high concentration of thermally sensitive ketone and carboxyl functionalities that decomposed easily, leading to a high C/O ratio in the resulting T-RGOBMs. However, when chlorate oxidizer was used, the resulting GOs (GO-BR, GO-ST, and GO-HO) contained primarily hydroxyl functional groups which were more thermally stable and resulted in T-RGOBMs with a lower C/O ratio and SSA[30].

The effect of sonication time and annealing temperature on the hydrophilicity of Graphene oxide film-containing chitosan (GOF-C) was investigated (**Fig. 2b, c, d,** and **e**). The results showed that the hydrophilicity of the resulting film increased with increasing sonication time, as the GOF-C became thinner and smaller, thereby enhancing the surface chemistry and wettability. Additionally, the hydrophilicity of the film decreased with increasing annealing temperature, which can be attributed to the elimination of more AOGs that contribute to the hydrophilic properties of GOF-C [69].

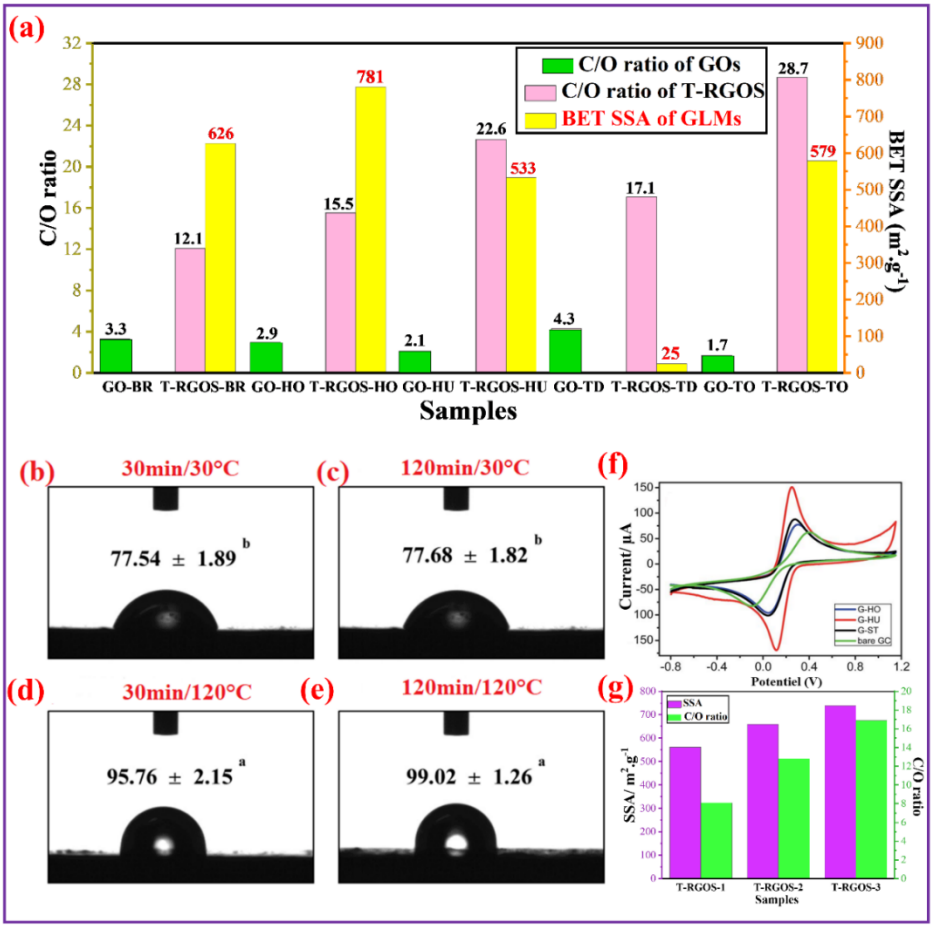

Figure 2. **(a)** Impact of oxidation method on structure and specific surface area of T-RGOSs [30]. (**b, c, d,** and **e**) Contact angle tests of GO film containing chitosan treated at 30 and 120°C, and prepared using GO sonicated for 30 and 120 min [69]. **(f)** Electrochemical behavior of various T-RGOBMs(G) derived from GOs prepared by Hofmann (HO), Hummers (HU), and Staudenmaier (ST) methods [61]. **(g)** effect of the size of graphite on the SSA and C/O ratio of the resulting T-RGOBMs (T-RGOS -1, T-RGOS -2, and T-RGOS -3 are derived from graphite with corresponding grain sizes of 604, 107, and 57 µm) [65]

Table 1. Impact of the oxidation and annealing conditions on the specifications and properties of the resulting Thermally reduced graphen oxide sheets (T-RGOBMs)

Graphite	Oxidation conditions	Annealing Conditions	GO C/O ratio	T-RGOS C/O ratio	Electrical conductivity ($S.m^{-1}$)	Porosity	References
Commercial GO	Hummers	500°C in nitrogen atmosphere	2.47	/	/	130	[73]
	Brodie		2.85			550	
Graphite (2–15 µm)	Brodie	1000°C in nitrogen atmosphere	3.3	12.1	/	626	[30]
	Hofmann		2.9	15.5		781	
	Hummers		2.1	22.6		533	
	Staudenmaier		4.3	17.1		25	
	Tour		1.7	28.7		579	
Graphite (<50µm)	Staudenmaier	1000°C in nitrogen atmosphere	2.5	24.1	/	/	[61]
	Hofmann		1.8	18.2			
	Hummers		1.1	19.3			
Graphite (604µm)	Brodie	1100 °C in nitrogen atmosphere	2.1	8.1	6850	562	[65]
Graphite (107µm)			2	12.8	5770	659	
Graphite (57µm)			1.9	16.9	9680	739	
Graphite (44 µm)	Modified Hummers Oxidation time (30min)	1100 °C in argon atmosphere	/	/	/	342	[74]
	Modified Hummers Oxidation time (1h)					370	
	Modified Hummers Oxidation time (3h)					453	
	Modified Hummers Oxidation time (1day)					442	
	Modified Hummers Oxidation time (3day)					484	

4.2 *Effect of the confined water*

Studies have shown that the amount of water stored in GOBMs plays a significant role in its thermal decomposition process. GOBMs have the ability to absorb and retain moisture within their structure, which. The ability is directly correlated to the concentration of AOGs present [49]. In the presence of confined water within GOBMs, it has been found that thermal annealing can promote the formation of oxygen-containing free radicals. Ultimately, these radicals target hydroxyls, carbonyls, and carboxyls with a preference for edge defects over basal plane defects [75]. In addition, it has been verified that confined water molecules indeed play a crucial role by engaging with etch holes on the basal plane, effectively passivating them. This interaction results in the release of CO_2 and the subsequent formation of ester carbonyl and ketone groups [76].

4.3 *Effect of lattice defects*

Harsh oxidation typically results in the disruption of the graphene lattice through the formation of CO_2. The removal of carbon atoms from GO creates lattice defects that are irreversible and should be regarded as permanent [66,77]. Moreover, these lattice defects can undergo expansion during the heat treatment reduction process, or new defect sites can be generated, leading to increased damage within the sp2 domains of the resulting T-RGOBMs. This is primarily due to the removal of carbon from the lattice as reaction products, including CO_2 and CO molecules [78]. The presence of lattice defects in T-RGOBMs disrupts their regular atomic arrangement, leading to a range of electronic and transport property modifications. These defects are often undesirable in applications requiring high electrical conductivity and pristine electronic properties [79]. Through precise manipulation of factors during the oxidation process, such as the size of the starting graphite powder, using a low oxidation temperature, and injecting oxidizing agents in a controlled manner, large sheets of GO can be produced with minimal lattice defects[80].

More importantly, in the presence of a carbon source, lattice defects may not be enlarged and can even be repaired during the heat treatment of GOBMs. For instance, Ethanol has been observed to play a role in mending holes by promoting the creation of new hexagonal carbon rings during heat treatment of GOBMs. During the decomposition of ethanol and its integration into the holes of T-RGOBMs, it leads to the formation of fresh hexagonal carbon rings, accompanied by the addition of AOGs like ethers and carbonyls. These oxygen-decorated groups within the etch holes react with other nearby AOGs, reopening the ring for additional carbon integration, ultimately enhancing the graphitization of T-RGOBMs [78,81]. Grimm et al. conducted annealing of GOBMs in the presence of an Ar/H_2/isopropanol flow. This process was aimed at repairing the graphitic domains in T-RGOBMs by reducing the decorated vacancy sites and subsequently introducing carbon into these sites [82].

4.4 *Effect of impurities*

The presence of impurities in GOBMs, whether derived from the graphite starting material or the oxidation process, remains a persistent concern. These impurities substantially affect not only the physicochemical properties of resulting T-RGOBMs but also the thermal decomposition behavior of GOBMs. This matter is of paramount significance, particularly when contemplating the use of T-RGOBMs in electrochemical sensing or energy-storage devices. Natural graphite used in the preparation of GO retains various mineral and metallic impurities, which are intercalated between stacks of adjacent graphene layers. It has been evident that the metallic impurities within GO can significantly impact, and in some cases, overpower the physicochemical properties of the resulting T-RGOBMs [83]. Ambrosi et al. conducted a study demonstrating that metallic impurities originating from the graphite material persist in the resulting GO even after its heat treatment at 1050°C. Their research also highlighted that these impurities exert a significant influence on the electrocatalytic properties of the resulting T-RGOBMs[84].

Furthermore, upon the oxidation of graphite, a substantial amount of highly oxidizing chemicals, including potassium salts like $KMnO_4$ and $K_2S_2O_8$, may be involved. These chemicals can potentially transform into various forms of potassium compounds, such as KNO_3, KOH, K_2SO_4, and KCl, among others. These impurities can serve as catalysts, thereby facilitating and accelerating the decomposition of GOBMs during heat treatment. This can result in a sudden increase in interlayer pressure and temperature, potentially leading to an explosion [85,86]. Qiu et al. conducted a study that elucidated the role of potassium impurities in inducing an explosive reduction mode of GO. They immersed a GO cake in a KOH solution, and thermal analysis revealed the absence of a water endotherm, along with the explosion of the cake. This observation indicated a promoting effect of potassium hydroxide. Importantly, the onset temperature for the exotherm was approximately 50°C lower compared to pure GO cake [85].

Additionally, the use of sulfuric acid during the oxidation process may introduce sulfur species in the form of both organic sulfates and inorganic sulfates. Organic sulfates decompose at approximately 200°C, producing the highly toxic gas SO_2. Furthermore, these species may have a significant impact on the physicochemical properties of GOBMs and their thermal behavior [87,88].

4.5 *Effect of the size, morphology, and physical form of GOBMs*

The formation of GOBMs is closely tied to the physical form required for their intended applications. The physical form is determined by the necessary T-RGOBMs, which have specific properties that make them suitable for different uses. The preparation of GOBMs usually involves obtaining graphene oxide sheets (GOS) through the mechanical splitting of GO into single or few-layer sheets using techniques like sonication. Further, GOS dispersion can be transformed into a free-standing graphene oxide film (GOF) using methods like drop casting, vacuum filtering, and spin coating. Graphene oxide aerogel (GOA) can be attained by freeze-drying GOS dispersion. On the other hand, T-RGOBMs can be prepared through the thermal annealing of GOBMs. Thermally reduced graphene oxide sheets (T-RGOS) may be produced by thermal reduction of GOS or by undergoing thermal exfoliation-reduction of GO. Thermally reduced graphene oxide film (T-RGOF) and aerogel(T-RGOA) can be obtained by thermal reduction of GOF and GOA. **Fig. 3a** presents comprehensive, step-by-step guidance for crafting GOBMs and T-RGOBMs.

T-RGOFs can be produced through the heat treatment of GOF without compromising their essential flexibility [19]. Due to their lightweight composition, exceptional porosity, and elevated electrical conductivity, they are widely endorsed for energy storage purposes in foldable and portable electronics, since they may be used without the need for a current collector [89]. On the other hand, T-RGOSs exhibit a two-dimensional structure with ultra-thin layers, exceptional porosity, and surfaces adorned with AOGs, making them promising candidates for various intriguing applications [90], including energy storage, and sensing. Moreover, T-RGOSs may also

function as a beneficial additive in composites, providing enhanced thermal and electrical conductivity [91–93]. This addition improves particular performance characteristics such as interference shielding [94] and flame retardancy [95]. Lastly, T-RGOA, characterized by extremely low density (a few milligrams per cubic centimeter), interconnected pores, and superior specific surface area (SSA), holds promise in applications such as oil absorption [96], heavy metal water decontamination [97], and interference shielding [98].

4.5.1 *Effect of size and morphology of GOBMs on the physicochemical and performance of T-RGOBMs*

The size and morphology of GOBMS, which are greatly influenced by preparation variables, have a significant impact on the physicochemical properties of the resulting T-RGOBMs.**Table 2** provides a concise summary of these effects. Notably, the initial concentration of GOS suspension used in the preparation of GOA has a substantial and far-reaching impact on its bulk density, thereby influencing the physicochemical properties of the resulting T-RGOA, including thermal and electrical conductivity [99,100]. In the study conducted by Chang et al., four distinct T-RGOA samples were prepared using different concentrations of GO suspension through a process involving supercritical ethanol drying and subsequent heat treatment at 1500°C under a nitrogen atmosphere. The results of this study demonstrate that an increase in the concentration of the GOS suspension leads to higher porosity, as well as improved electrical and thermal conductivity in the T-RGOA. This phenomenon is attributed to the enhanced bulk density of the resulting T-RGOA that arises from the elevated concentration of the initial GOS suspension [101]. The microwave absorbing performance has been found to be strongly associated with the morphology of T-RGOA. Zhang et al. investigated the impact of the initial concentration of GOS suspension on the microwave-absorbing performance of the resulting T-RGOA. Their findings revealed that increasing the initial GOS suspension concentration from 0.3 to 0.6 $mg.ml^{-1}$ significantly enhanced the microwave absorption effectiveness, reaching a peak value of 34 at 13.1 GHz. However, T-RGOA produced from a 0.9 $mg.ml^{-1}$ GOS suspension exhibited reduced microwave absorbing capabilities. These results suggest that the optimal concentration for achieving the best microwave absorption is 0.6 $mg.ml^{-1}$. This concentration enables self-assembled T-RGOA to attain an ideal morphology for optimal microwave absorption performance [102]. The thickness of the GOF was identified as a critical factor affecting the properties and performance of the resulting T-RGOF. The thickness of GOFs can be controlled through various preparation variables in the chosen technique. For example, in methods involving vacuum filtering or solution casting, variables such as the concentration and quantity of the GOS can be adjusted. Additionally, when spin-coating is employed, the spin speed serves as a variable for controlling thickness. Papamatthaiou et al. prepared GOFs with two different thicknesses by spin-coating at different spin speeds, specifically 3000 rpm and 6000 rpm. Subsequently, both GOFs underwent heat treatment at 180°C in an Ar-H_2 environment for 30 minutes on multiple occasions. Following exposure to several air/vacuum cycles for both T-RGOFs, it was observed that the thicker T-RGOF (produced at 3000 rpm) rapidly lost its ability to sense humidity within a brief period, typically less than one week. In contrast, the thinner T-RGOF (produced at 6000 rpm) retained its humidity-sensing capability for approximately two weeks. However, the thicker T-RGOF exhibited higher sensitivity to changes in humidity [103]. The lateral size of T-RGOSs resulting from the thermal exfoliation of GO plays a crucial role in determining their physicochemical properties [104]. Specifically, the electrical conductivity of graphene aggregates is heavily influenced by the contact resistance between the individual sheets. When the sheets are larger in lateral size, there are fewer sheet-to-sheet contacts for a given number of conducting paths. Consequently, this reduction in the total number of contact points results in an improvement in conductivity. Lin et al. demonstrated that the electrical conductivity of T-RGOF produced through heat treatment at 1100°C from GOF prepared by vacuum filtering larger-sized GOS is significantly higher than that of T-RGOF prepared from smaller-sized GOS [105]. Moreover, larger sheets prove to be more effective in bearing loads when T-RGOS is employed as a reinforcing filler in composite materials [106,107].

Table 2. Impact of size and morphology of GOBMs on the pysicochemical properties and performances of the resulting T-RGOBMs

GOBMs	Heat treatment conditions	Preparation variables		Physicochemical properties and performance of the resulting T-RGOBMs		References
GOA prepared at different GO Concentrations	1500°C in nitrogen atmosphere	Concentration /$mg.ml^{-1}$	T-RGOA S_{BET}/ $m^2.g^{-1}$	Thermal Conductivity/$W.m^{-1}.K^{-1}$	Electrical Conductivity/$S.m^{-1}$	[101]
		1	336.5	0.036	53.5	
		2	384.0	0.041	95.0	
		5	423.1	0.053	143.3	

		10	440.8	0.067	157.3	
	600°C in Ar atmosphere	Concentration /mg.ml^{-1}	Bulk density/mg.cm^3		Microwave absorption effectiveness/ dB	[102]
		0.3	0.9		Max -15 at 18 GHz	
		0.6	1.6		Max -34 at 13.1 GHz	
		0.9	2.4		Max -22 at 15.6 GHz	
GOF prepared by spin coating at different spin speeds	180°C in Ar-H_2 atmosphere	Spin speed/rpm	Operational lifespan/week		sensitivity	[103]
		3000	<1		0.6	
		6000	2		0.4	
GOF prepared by vacuum filtering from GOS of varying sizes	1100°C in Argon atmosphere	Size of GOS/ µm	Young's modulus of GOF/ GPa		Electrical Conductivity/S.m^{-1}	[105]
		1	5.2		50000	
		3	6.9		75000	
		32	7.5		125000	
		272	13.1		139000	

4.5.2 *Effect of the geometry and physical form on the thermal decomposition of GOBMs*

The geometry and the physical form of GOBMs can also have a significant impact on the thermal decomposition process. This is because the geometry can affect how heat is conducted and exchanged with the environment, the number of sites where reduction can occur, and how long the engendered gases are retained. These factors can all influence the overall mechanism of the thermal decomposition of GOBMs. The effect of the geometry of GOBMs on thermal decomposition has been well-documented in various studies. For instance, Klemeyer et al. elaborated two GOMBs of varying densities and subjected both to identical thermal treatment conditions. The study found that the reduction process occurred more rapidly when the density of GOBMs was higher. This can be attributed to the fact that the sheets composing the GOMBs are situated in closer proximity, thereby increasing the number of reduction sites. Additionally, the duration of gas retention between the GOMB sheets is prolonged, leading to an even greater enhancement of reduction. [108]. Moreover, Pan et al. have shown that GOF experiences faster thermal decomposition when compared to GO powder, owing to the enhanced thermal conductivity within the stacked GOS and the restricted heat exchange with the surrounding environment [109].

Furthermore, the geometry of GOBMs samples can have a tremendous impact on the explosive mode of reduction, which refers to the rapid and exothermic release of gases such as CO, CO_2, and H_2O. The geometry of the sample can affect the heat conduction and exchange with the surrounding environment, which influences heat and mass transfer of the internal temperature and pressure [85]. Losic and colleagues studied the thermal behavior of various GOBMs with different physical forms, such as GO paste, GO powder, GO film, and GO aerogel. Results of thermal analysis techniques are shown in **Fig. 3b.** It can be seen that GO in paste and powder forms had lower reduction temperatures (at 196 and 197 °C) for micro-explosions when compared to the film and aerogel (at 210 °C and 214 °C). The study also found that GO film is more flammable than the other samples and had the ability to self-ignite in low-oxygen environments [51].

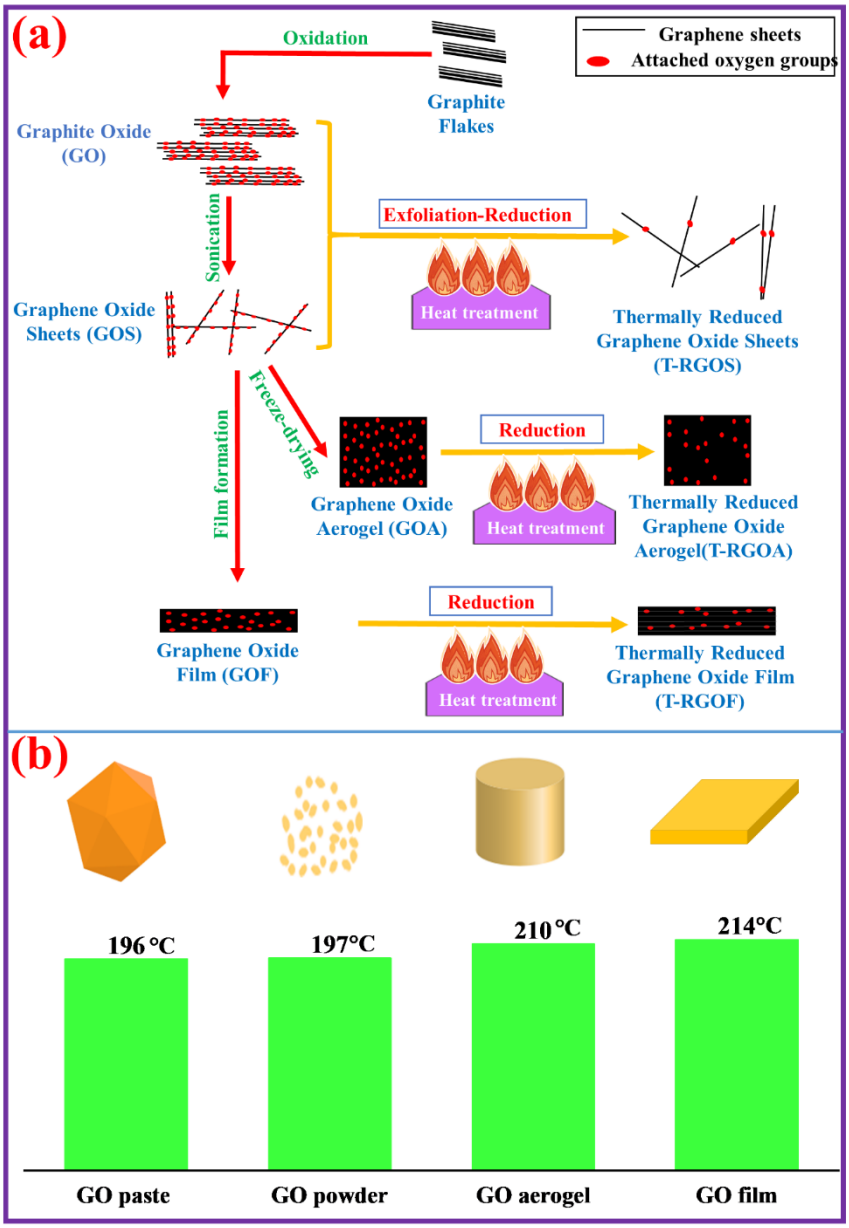

Figure 3. **(a)** a step-by-step guide to crafting GOBMs and T-RGOBMs: a detailed schematic illustration**; (b)** impact of physical form of GOBMs on thermal reduction temperature [51]

5. Effect of the heat treatment conditions of GOBMs on the physicochemical properties of the resulting T-RGOBMs

Investigating the impact of annealing conditions on the structure and physicochemical properties of the ensuing T-RGOBMs is crucial as it plays a significant role in determining the final physicochemical properties of T-RGOBMs and their suitability for specific applications. The annealing conditions such as temperature, heating rate, pressure, and atmosphere can influence the thermal decomposition of GOBMs, which in turn affects the overall properties of T-RGOBMs. By understanding how these factors affect the structure and properties of RGOBMs, researchers and practitioners can develop thermal approaches to precisely fine-tune the properties of T-RGOBMs toward specific applications.

5.1 *Effect of annealing temperature*

The temperature at which thermal annealing is performed exerts the most profound influence on the ultimate structure of T-RGOBMs and their physicochemical properties, such as electrical conductivity, thermal

conductivity, and porosity [110–112]. Depending on the end-use application, annealing temperature may be used as a monitoring tool to tune the physicochemical properties of GOBMs. The conversion of GOBMs can be achieved across a wide temperature range, spanning from low temperatures (e.g., 150°C) [113–115] to high temperatures (e.g., 2000°C) [116,117].

Raising the treatment temperature has been found to be an effective strategy for eliminating AOGs from GOBMs. During heat treatment, the covalent bonds between the oxygen and carbon atoms in the GOBMs break, releasing the oxygen atoms and resulting in a reduced form of the material. Several studies have investigated the impact of increasing temperature on the structure of the resulting T-RGOBMs in terms of AOGs removal effectiveness. For example, it was found that the C/O ratio of GOBMs can be improved from 2.8 for the initial material to 8.9 at 500°C, 13.2 at 700°C, and 14.1 at 900°C when the reduction of GOBMs is performed in ultra-high vacuum(UHV) [118]. Furthermore, T-RGOS resulting from the reduction of GOBMs at temperatures ranging from 2000 ºC to 2400 ºC were almost entirely devoid of oxygen and exhibited a graphite-like structure owing to an increase in Sp2 domains in T-RGOS [119]. Additionally, a thorough examination of the effect of temperature on AOGs reveals that their thermal stability varies depending on the type of group. Accordingly, annealing at temperatures above 650°C is sufficient to completely remove hydroxyl groups, while carbonyl groups require temperatures above 1700°C for removal [120].

Recent studies have consistently demonstrated that the electrical and thermal conductivity of T-RGOBMs increases as the annealing temperature increases. This suggests that heat treatment at high temperatures could be a potential approach to produce T-RGOBMs for applications requiring high conductivities [121–127]. The reason for this enhancement is that, as the temperature increases, more AOGs are removed. AOGs can act as defects in the material, hindering the flow of electrons and decreasing conductivity. Once these AOGs are removed, the remaining T-RGOS can stack more closely together, resulting in a marked increase in both electrical and thermal conductivity.

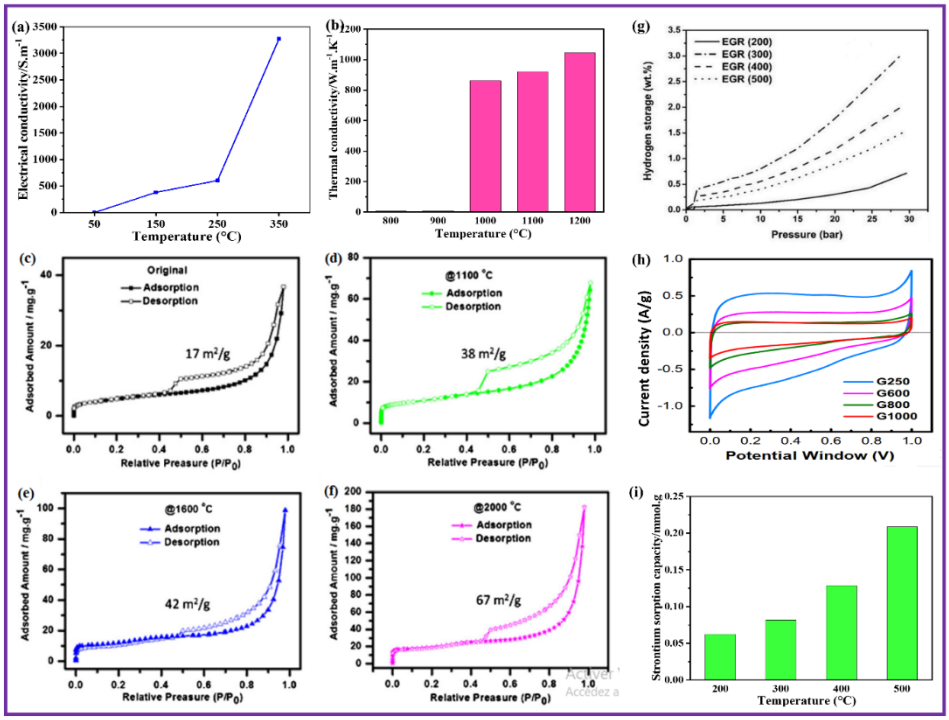

Figure 4. Effect of annealing temperature on the physicochemical properties of T-RGOBMs; (a) elecrical conductivity [19]; (b) thermal conductivity [16]; (c, d,e, and f) specific porosity [116]. Effect of annealing temperature on the performances of T-RGOBMs; (g) specific capacitance [128]; and (h) hydrogen storage capacity [14]; sorption capacity [73]

Various studies have examined the effect of increased temperature on the conductivity of the resulting T-RGOBMs. For example, Akbi et al. examined how annealing temperature affects the electrical conductivity of the resulting T-RGOF (**Fig. 4a**). Results indicate that as annealing temperature increases, so does electrical conductivity, which reaches 3275 $S.m^{-1}$ at 350°C. This improvement is attributable to the evaporation of the stored water, the restoration of the Sp2 carbon character, and the elimination of AOGs [19]. Chen et al. demonstrated the influence of temperature annealing on the thermal conductivity of T-RGOF (**Fig. 4b**). Consequently, when the temperature rises, a simultaneous change from Sp3 to Sp2 character removes additional AOGs from the T-

RGOF resulting in an increase in thermal conductivity, which reaches 1045 $W.m^{-1}.K^{-1}$ at 1200 °C [16]. The effect of reduction temperature on the thermal and electrical conductivity of T-RGOF has also been demonstrated. Accordingly, T-RGOF reduced at a higher temperature displays the maximum thermal and electrical conductivity [127].

Temperature can significantly impact the morphology of the T-RGOBMs, causing the exfoliation of sheets and the formation of pores. High-temperature treatment (1100-2000°C) has been shown to improve absorption performance and increase the pore size of T-RGOS. In addition, the BET analysis (**Fig. 4c, d, e, and f**) of the resulting T-RGOS indicated a significant increase in the specific surface area (SSA) [116]. The consideration of the extent of exfoliation has significance in T-RGOMBs due to its pivotal role in determining their physicochemical characteristics. Research has shown that the temperature of heat treatment significantly influences the degree of exfoliation. According to McAllister's theoretical findings, it is essential to exceed a temperature of 550°C in order to obtain effective exfoliation of Staudenmaier-prepared GO. Once the temperature exceeds 550°C, the rate at which AOGs decompose in GO becomes greater than the rate at which the evolved gases diffuse. As a consequence, the pressures experienced surpass the cohesive van der Waals forces that hold GOSs together [43]. Cao et al. performed a study to examine the influence of treatment temperature on the degree of exfoliation in T-RGOS. They accomplished this by exposing modified Hummers-prepared GO to different temperatures in the presence of a nitrogen environment. The results of their study demonstrated that increasing the temperature from 550°C to 1200°C led to a decrease in the number of layers that constitute T-RGOS, declining from 3 to 2 layers. The observed result may be ascribed to the phenomenon wherein elevated temperatures expedite the rate of disintegration of AOGs. The acceleration mentioned above induces elevated pressures, hence leading to a more pronounced exfoliation process characterized by a reduced number of layers [129]. Adjusting the extent of exfoliation can be employed to control the dielectric properties of T-RGOS. A comparison between two T-RGOBMs, one prepared by annealing GOS at 400°C and the other at 1000°C under argon atmosphere, revealed that the T-RGOS prepared at 400°C exhibited higher permittivity. This was due to its lesser degree of exfoliation and a greater presence of AOGs in the T-RGOS prepared at 400°C [130].

The temperature used during annealing can greatly impact the performance of T-RGOBMs in a variety of applications [131,132]. By carefully adjusting this parameter, the performance of T-RGOBMs can be optimized for superior results. Many studies have explored the effect of annealing temperature on the properties and performance of the resultant T-RGOBMs, as summarized in **Table 3**. Supercapacive performances of T-RGOS may be improved by adjusting the temperature of heat treatment (**Fig. 4g**). Further research into the effect of temperature reduction on the T-RGOS's capacitance at temperatures ranging from 250 to 1000 °C revealed a decrease in capacitance as the temperature increased due to the elimination of AOGs, which offers additional pseudocapacitance via faradic redox processes [128].

Le et al. investigated the strontium sorption capability of T-RGOS produced at varied temperatures in ambient air (**Fig. 4i**). Consequently, raising the temperature of treatment improves the sorption capacity, which reaches a maximum of around 0.2 mmol/g at *T*=500°C. This finding may be credited to the fact that, at elevated temperatures, T-RGOS react with oxygen, resulting in a greater density of AOGs and defects that can serve as adsorption sites. To investigate the influence of temperature reduction on the performance of T-RGOS as flame retardants for polyester (PS), GO was thermally treated at 200°C, 500°C, and 800°C. Due to the elimination of additional AOGs and the barrier effect caused by the expanded and lamellar structure of T-RGOS, incorporation of polyester with T-RGOBMs treated at 800°C significantly increased the flame retardancy, reducing the releasing energy rate by 48% and the ignition time by 53% [133]. Singh et al. revealed that the exfoliation temperature has a significant impact on the porosity and pore size of T-RGOS, resulting in varying hydrogen storage capacities (**Fig. 4i**). Exfoliating GOS at 200 °C is ineffective for layer separation, resulting in the lowest ability to absorb hydrogen. At *T*= 300 °C, T-RGOS displays a high SSA of 248 $m^2.g^{-1}$ and an increased pore volume of 1.4 $cm^3.g^{-1}$, resulting in a maximum hydrogen absorption capacity (3.12%). However, subsequent increases in exfoliation temperature (*T*=500°C) resulted in a drop in the ability to absorb hydrogen because of the layer degradation and rupture caused by the high exfoliation temperature [14].

Table 3. Impact of the annealing temperature on the properties and performance of the resulting T-RGOBMs

T-RGOBMs	Application	Annealing temperature (°C)	SSA/ inter-layer spacing	Electrical/ thermal conductivity	performance		References
T-RGOS	Anode for Li-ion Battery	300	234 $m^2.g^{-1}$	/	Charge/discharge capacity at a current density of 30 mA/g	780 $mAh.g^{-1}$	[134]
		400	403 $m^2.g^{-1}$			1220 $mAh.g^{-1}$	

		500	62 $m^2.g^{-1}$			615 $mAh.g^{-1}$	
		600	213 $m^2.g^{-1}$			529 $mAh.g^{-1}$	
T-RGOS	Electrode for supercapacitor	250	309 $m^2.g^{-1}$	/	Specific capacitance was determined using a three-electrode system at a scan rate of 3 $m.V.s^{-1}$	170.5 $F.g^{-1}$	[128]
		600	293 $m^2.g^{-1}$			107.7 $F.g^{-1}$	
		800	302 $m^2.g^{-1}$			58.9 $F.g^{-1}$	
		1000	434 $m^2.g^{-1}$			47.5 $F.g^{-1}$	
T-RGOS	Hydrogen storage	200	46 $m^2.g^{-1}$	/	Hydrogen uptake at -196 °C under 30 bar	0.71 weight %	[14]
		300	248 $m^2.g^{-1}$			3.12 weight %	
		500	135 $m^2.g^{-1}$			1.53 weight %	
T-RGOA	Electromagnetic shielding	400	211 $m^2.g^{-1}$	13.9 $S.m^{-1}$	Electromagnetic reflection efficiency in the range of 8-10 GHz	39-22%	[135]
		600	208 $m^2.g^{-1}$	20.6 $S.m^{-1}$		38-29%	
		1000	211 $m^2.g^{-1}$	78.9 $S.m^{-1}$		60-54%	
T-RGOF	Membrane	160	5.8 Å	/	Water vapor transmission rate	1380	[136]
		200	4.9 Å			170	
T-RGOF	Extreme Temperature Sensor	1000 K	/	5.2 $S.m^{-1}$ 46.1 $W.m^{-1}.K^{-1}$	Temperature sensitivity at 300 K and dynamic range	/	[137]
		3000 K		1481 $S.m^{-1}$ 118.7 $W.m^{-1}.K^{-1}$		0.2305 $\mu\Omega.cm.K^{-1}$ 24.77 dB	
T-RGOF	Gas sensor	150	81.6 $m^2.g^{-1}$	669 $S.m^{-1}$	SO_2 sensing response at 27 °C	1.5%	[138]
		300	143.3 $m^2.g^{-1}$	1576 $S.m^{-1}$		2.1%	
		800	285 $m^2.g^{-1}$	9895 $S.m^{-1}$		3.2%	
T-RGOF	supercapacitor	250	306.9 $m^2.g^{-1}$	22730 $S.m^{-1}$	Specific capacitance was determined using a three-electrode system at a current density of 0.5 $A.g^{-1}$	101.9 $F.g^{-1}$	[89]
		350	492.4 $m^2.g^{-1}$	30300 $S.m^{-1}$		198.2 $F.g^{-1}$	
		450	554.3 $m^2.g^{-1}$	35710 $S.m^{-1}$		350.4 $F.g^{-1}$	

5.2 *Effect of the rate of heating*

The rate of heating is a significant variable that exerts a profound influence on the thermal decomposition of GOBMs, as well as on the physicochemical properties of the resulting T-RGOBMs, with a particular emphasis on porosity. When a low heating rate, typically below 10°C.min^{-1}, is employed during the heat treatment of GOBMs, it leads to a gradual release of gases resulting from the decomposition of AOGs. This gradual decomposition results in a lower amount of product gas, which does not surpass the quantity of gas that can escape from the sample. As a result, the interlayer pressure does not exceed the van der Waals forces that hold the GO sheets together, preventing the expansion of the resulting T-RGOBMs' structure [43]. Conversely, when rapid heating is applied, exceeding 10°C.min^{-1}, the rates of heat and product gas generation outpace the rates of heat and gas removal from the sample. At this juncture, the interlayer pressure between the GO sheets significantly exceeds the van der Waals forces that normally bind them together. This leads to an explosive reduction-exfoliation phenomenon, resulting in a fluffy and highly porous structure (as depicted in **Fig. 5a and Fig. 5b**) in the resultant T-RGOBMs [46,139–141]. The rate of heating can also have a significant impact on the extent of exfoliation in the resulting T-RGOS. Applying rapid heating during the heat treatment process can lead to a high degree of exfoliation. For example, Schniepp et al. successfully achieved single-layer T-RGOS by employing a rapid heating process at a rate of 2000°C.min^{-1} until reaching 1050°C, resulting in an impressive specific surface area (SSA) of 1500 $m^2.g^{-1}$ [44]. Furthermore, elevating the reduction temperature leads to a greater degree of exfoliation [43,129]. Conversely, when low heating rates are applied, increasing the temperature during reduction results in T-RGOS with a reduced degree of exfoliation. For instance, at a heating rate of 5°C.min^{-1}, raising the temperature from 127°C to 2400°C increases the number of layers forming T-RGOS from 1 to 6 layers [119].

Table 4 presents a curated selection of cases where the effective utilization of rapid heating has been explored for the production of porous T-RGOBMs, tailored to serve various advanced applications. Qiu et al. elucidated the influence of the increasing external rate of heating on the porosity of T-RGOBMs produced by explosive exfoliation. Results reveal that beyond a critical heating rate, further increments in the external heating rate fail to yield additional enhancements in surface area. Instead, all resulting T-RGOBMs consistently fall within the range of 350 to 400 m^2.g. This "heating-rate independence" phenomenon arises due to local self-heating within the sample. With a heating rate of 10°C/min or higher, the exothermic reaction accelerates to the point where it induces a noticeable divergence in the temperature of the GOBMs compared to its surroundings. Consequently, this leads to an increased rate of heating perceived by the sample. Once the disproportionation reaction is initiated, the fast self-heating dominates the total rate of heating, rendering the externally applied rate of heating less influential. Consequently, further elevations in the external heating rate do not alter the total rate of heating, the kinetics of the disproportionation reaction, or the porosity of the resulting T-RGOBMs [142]. Yang et al. conducted research to explore the connection between heat treatment conditions for GOBMs in order to achieve efficient reduction into T-RGOBMs. Their findings revealed that at higher heating rates, GOBMs required a shorter duration and lower temperature for effective reduction. These results underscore the importance of aligning the duration and temperature of heat treatment with the chosen heating rate [140]. Known et al. achieved the successful preparation of a flexible and highly porous T-RGOF through rapid heating while preserving its structural integrity. This was accomplished by sandwiching the GOF between two borosilicate glass substrates during the heat treatment process. However, when the structure of the GOF was subjected to fast heating without such confinement, it was found to be compromised and destroyed [139]. To produce T-RGOF with exceptional performance in supercapacitors, Ye et al. employed a combination of rapid heating under pressure and chemical graphitization, resulting in a porous T-RGOF doped with iodine groups. The rapid heating under pressure was carried out using a pedal sealing machine at a temperature of 200°C for 5 minutes, while chemical graphitization utilized HI/acetic acid as a chemical reducing system. During the rapid heating under pressure, there was a swift decomposition of AOGs, leading to the generation of a significant volume of gases. This sudden increase in intersheet pressure caused the separation of sheets and the formation of a porous and fluffy structure [143].

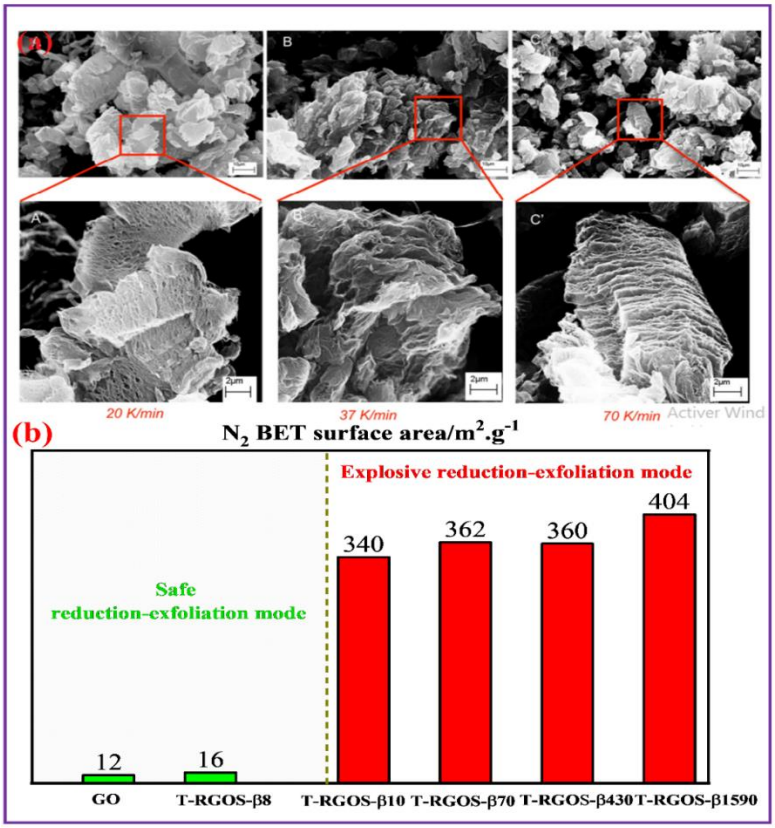

Figure 5. (a) SEM images of T-RGOS prepared by thermal exfoliation at different heating rates**; (b)** Effect of heating rate on the resulted porosity of T-RGOBMs [142]. The T-RGOBMs, identified as T-RGOS -β8, T-RGOS -β10, T-RGOS -β70, T-RGOS -β430, and T-RGOS -β1590, are subjected to heating processes at varying rates of 8, 10, 70, 430, and 1590°C.min^{-1}, respectively [142]

Table 4. Examples of monitoring the rate of heating to increase the porosity of T-RGOBMs

T-RGOBMs type	Heat treatment conditions	Heating rate (°C.min^{-1})	BET SSA (m^2.g^{-1})	References
T-RGOS	500-900 °C inert atmosphere	40 70 1590	362 360 404	[142]
T-RGOF	1050 °C Ambient air	100	350	[144]
T-RGOS	250 1000°C UHV	30	309 434	[128]
T-RGOF	200°C ambient air	40	180.02	[143]
T-RGOF	250°C ambient air	10	500 970	[139]
T-RGOS	200°C Ambient air	5 10 50	144 250 580	[140]
T-RGOS	350°C UHV	10	550	[73]

5.3 *Effect of the period of heat treatment*

The period of time allocated for heat treatment has a profound impact on the structure and physicochemical properties of GOBMs. Previous research has illustrated that extending the period of reduction results in a narrowing of interlayer distance and an increase in the C/O ratio. The drop in interlayer distance is attributable to the removal of water and AOGs, while the increase in the C/O ratio is due to exclusion of AOGs [145,146]. Chen et al. delved into the transformation of the C/O ratio and electrical conductivity in T-RGOF that underwent treatment at a relatively low temperature of 400°C. **Fig. 6a** showcases the results of their findings, which reveal that prolonged treatment leads to a remarkable rise in both the C/O ratio and electrical conductivity. This is owing to the elimination of AOGs, which results in a notable enhancement of the Sp2 domains and a marked decrease in sheet resistance [46].

Moreover, the annealing period can serve as a crucial parameter in optimizing the laminar channels in GOF, thereby resulting in improved performance of the membrane nanofiltration. For example, Li et al. studied the impact of mild annealing at 80 °C on water permeance and Na_2SO_4 selectivity. The data presented in **Fig. 6b** showcases the remarkable impact of thermal annealing on water permeance and salt rejection. The results reveal that after thermal annealing, the water permeance dropped from 7.4 to 4 L.m^{-2}.h^{-1}.bar^{-1} and the salt rejection of Na_2SO_4 rose from 57.7% to a substantial 90.9%. This is attributed to the narrowing of the laminar channels [114].

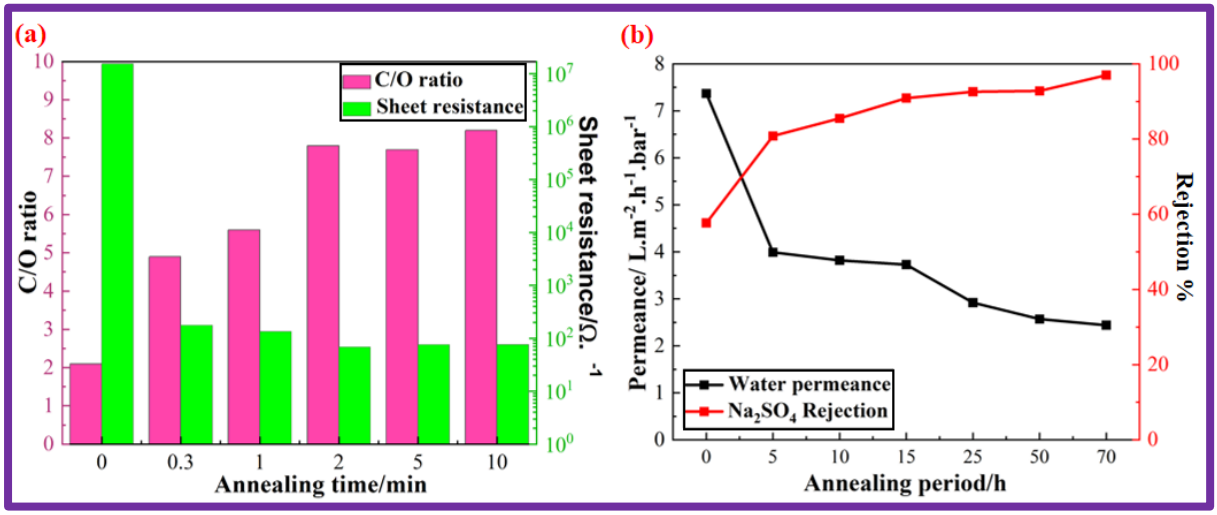

Figure 6. Impact of annealing time on (a) C/O ratio and sheet resistance of GOF and (b) water permeance and Na_2SO_4 rejection of GOF-based membrane [114]

The determination of the required time for thermal reduction under specific annealing conditions is of utmost importance for the large-scale manufacture of T-RGOBMs. Sengupta et al. studied the evolution of transformations in GO during thermal reduction at 350°C. The analysis revealed that the elimination of AOGs from GOBMs began with the gradual removal of carboxylic and hydroxyl groups. After seven minutes of heating, most of the hydroxyl, carboxylic, and carbonyl groups were eliminated from the lattice, leading to the exfoliation of the material due to the intense pressure placed on the layers of GO [28].

5.4 *Effect of annealing atmosphere*

The choice of annealing atmosphere during heat treatment can have a profound impact on the structure and performance of resulting T-RGOBMs. Hence, careful consideration of the desired properties is necessary to select the appropriate annealing atmosphere for a specific application. Several atmospheres were employed including, inert gases like Nitrogen (N_2) [139,147] and Argon [148], oxidizing atmospheres such as ambient air [19,149,150], reducing atmospheres such as Hydrogen (H_2) [151], mixed gases atmospheres like Argon-Hydrogen (Ar-H_2) [152–154], and Ultra-high-vacuum (UHV) [118]. UHV has been recognized as the optimal environment for thermally annealing GOBMs, generating almost oxygen-free T-RGOBMs without the introduction of impurities. Furthermore, the use of UHV may boost the pressure gradient force exerted on annealed GOBMs, hence promoting their exfoliation [92,155]. The thermal treatment of GOBMs in oxidizing atmospheres such as ambient air was seen as a viable method for enhancing some properties, such as pseudocapacity [156] and sensitivity [110], by introducing more AOGs through the reaction of the structure's carbon atoms with the oxygen of the air (**Fig. 7a**) [19].

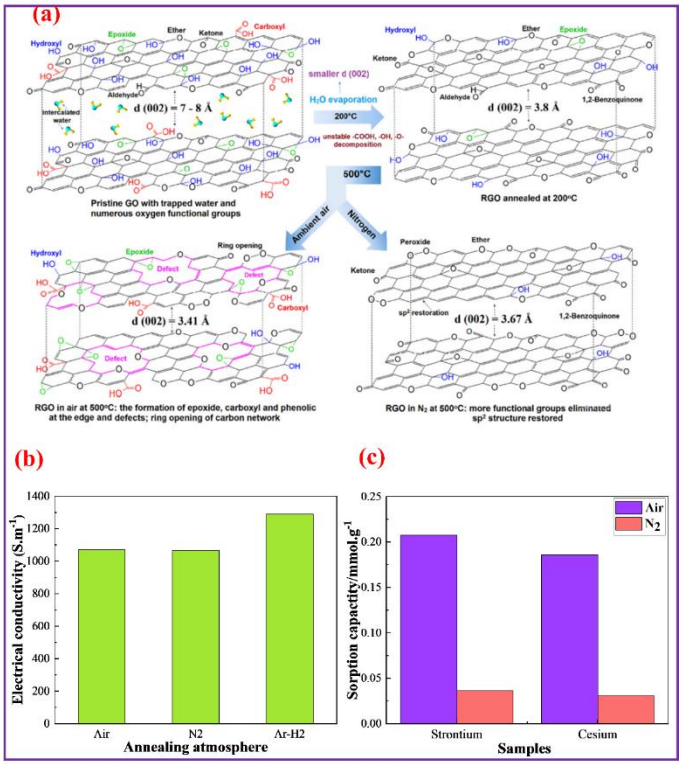

Figure 7. Schematic ilustration shows the influence of varying atmosphere (air and N_2) on the structure of T-RGOBMs during thermal annealing [110]; (b) Effect of annealing atmosphere on electrical conductivity [5]; (c) Effect of annealing atmosphere on the sorption capacity [110]

To alleviate the oxidation of carbon structure, an inert gas such as N_2 and Ar, and a reducing atmosphere such as H_2 may be utilized to produce free-impurities T-RGOBMs with a high degree of reduction. Wang et al. used a two-step thermal process to convert GOF to T-RGOF with record-breaking electrical conductivity (6400 $S.cm^{-1}$). The thermal reduction stage was conducted in an Ar environment at 1000 K, followed by joule heating at 3000 K [148]. The addition of a small portion of H_2 to Ar results in an increase in the reduction efficiency. In this context, Xu et al. proposed an effective strategy to prepare T-RGOBMs. After tweaking GO's oxidation parameters, the exfoliation-reduction process was conducted in an Ar-H_2 environment. It is found that the majority of AOGs were successfully eliminated [157].

Yang et al. investigated the thermal reduction of GOBMs under three distinct environments, Ar, Ar-H_2, and UHV at temperatures of 500 °C. The results showed that using UHV is more effective to reduce GOBMs, resulting in high-quality T-RGOBMs with a C/O ratio of 8.9 compared to Ar gas (6.8) and Ar-H_2 gas (7.2) [118]. The effect of heat treatment in various environments on electrical conductivity was extensively investigated [5,158]. Wang et al. investigated the effect of thermal treatment at various atmospheres (Air, Ar-H_2, and N_2) on the electrical conductivity of T-RGOBMs (**Fig. 7b**). They found that using Ar-H_2 atmosphere results in greater conductivity than the use of N_2 and ambient air due to the recovery of more Sp2 domains [5].

The annealing environment has been found to have a profound influence on T-RGOBMs' performance, according to various studies. As stated in **Table 5**, several studies have investigated the influence of the annealing environment on the properties and performance of the resulting T-RGOBMs. Le et al. studied the influence of air and nitrogen annealing atmospheres on the heavy metals sorption performance of T-RGOS (**Fig. 7c**). They discovered that T-RGOS treated with ambient air had a greater sorption capacity than T-RGOS treated with N_2. T-RGOS reacts with oxygen in ambient air, resulting in a higher concentration of AOGs and flaws that could serve as adsorption sites [110]. The environment of annealing also affects the capacitance performance of the resulting T-RGOBMs. Due to the carbon structure's reactivity with oxygen, AOGs are introduced to T-RGOBMs during the treatment of GOBMs in ambient air, increasing the pseudocapacitive contribution [89]. However, vacuum treatment of GOBMs eliminates AOGs, lowering the pseudocapacitive performance of the resulting T-RGOBMs [128]. Shiravizadeh et al, in contrast, studied the effect of the atmosphere on the photocatalytic performance of GOMB during thermal treatment. Annealing in hydrogen improved the photocatalytic efficiency of the T-RGOBMs, but annealing in air diminished it [159].

Table 5. Impact of the annealing temperature on the properties and performance of the resulting T-RGOBMs

T-RGOBMs	Application	Annealing atmosphere	SSA/ inter-layer spacing	Electrical conductivity/ sheet resistance	performance		References
T-RGOF	Heavy metal adsorption	Air	/	/	Strontium sorption capacity in mmol per gram of T-RGOF prepared at 500°C	0.21 $mmol.g^{-1}$	[110]
		N_2				0.04 $mmol.g^{-1}$	
T-RGOS	Electrode for lithium-ion battery	Air	/	1068 $S.m^{-1}$	Capacity of vanadium oxide- T-RGOBMs //lithium battery measured at 6 $A.g^{-1}$	144 $mA.h.g^{-1}$	[5]
		N_2		1065 $S.m^{-1}$		/	
		Ar-H_2		1289 $S.m^{-1}$		/	
T-RGOS	Supercapacitor	Air		/	Maximum specific capacitance in farads per gram of T-RGOF.	124 $F.g^{-1}$	[160]
		N_2				148 $F.g^{-1}$	
T-RGOF	/	UHV (177°C)	/	194	/	/	[158]
		Air (300°C)		245			
		N_2 (600°C)		1130			
T-RGOF	Counter electrode for dye-Sensitized Solar Cells	Ar	/	/	Power conversion efficiency	2.23%	[161]
		N_2				3.34%	
		Air				5.89%	
T-RGOF	flexible electrodes	Ar	/	8100 $S.m^{-1}$	/	/	[151]
		H_2		5000 $S.m^{-1}$			
T-RGOF	flexible electrodes	CH_2	/	3.07 $k\Omega.m^{-1}$	/	/	[162]
		Ar		1120 $k\Omega.m^{-1}$			
		H_2		2540 $k\Omega.m^{-1}$			

5.4.1 *Doping T-RGOBMs by thermal annealing in presence of heteroatoms sources*

Heat treatment is a common route for heteroatom doping of T-RGOBMs. The process typically involves heating GOBMs in the presence of nitrogen, iodine, sulfur, boron, or phosphorus sources, creating the highly sought-after heteroatom-doped T-RGOBMs (DT-RGOBMs) (**Fig.8a**). The incorporation of these heteroatoms into the resulting T-RGOBMs structure leads to remarkable changes in its physicochemical properties [163], elevating its performance to new heights, including increased sensing abilities, catalytic activity, and photoresponse [164–166]. Regarding the literature, several studies have employed heat treatment as a means of doping T-RGOBMs. This is achieved by combining GOBMs with precursors that contain heteroatoms or

subjecting them to specific environmental conditions [167,168]. For instance, Nitrogen DT-RGOBM (N-DT-RGOBM) may simply be synthesized by annealing GOBM under ammonia gas [169] or by using precursors for Nitrogen atoms such as urea [170], melamine [171], and Hexamethylenetetramine [172]. Furthermore, the sulfur DT-RGOBM (S- DT-RGOBM) may be achieved by the use of precursors like thiophene/bithiophene [173], or thermal annealing under H_2S, SO_2, CS_2 atmosphere [48,168].

Doping T-RGOBM with Boron (B-DT-RGOBM) may also alter its electronic structure, leading to various astonishing features and potential applications [174]. It may merely be achieved by several routes like the thermal treatment of GOBMs under the BF_3 environment [175] or by combining GOBMs with precursors such as B_2O_3 during the thermal treatment [167]. Furthermore, the phosphorus atom is regarded as an effective dopant for T-RGOBMs in order to enhance their quality. Phosphorus-doped T-RGOBM may simply be prepared by thermally heating a combination of GOBMs and precursors like 1-butyl-3-methylimidazolium hexafluorophosphate [176] and ammonium phosphate monobasic [177]. Halogenation of T-RGOBMs may also be achieved by the thermal treatment of GOBM under a halogen atmosphere [178]. The most common halogenation of T-RGOBMs involves iodine groups as a result of their increased electrical conductivity and catalytic activity [179]. It can be prepared by combining GOBMs with a source of iodine like KI [180] and iodine solution [181] or by reducing GOBMs directly in an iodine environment [182].

Dual-heteroatom-doping of T-RGOBMs may lead to unique physical and chemical features as well as potential applications [183]. Thermal annealing was currently used to dope T-RGOBMs with two different heteroatoms such as sulfur-nitrogen [184], boron-nitrogen [185], iodine-nitrogen [186], and so on.

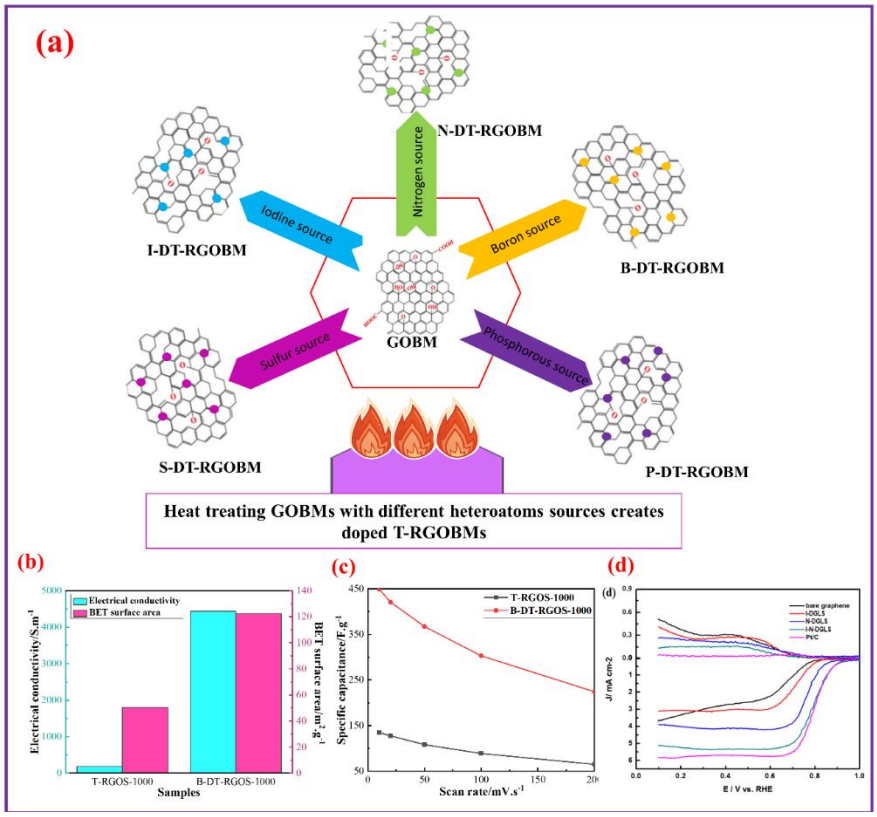

Figure 8. (a) Thermal treatment routes to prepare different heteroatom-doped T-RGOBMs; (b) Effect of boron doping on the electrical conductivity and BET surface area of T-RGOS [167]; (c) effect of boron doping on the supercapacitive performance of T-RGOS [167]; (d) effect of iodine-nitrogen co-doping on the catalytic performance for oxygen reduction reaction: onsets potential determined from cyclic-voltammetry tests [186]

The incorporation of heteroatoms into T-RGOBMs may greatly enhance their physicochemical features. Yeom et al. incorporated boron heteroatoms into the structure of T-RGOS as an example. Electrical conductivity rose from 181 for T-RGOS without boron doping to 4434 $S.m^{-1}$ after boron doping, while BET surface area increased from 50 to 122 $m^2.g^{-1}$ after boron doping, according to investigations (**Fig. 8b**). As a result, the supercapacitive performance of T-RGOS was enhanced by tripling the specific capacitance from 135 to 448 $F.g^{-1}$ (**Fig. 8c**). Furthermore, dual-heteroatom-doping was reported to be more effective than single-heteroatom-doping. According to zhan et al., Nitrogen-Iodide-DT-RGOS exhibits higher catalytic performance for reduction

oxygen reaction than Iodide-DT-RGOS, N-DT-RGOS, and Graphene (**Fig. 8d**). This discovery may be attributed to the high density of defects induced by doping and the synergistic action of I/N and T-RGOS [186].

5.5 *Annealing in a confined space under the effect of pressure*

Heating GOF in an unrestricted environment results in a fragmented T-RGOF with numerous breaks. However, when pressure is applied to GOF in a confined space during heat treatment, it results in the formation of T-RGOF with an ordered and compact structure (as seen in **Fig. 9**), which can result in improved electrical and mechanical properties. Many investigations, as shown in **Table 6**, have examined the effect of annealing in a confined space and under pressure on the physicochemical properties of the resulting T-RGOBMs. Exerting pressure can also help to minimize defects and wrinkles in the resulting T-RGOBMs, leading to a higher-quality material with fewer impurities. Importantly, applying high pressure upon heat treatment of GOBMs significantly reduces the temperature required for the graphitization of T-RGOBMs and accelerates the transformation of non-crystalline structures into their crystalline counterparts [187]. Research shows that the structure of T-RGOBMs reduced at 260°C under 4 MPa is almost identical to that of T-RGOF reduced at 1000°C at ambient pressure [188].

Chen et al. may alleviate T-RGOF's expansion after heat treatment by sandwiching GOF between two stacked wafers. After thermal reduction, the morphology of the film was found to be retained. The pressure exerted by wafers on GOF prevents layer expansion and fractional displacement caused by the release of gases generated from GOF's decomposition. The resulting T-RGOF displays remarkable electrical conductivity, boasting a conductivity value of 272 $S.cm^{-1}$ [189]. GOFs have a tendency to undergo explosive exfoliation when subjected to high heating rates, leading to a total loss of structural integrity. To mitigate this issue, it has been demonstrated that inserting GOFs between inert plates during heat treatment at 250°C can preserve the initial form of the film. This results in the production of T-RGOFs that boast both high electrical conductivity and microporosity [139].

To control the thickness of T-RGOF and preserve its integrity, Chen et al. employed two parallel quartz Plates with a Precisely Aligned Gap to Confine the Expanding GOF to a Consistent and Specified Thickness [190]. Combining high temperature and pressing, according to another research, preserves a tightly packed GOF structure and improves the graphitization of T-RGOF by promoting the removal of AOGs. The resulting T-RGOF exhibits remarkable electrical and thermal conductivities [187].

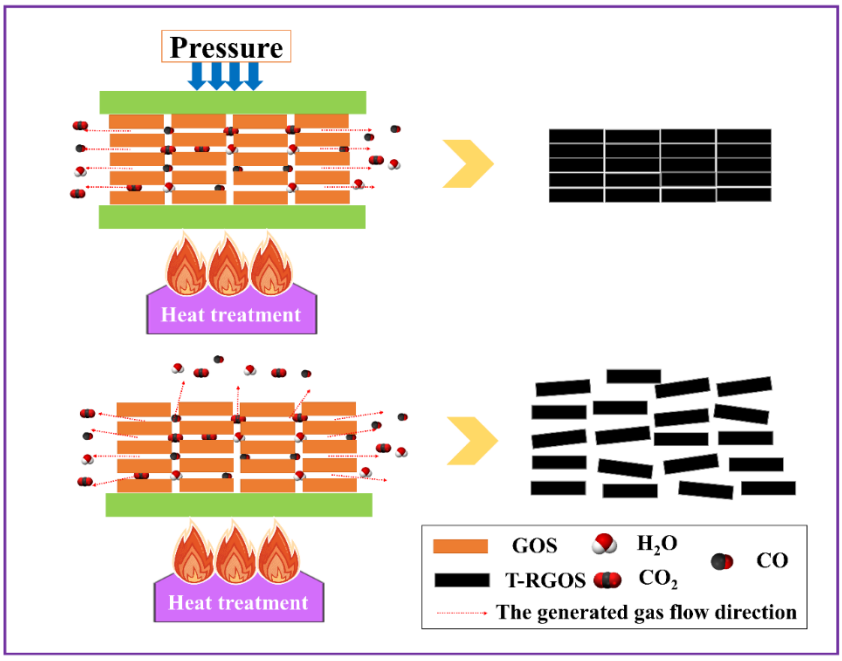

Figure 9. Schematic illustration showing the difference between the heat treatment of GOF in open and confined spaces

Table 6. Annealing in a confined space and under pressure and its impact on the electrical conductivity/ resistivity of resulting T-RGOBMs

T-RGOBMs type	Strategy	Heat treatment conditions	Electrical conductivity/ resistivity	References

T-RGOF	Sandwiching between two carbon plates	1050 °C	6900 $S.m^{-1}$	[144]
T-RGOF	Sandwiching between borosilicate glass and stainless-steel plates	250 °C	757 $S.m^{-1}$	[139]
T-RGOS	hydrogen atmosphere under high pressure	500 °C 100 bar	1.14 $\Omega.m^{-1}$	[191]
T-RGOF	UHV under hot press furnace	2000 °C 294 bar	310000 $S.m^{-1}$	[187]
T-RGOF	Argon Sandwiching between two Si stacked wafers	800 °C	27200 $S.m^{-1}$	[189]
T-RGOF	Ambient air confined between two parallel quartz slides	1000 °C	1190 $S.m^{-1}$	[190]

6. Optical properties optimization of GOBMs through heat treatment

Heat treatment is not only used to adjust the physicochemical properties of T-RGOBMs but also to fine-tune their optical properties, which are crucial for applications in optoelectronics and photonics. According to Schmiedova et al., the heat treatment route is likely the best method for reducing GOBMs to enhance their optical properties. They found that the refractive index of T-RGOBMs produced through heat treatment is 1.993, which is higher than those produced chemically (1.839) and with UV treatment (1.873). The lower refractive index in chemically and UV-reduced RGOBMs is attributed to the higher defect content resulting from these reduction methods [192]. Politano et al, reported on the heat treatment of GOF, showing that GOF prepared by dip-coating and thermally annealed at 450°C for 20 minutes in an Ar atmosphere exhibited improved optical conductivity and absorption coefficient. After the heat treatment, the quantity of AOGs decreased, and a transition from sp3 to sp2 hybridization occurred. This change resulted in a variation in the coverage of functional groups, thereby altering the electronic density of states of the T-RGOF[193]. Cao et al. established a correlation between defect density in T-RGOBMs and optical constants, specifically the refractive index and extinction coefficient. Their findings indicate that fewer defects in T-RGOBMs lead to higher density and, consequently, increased optical absorption[194]. Jung et al. examined the impact of heat treatment and the extent of exfoliation on the optical properties of T-RGOBMs. They demonstrated that thermally treating the material in a vacuum enhances its optical properties. Furthermore, multiple layers of GO showed more significant changes in optical properties compared to single layers. Thermal reduction removes interlamellar water layers, resulting in an increased refractive index, and reduces the AOGs content of GO layers, significantly increasing the extinction coefficient [195].

The refractive index is a crucial parameter that can effectively monitor the size and thickness of GOBMs during heat treatment. Guo et al. propose an efficient and accurate method to determine the layer number of GO by leveraging its thermally enhanced optical contrast through vacuum heating. The observed changes in thickness and chemical structure are attributed to the removal of intercalated water and oxygen-containing groups during thermal treatment. This process results in an increase in both the refractive index and absorption coefficient, approaching the values of intrinsic graphene [196].

7. Thermal annealing-induced transformations and mechanisms in GOBMs

7.1 *Unveiling structural transformations in GOBMs through heat treatment*

To address a number of crucial concerns regarding GOBMs' thermal decomposition and the controllability of the production of T-RGOBMs, it is essential to identify transformations that occur in GOMBs during thermal annealing [197]. The thermal annealing of GOBMs leads to structural and morphological changes, which result in altered properties of the resulting T-RGOBMs. Previous studies have been conducted to identify transformations during GOBMs thermal decomposition [45,198]. Huh investigated in detail transformations that occur in GOBMs in the temperature range between ambient and 2000 °C. As shown in **Fig.10a**, six significant transformations were identified during the thermal annealing of GOBMs. The first transformation occurs between room temperature and 130°C, where absorbed water partially vaporizes, causing shrinkage of the GOBMs lattice. In the second stage (140-180°C), there is a significant loss of water, leading to partial exfoliation of T-RGOBMs. The third stage (180-600°C) is associated with the removal of carboxyl groups, resulting in further contraction of the T-RGOMBs lattice. Lattice expansion of T-RGOBMs occurs in the temperature range of 600-800°C, caused by outgassing from the decomposition of remaining carboxyl and hydroxyl groups. The elimination of remaining

hydroxyl and epoxide groups leads to a high number of defects within the temperature range of 800-1000°C. The last transformation, occurring between 1000-2000°C, involves the bottom-up formation of T-RGOBMs crystal layers and a decrease in the number of defects. [45]. Ganguly et al. examined GOMBs' deoxygenation process during vacuum heat at a range of temperatures between ambient and 1000 °C. Interestingly, it has been discovered that carboxyl groups on the edge plane are indeed very unstable, while carbonyl groups seem to be harder to eliminate. Furthermore, phenol groups were generated through the moderate interaction of basal plane epoxide with neighboring hydroxyl groups at 400 °C. At temperatures as high as 1000°C, phenolic groups prevail over carbonyl groups and survive [198]. Pelaez-Fernandez et al. analyzed AOGs decomposition upon heating of GOMBs in temperatures from 70 to 1200°C using in situ techniques [199]. It has been revealed that physically and chemically absorbed water evaporated at temperatures below 100°C and between 130 and 180°C, respectively. In addition, epoxide groups may be removed at temperatures below 300°C, but carbonyl and ether groups are removed at temperatures over 300°C in the temperature ranges 500-700°C and 700-900°C, respectively. Furthermore, the elimination of hydroxyl groups appears obviously more difficult at temperatures over 1000°C. Akbi et al. identified transformations that occurred during the thermal annealing of GOF under a nitrogen atmosphere by deconvolution of derivative thermogravimetry. Accordingly, six transformations take place in GOF during its heat treatment, including evaporation of physisorbed and chemisorbed water, rearrangement and elimination of AOGs, disproportionation reaction, elimination of sulfur groups, and degradation of the carbon framework (**Fig. 10b**) [29].

Shen et al. disclosed transformations that take place at low-temperature thermal annealing of Hummers' GO. The findings imply the existence of four major stages: In the first phase, which occurs below 100°C, physisorbed water is released. The second step (160 to 210 °C) removal of unstable AOGs. Elimination in the third stage (210-300 °C) of sulfur groups and stable AOGs. Fourth stage degradation (210-300 °C) of the carbon network and the very stable AOGs [200].

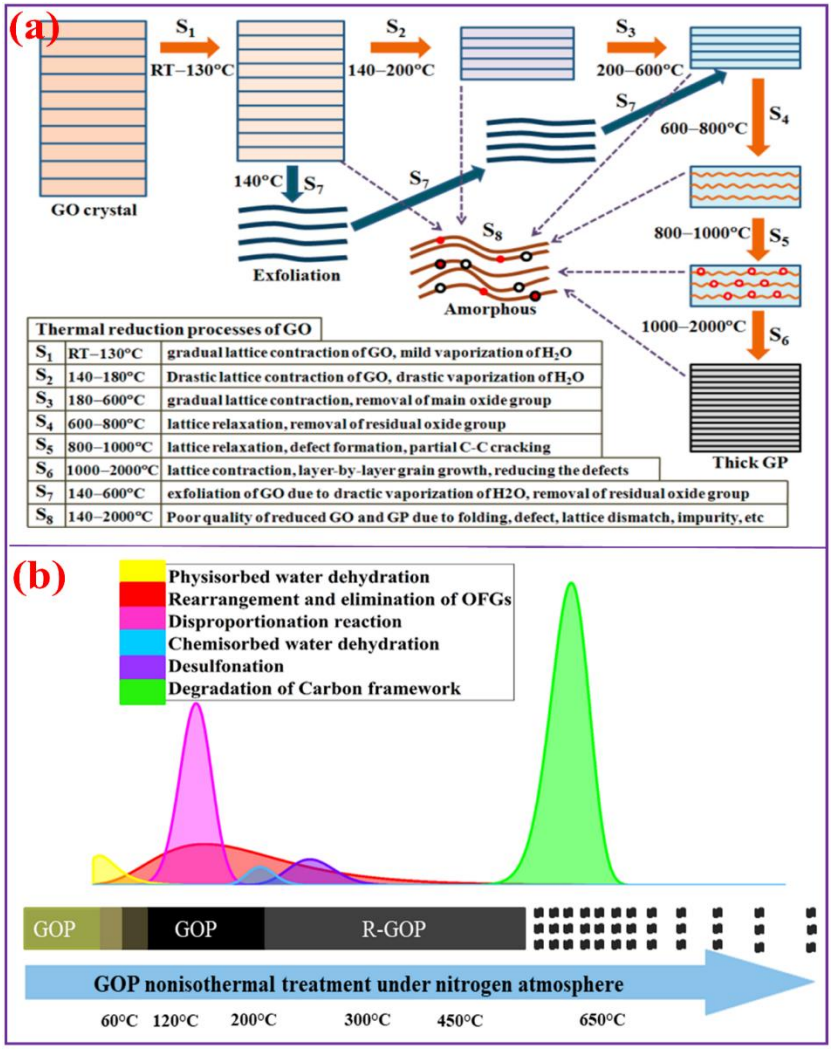

Figure 10. (a) An illustration showcasing the thermal reduction process of GO, ranging from room temperature to 2000°C [45]. (b) Illustrating the Transformations of GOF during Heat Treatment (removal of water molecules, decomposition and rearrangement of different AOGs, degradation of the carbon skeleton) [29]

Gao et al. used the computational method to investigate the thermal reduction of GOMBs under UHV. As a result, thermal treatment at high temperatures promotes the removal of hydroxyl and carboxyl groups. Additionally, thermal reductions of hydroxyls connected to the inside of an aromatic structure are less difficult than those of hydroxyls linked to the aromatic structure's edges [120]. Acik et al. monitored the CO_2 and CO generated during the thermal annealing of GOMBs. At temperatures below 200 °C, CO_2 is reported to be a byproduct of the decomposition of esters, lactones, anhydrides, carboxyls, and lactols groups linked to the basal planes or the edges, whereas at temperatures between 250 and 750 °C, CO is associated with the decomposition of phenols, ethers, quinones, and carbonyls [201].

Le et al. investigated the transformations resulting from thermal annealing of GOF under nitrogen and air atmosphere. Thermal annealing at low temperatures (<200°C) under both atmospheres leads to the removal of unstable AOGs; moreover, both atmospheres result in almost the same structure, indicating the negligible influence of the surrounding environment at low temperatures. At high temperatures (200<T< 500 °C), under an air atmosphere, carbon atoms start to react with oxygen, generating AOGs and defects; however, under a nitrogen atmosphere, AOGs continue to be removed, leading to an increase in a C/O ratio. Furthermore, under an air environment, GOF completely decomposes at 700 °C, however, it retains 20% of its initial mass under a nitrogen atmosphere [110].

Overall, both the quality of GOBMs and the annealing conditions greatly impact the transformations that occur in GOBMs during heat treatment. The quality of GOBMs influences the content of the starting material, while annealing conditions determine the extent and rate of transformations during thermal annealing.

7.2 *Mechanisms behind the thermal reduction of GOBMs*

Understanding the mechanisms of reactions that occur in GOBMs during heat treatment is crucial for identifying alternate approaches that might decrease the density of carbon evolution-induced defects [202]. Bagri et al. elucidated mechanisms of chemical transformations that occur in GOBMs upon heat treatment. By the use of theoretical simulations, it has been proved that during heat treatment of GOBMs, a highly thermally stable ether and carbonyl group was formed via the alteration of the original hydroxyl and epoxy groups, and that prevents its total transformation to pristine graphene. Furthermore, the aforementioned groups cannot be eliminated without harming the carbon network to which they are attached [70]. Larciprete et al. proposed a dual-path mechanism for the reduction of GOBMs into T-RGOBMs driven by AOGs density. For GOBMs with low AOGs coverage, The thermal reduction proceeds by releasing just O_2 from epoxide group pairs through cycloaddition, with the carbon network remaining intact. However, for GOBMs with high AOGs coverage, the formation of ether epoxy pairs promotes the removal of CO/CO_2 mixtures, hence consuming the carbon network[202]. Foller et al. demonstrated that it is possible to enlarge graphitic domains in GOBMs at low temperatures without eliminating AOGs. The heat treatment of GOBMs at T=80 °C has been reported to result in an increase of Sp2 carbon and hydroxyl groups and a decrease in epoxy groups, which may be attributed to binary reactions between adjacent AOGs and/or C–H [113]. Acik et al. displayed the effect of GOMB-intercalated water in a separate study by observing the alterations that occur in the single and multilayer GOMB during thermal annealing. The results indicate that intercalated water in multi-layered GOMB plays an important role, creating defects in the structure and leading to the formation of ketone and ester carbonyl groups [203]. Based on molecular dynamic simulations, Yang et al. investigated the degradation processes of GOBMs from two perspectives: (1) Transformations in the structure that occurred in the carbon network and (2) the removal of the AOGs. It has been established that at low temperatures, the elimination of AOGs is dominant with the introduction of a few defects into the carbon network. At high temperatures, the decomposition of the carbon network becomes dominant. The orbital flipping from the Sp3 character to Sp2 one results in significant disorder, and amorphous transformation. Leftover oxygen mostly resides as hydroxyl groups, along with a tiny quantity of epoxide groups and bridged oxygen, while residual hydrogen predominantly exists as hydroxyl groups. The quantitative analysis reveals that the decomposition mechanism of GOBMs is reliant on AOGs amount and OH/O ratio [204].

7.3 *Kinetics of thermal reduction of GOBMs*

As a means of illuminating the associated mechanisms, the kinetic investigation of reactions that occur in GOBMs during thermal annealing may be used as a potential approach [19,205]. Yin et al. proved that the disproportionation reaction is kinetically directed. The reduction reaction of GOBMs should be spontaneous

according to the laws of thermodynamics, which means that it can occur at relatively low temperatures, owing to the exponential connection between reaction rate and temperature. Furthermore, benefiting from the high energy release of the disproportionation reaction, and using nonisothermal analytical data derived from DSC and the Kissinger model, the activation energy of the disproportionation reaction is assessed to be 167 $kJ.mol^{-1}$ [206]. Barroso-Bujans et al. gave insight into the mechanism of thermal reduction of GOBMs synthesized by Brodie. It has been established that the disproportionation reaction involves two distinct pathways; the 2D-diffusion mechanism ($f(\alpha)=-1/\ln(1-\alpha)$, 135.85 $KJ.mol^{-1}$) which occurs mostly between interlayers, and the autocatalytic process ($f(\alpha)=\alpha^4(1-\alpha)n^{3/2}$, 159.18 $KJ.mol^{-1}$) which happens at the surface, suggesting that the deoxygenation begins in the interlayer and that the diffusion of the generated gas is responsible for the exfoliation of tightly packed layers. When GOBMs lose around 10 wt%, the autocatalytic process becomes significant and reactions begin to occur mostly on the outer surface of GOBMs layers. The newly produced surfaces then catalyze the release of more CO_2 and H_2O [207]. McAllister et al. detailed on the other hand the mechanism of thermal exfoliation of GO synthesized by the Staudenmaier route. They found that the exfoliation of GO occurs when the interlayer pressure is superior to the van der Waals forces keeping the GO sheets stacked together and the rate of decomposition of AOGs surpasses the rate of diffusion of the generated gases. It has been established that the thermal exfoliation mechanism follows the second-order ($f(\alpha)= (1-\alpha)^2$) with respect to oxygen concentration [43]. Accordingly, the synthesis technique and C/O ratio of GO are definitely crucial factors in defining its disproportionation reaction mechanism. According to Świniarski et al., the thermal annealing of thin GOF may be considered as a single kinetic process with an activation energy of 90.7 $KJ.mol^{-1}$ [208]. In the other side, by using a model-free approach [209], akbi et al. studied the disproportionation reaction during nonisothermal annealing under ambient air. Results show a lower activation energy of 88.8 $KJ.mol^{-1}$ than that observed under inert gas [206]. This can be explained by the fact that air includes around 21% oxygen. Oxygen may alter the rate of decomposition of GOF, resulting in a quicker decomposition, but an inert environment does not react with GOF. Shen et al. found that the activation energy of the decomposition process increases throughout the deterioration process. This is due to the fact that the most vulnerable groups deteriorate first during heat treatment [200]. Utilizing temperature-dependent resistivity tests, the kinetics of thermal reduction of a single layer GOS were investigated under high vacuum. The estimated activation energy was 154.66 $KJ.mol^{-1}$; additionally, the mechanism follows the second-order ($f(\alpha)= (1-\alpha)^2$). Furthermore, a temperature-programmed desorption test has been performed to monitor the kinetics of thermal reduction of multi-layered GOF under UHV. The principal desorption products of the decomposition of GOF at temperatures up to 300 °C were discovered to be H_2O, CO_2, and CO, and minor quantities of O_2 [210]. The thermal reduction of GOBMs was also investigated by Aukstakojyte et al. It has been revealed that the activation energy of GOBMs was assessed by Ozawa and Kissinger and found to be 142 $KJ.g^{-1}$. Additionally, the mathematical kinetic model was determined by Borchardt-Daniels's approach. Accordingly, the mechanism is ($f(\alpha)= (1-\alpha)^{0.7}$), suggesting that the thermal degradation of GOBMs involves successive zero and first-order reactions [211].

8. Mitigating Risks and Ensuring Safety in the Heat Treatment of GOBMs

GOBMs have long been recognized as exceptionally sensitive materials when exposed to moderate heat, and their thermal decomposition can occur explosively at temperatures near those commonly encountered during routine drying processes. Whether in a laboratory or a factory setting, the rapid reduction of GOBMs carries the alarming risk of triggering catastrophic explosions or fire hazards. Additionally, when dealing with large-scale quantities of GOBMs, a range of dangers emerges, encompassing heat generation, the potential for fires, the release of gases, overpressure issues, and the risk of pressure or shock waves. This risk is especially pronounced when GOBMs experience explosive reduction within confined spaces or open environments. The situation becomes particularly critical in cases where unforeseen events, such as self-heating and spontaneous ignition, result in unexpected thermal runaway reactions during storage and handling [86]. Consequently, for safety concerns, it is essential to find and control critical conditions promoting the safe mode of GOBMs decomposition during thermal annealing [85,212,213]. Qiu et al. gave a comprehensive thermochemical and kinetic analysis of GO exothermic disproportionation reaction in an effort to find the circumstances and material compositions that prevent explosive occurrences throughout large-scale storage and handling. As a result, epoxide groups were found to be principally responsible for the energetic character of GOBMs; additionally, it has been shown that residual potassium catalyzes the disproportionation reaction, lessening the temperature by about 50°C and lowering the energy release [214].

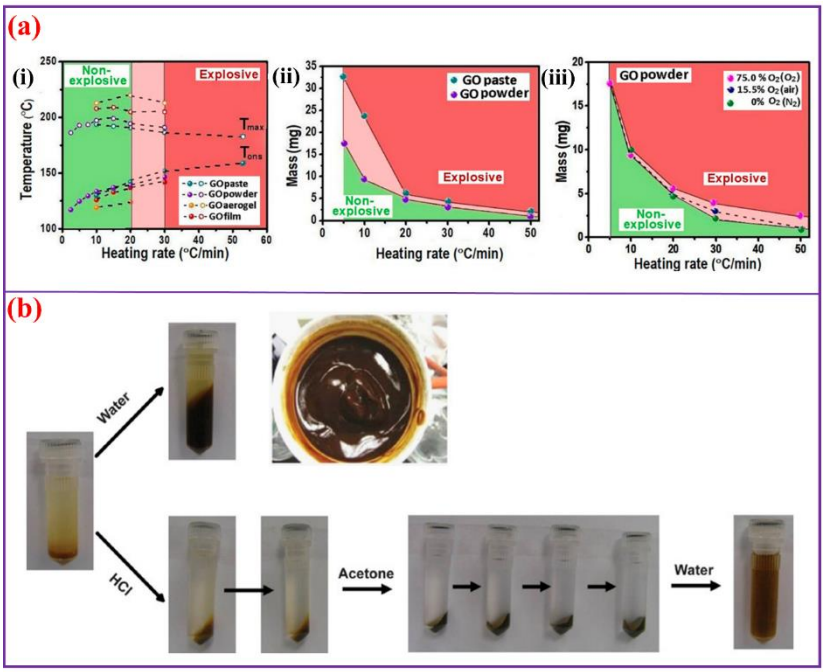

Figure 11. (a) Effect of some parameters on the mode of thermal reduction of GOBMs, (i) heating rate, (ii) geometrical form, and (iii) atmosphere oxygen content. Red (explosif mode) and green (safe mode) [51]. (b) A diagram depicting an improved purification process involving two steps with acid and acetone. The vial on the far left contains as-prepared GO, which significantly expands and forms a gel when washed with water, making filtration or centrifugation challenging. This issue, however, is resolved when rinsing with HCl (pH = 0). Subsequently, acetone is employed to eliminate the remaining acid. Again, when water is used for purification, gelation occurs as the pH increases. Eventually, the dispersion of GO in water can be achieved by means of solvent-exchange subsequent to the final acetone wash, or by directly dispersing the dehydrated GO solid product. [86]

Furthermore, the explosive mode of the thermal reduction results from the gas and energy releases of GOBMs disproportionation reaction in conjunction with the dimension/mass of GOBMs sample, which determines the heat and mass transfer of the inbuilt temperature and pressure. It has also been established that the explosive mode of thermal reduction is neither induced nor facilitated by the intercalated water molecules [85]. Lakhe et al. investigated the explosive reduction mode of GOBMs by tracking the temperature and pressure during thermal annealing. Results show that the explosive mode of GOBMs reduction is highly dependent on the sample size. Indeed, increasing size causes uncertainty owing to hotspots, material heterogeneity, and decreasing surface-to-volume ratio. The temperature and the pressure output for 0.5 grams of GOBMs are on the scale of thousands of degrees Celsius per minute and thousands of pascals per minute, correspondingly. In addition, the investigation of the thermal stability of GOBMs from various sources revealed that the SSA of GOBMs has a substantial impact on the reduction mode of GOBMs. If SSA is small, the reaction rate will overwhelm the heat dissipation rate, leading to an explosive mode of reduction [212]. Aiming to shed light on the flammability and thermo-explosivity settings of GOBMs, the effect of the GOBMs form, heating rate, temperature, mass of the sample, and the atmosphere on the explosivity and the flammability of GOBMs during heat treatment was explored by Losic et al. (**Fig. 10a**). Accordingly, GOBMs in form of powder and paste have lower temperature barriers for initiating micro-explosions than GOBMs in form of aerogels and GOF, independently of the annealing atmosphere (**Fig. 10a i** and **ii**). Also, it has been revealed that GOF is combustible and the flame may rapidly spread across the whole GOF in a low oxygen content (about 11%), indicating a substantial fire danger (**Fig. 10a iii**) [51,86].

For safety considerations and to reduce the risk of GOBMs explosion during heat treatment, several solutions have been suggested in the literature.

Efficient techniques for the purification of GO:

As mentionned above GOBMs became highly flammable if the purification of GO is not done properly and still contaminated with impurities such as K^+ and SO_4^{2-}, which induce their explosion mode of reduction. It has been discovered that the flammability of GO increases as its impurity content rises. For example, one weight percent of KOH was enough to cause the combustion of GOBMs. For safe handling, inorganic impurities in GOBMs should be reduced (<0.1%) so that they are very stable against combustion; thus, an effective strategy to purify GO is in great demand. Normal GO purification is impeded by its propensity to gel when the pH level rises after rinse. It has been discovered that the acid/acetone washing technique (**Fig.10b**) is excellent for inhibiting gelation and hence improving purification [86,215]. Moreover, Mrózek et al. demonstrated that the repeated cycles

of aggregation and dispersion of GO in a NaCl solution represent a cost-effective and efficient technique for purifying GO. it does not alter the nature of AOGs or the morphology of the GO sheets. When scalability is a concern, the membrane-based purification of GO is considered to be the most effective method. Combining brief dead-end filtration dialysis, prefiltration of acidified GO dispersions, and cross-flow filtration reduces process time and water consumption. In addition, this method permits simple final-stage concentration of the aqueous GO dispersion [216]. Another method reported, hollow fiber diafiltration, removes nearly all ionic contaminants from GO [217].

Reducing the energy released during the reduction of GOBMs

Reducing the enthalpy of decomposition is also considered a potential strategy for directing the thermal reduction into a safe mode. Introducing certain compounds may inhibit the highly energetic decomposition of GOBMs. Aukstakojyte et al. investigated the influence of carbon suboxide on the thermal decomposition of GOBMs. Apparently, the introduction of carbon suboxide reduces the energy released from the decomposition of GOBMS. It has been found that was reduced from 1487 to 1184 $KJ.g^{-1}$; additionally, the activation energy was decreased by about $27KJ.g^{-1}$ [211]. In a separate study, Barkauskas et al. studied the influence of nitrogen-based dyes on the thermal decomposition of GOBMs. Adding 20% of Auramine O results in a reduction of the released energy from 1510 to 1064 $KJ.g^{-1}$ [218].

9. Recent Advances in the Strategies of Heat Treatment for the Development of T-RGOBMs for Advanced Applications

The heat treatment route provides a high degree of versatility in producing T-RGOBMs with tailored physicochemical properties, specifically designed for particular applications (**Fig. 17**). This section focuses on the latest developments and fine-tuning strategies involving heat treatment to tailor the properties of GOBMs for a range of exciting applications, including supercapacitors, gas sensing, and electromagnetic interference shielding.

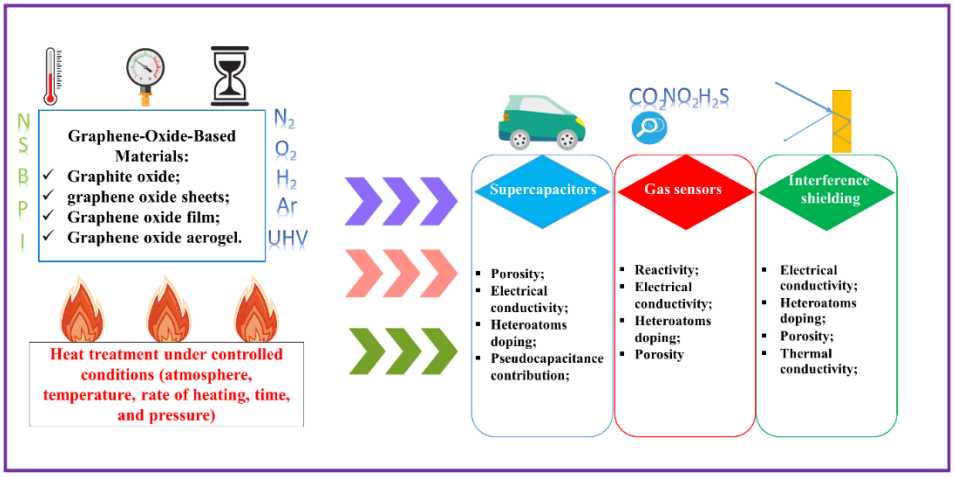

Figure 12. Heat Treatment for Tailoring GOBMs Properties for Potential Applications (Supercapacitors, Gas Sensors, and Electromagnetic Shielding): Schematic Representation

9.1 *Strategies for developing T-RGOBMs for supercapacitors*

At present, there is a substantial demand for energy storage technologies, particularly flexible supercapacitors, which exhibit high-rate capability and an extended cycle life. This makes them a promising candidate for various emerging technologies, including foldable mobile phones, wearable devices, and electric vehicles. However, the key hindrance to their wider adoption remains their limited storage capacity. To overcome this challenge and ensure a high storage capacity, it is imperative to develop new active materials with exceptional features specifically designed for supercapacitors. T-RGOBMs are being prominently considered for this purpose due to their remarkable physicochemical properties. These materials possess an exceptionally large surface area, excellent electrical conductivity, high content of AOGs, tailored porosity, and the potential for doping.

In the quest to prepare T-RGOBMs for supercapacitor applications, various heat treatment strategies are available for modifying their structure. The utilization of T-RGOFs is particularly appealing for streamlining and lightening the design of supercapacitors due to their exceptional flexibility and outstanding electrical conductivity.

Thermal treatment can effectively reduce GOFs without compromising their flexibility. In this context, AKBI et al. proposed a nondestructive thermochemical reduction approach to further enhance the storage capacity and rate capability of T-RGOF. The flexibility of the T-RGOF was preserved following reduction, and noteworthy improvements in its physicochemical properties were observed. The chemical reduction step improved electrical conductivity and introduced iodine groups through the use of HI as a reducing agent. Subsequently, the thermal reduction step conducted at 450°C under ambient air led to an expansion of the specific surface area (SSA), increased electrical conductivity, the introduction of oxygen-containing functional groups (AOGs) on the T-RGOF surface, and enhanced surface wettability for the T-RGOF. [89]. The thermal reduction-exfoliation of GO can also serve as an effective method to produce T-RGOSs with remarkable capacitive performance. Fouda et al. conducted experiments to assess the capacitive performance of an electrode fabricated using T-RGOSs at 350°C. The results demonstrated an impressive specific capacitance of 731 $F.g^{-1}$ at a scan rate of 10 $mV.s^{-1}$, and even when the scan rate was increased tenfold, it maintained a high value of 451 $F.g^{-1}$. This exceptional capacitive performance can be attributed to the expanded active surface area achieved through the reduction-exfoliation of GO during the heating process [219].

A multi-step thermal reduction process of GO under different atmospheres is also suggested as a key approach for tailoring the properties of T-RGOS for supercapacitor applications. In this context, Luo et al. employed a two-step thermal reduction method to reduce GO. The initial step is carried out under an Argon atmosphere at 500°C, which results in high porosity. The subsequent step is performed under ambient air at 400°C, introducing AOGs (carbonyl groups) into the T-RGOS' structure, potentially enhancing the pseudocapacitance contribution. When used as a supercapacitor electrode, the prepared T-RGOS exhibited a remarkable storage capacity and rate capability [156].

The reversible pseudocapacitive reactions facilitated by AOGs in T-RGOS can significantly enhance the overall specific capacitance. In a study by Chen et al., the impact of annealing temperature under vacuum conditions on the capacitive performance of T-RGOS was investigated. T-RGOS was produced through a two-step thermal annealing process. The first step involved rapid heating (30°C.min^{-1}) of GO, in the form of fine powder, from ambient temperature to 200°C, followed by a second step of heat treatment at higher temperatures for 20 minutes. Interestingly, an increase in the heat treatment temperature from 250 to 1000°C resulted in a decrease in specific capacitance from 171 to 48 $F.g^{-1}$. This reduction is attributed to the progressive elimination of AOGs as the heat treatment temperature increases [128].

Rate capability is a crucial characteristic of supercapacitors, allowing them to charge and discharge rapidly. This capability can be enhanced by optimizing the structure and improving the electrical conductivity of the active material. One effective approach to achieve this is through heat treatment, which decomposes AOGs, restoring Sp2 domains and increasing electrical conductivity. Moreover, this decomposition mainly generates H_2O and CO_2 gases, elevating the interlayer pressure and consequently expanding the T-RGOBMs. Luo et al. synthesized T-RGOA at 400°C under an argon atmosphere. When tested as a supercapacitor electrode, the resulting T-RGOA exhibited impressive rate capability, retaining 70% of its capacity even as the current density increased from 1 to 40 $A.g^{-1}$. This exceptional rate capability can be attributed to the well-preserved 3D porous structure following thermal treatment, in addition to the enhanced electrical conductivity [220]. To obtain T-RGOA with tailored prores and expanded SSA, KIM et al. activated a freeze-dried GO with two-step thermal annealing in two different atmospheres; first, under air at 650°C, and then under nitrogen at 600 °C. analysis attests to a large SSA of 653 $m^2.g^{-1}$. the T-RGOA -based electrode exhibits a superior specific capacitance of 372 $F.g^{-1}$ at 0.5 $A.g^{-1}$. The cyclic stability was also performed and the specific capacitance at the 10000 th cycle increased by 4% compared to the 1st cycle [221]. In another study, Yan et al. made a corrugated T-RGOS by exfoliating GO at 900°C followed by cryogenic treatment with liquid nitrogen. As an electrode for supercapacitor, the resulting T-RGOS exhibits an exceptional specific capacitance of 349.0 $F.g^{-1}$ at 2 $mV.s^{-1}$; moreover, a marked increase of 8% in specific capacitance is observed after 5000 cycles, indicating an outstanding stability in performance. This extraordinary performance might be attributed to the wrinkly morphology of the sheets, which hinders the agglomeration of the resulting T-RGOS, improving the accessible surface by electrolyte ions, and thus boosting the double-layer charge storage capacity [222]. T-RGOS commonly suffer from severe sheets restacking owing to hydrogen-bound involvement in the intercalated water and thus lose their advantageous characteristics such as high SSA. To remedy the problem of T-RGOS restacking, Lee et al. treated GO with a restacking-inhibitor *i.e.* melamine resin before thermal annealing, leading to the T-RGOS with an exceptionally large SSA of 1040 $m^2.g^{-1}$. As a result of using this T-RGOS as a supercapacitor electrode, a superior specific capacitance of 210 $F.g^{-1}$ was achieved, almost no capacitance loss for 20,000 cycles, and excellent rate capability [223].

As exciting materials for supercapacitor electrodes, heteroatoms single-doped, and multiple-doped T-RGOBMs have provoked a great deal of interest. Doping T-RGOBMs with heteroatoms *i.e.* N, P, I, and S enhances the electronic features, increases electrochemical reactivity, and facilitates the transfer of electrons,

which are crucial characteristics for achieving high capacitive performances [224,225]. Apparently, increasing the potential window (V) of supercapacitors is the most favorable to boost their energy density (E_d), owing to the fact that Ed is consistently related to the squared V ($E_d=1/2C_sV^2$). In this perspective, P-DT-RGOBMs were developed by the heat treatment of GO with phosphoric acid as a precursor at 800 °C under inert gas. The capacitive performances of P-DT-RGOBMs were investigated. It has been shown to have a large operating voltage window of 1.7 V, leading to a high energy density of 11.6 $W.h.kg^{-1}$ [226]. NS-DT-RGOBMs were extensively investigated as supercapacitor electrode material. For instance, Gopalsamy et al. developed NS-DT-RGOBMs by treating GO with the precursors of N and S atoms at high temperatures as 900°C under inert gas. NS-DT-RGOBMs were tested as an electrode for supercapacitors. Notably, an excellent specific capacitance of 442.0 $F.g^{-1}$ was attained at a high current density of 0.5 $A.g^{-1}$. More crucially, a stable cycle performance with a 1.4% loss of its initial capacitance after 10,000 cycles [227]. Ma et al. on the other hand, effectively constructed NS-DT-RGOBMs foam with customized porosity, increased SSA, and outstanding electric properties by using almost the same process. As a result, a high capacitance of 405 $F.g^{-1}$ at 1 $A.g^{-1}$ was attained [184].

9.2 *Strategies for developing T-RGOBMs for gaz Sensors*

Detection of particular gases in low quantities is of vital importance nowadays, not only for our everyday comfort and safety but also for our increasingly contaminated environment. Sensors are technical instruments that enable us to detect particular undesired and dangerous gases in our homes or surroundings. With the increasing complexity of dangerous gases and the need to detect more trace amounts of toxic gases, it is necessary to continuously develop and create highly sensitive and high-performance gas sensor materials. T-RGOBMs have remarkable properties, including high specific surface area, excellent electrical conductivity and semiconductivity, and abundant AOGs. Furthermore, heat treatment can be an effective path for fine-tuning the physicochemical properties of T-RGOBMs toward gas sensing applications.

Heat treatment may be used as a versatile route to convert GOBMs from insulators to semiconducting materials, making T-RGOBMs-made sensors favorable for gas sensing [118]. Park et al. monitored the change in the semiconducting behavior of T-RGOFs upon heat treatment. They observed that when exposed to ethanol gas, GOF displayed n-type semiconducting behavior, while T-RGOFs exhibited p-type behavior. the changeover may be ascribed to the variations in AOGs content [228]. To assess the impact of different heat treatment conditions on sensitivity performance, Wang et al. fabricated three variations of T-RGOFs. T-RGOF70 was produced at 70°C in an ambient atmosphere, while T-RGOF200 and T-RGOF500 were created at 200°C and 500°C, respectively, under vacuum conditions. These various T-RGOFs-based devices were then exposed to H_2 gas within a vacuum chamber to investigate their semiconducting behavior. Results revealed distinct behavior among the T-RGOFs. T-RGOF70 exhibited a significant decrease in resistance at ambient temperature upon exposure to H_2 gas, indicating its classification as an n-type semiconducting material. T-RGOF200, on the other hand, showed a negligible drop in resistance at ambient temperature and a substantial increase in resistance at higher temperatures, signifying its status as an asymmetric semiconductor. In the case of T-RGOF500, it demonstrated a substantial increase in resistance at both ambient and high temperatures, categorizing it as a p-type semiconducting material. These findings suggest that temperature fluctuations influence both the state density distribution and the size of the band gap in these materials. Additionally, the H_2-sensing performance of T-RGOF500 was evaluated using air as the gas flow, showing that the T-RGOF500-based device serves as an efficient H_2 sensor under room conditions. It exhibited moderate sensing performance, rapid response times, and excellent recovery characteristics [229]. As revealed by Zhou et al., heat treatment may also be utilized to fine-tune the chemically-made RGOF characteristics. RGOF made by hydrazine reduction is originally an n-type transition and it transforms into an n-p when exposed to NO_2 gas in a dynamic environment. It became p-type semiconducting after being heated to 300°C, but the p-n transition behavior did not occur once submerged in NO_2 [230]. AOGs also play an important role in the sensitivity performances of T-RGOBMs. Jung et al. constructed T-RGOS-coated silk by treating GOS-coated silk at 400 °C, using different rates of heating ranging from 1 to 5°.min^{-1}. The NO_2-sensing measurements were performed for the several prepared samples. Results show that the T-RGOS treated at 1°.min^{-1} exhibit the best performances with low response time (3.3 min) and maximum response. Structural investigation revealed that T-RGOS obtained with 1°.min^{-1} retains a higher proportion of AOGs, which results in a substantial improvement in NO_2 sensitivity performances [231]. In counterpart, Kumar and Kaur reduced GO at various temperatures of 150, 300, 600, and 800°C under an atmosphere, which contains argon(95%) and hydrogen(5%). As an SO_2 gas sensor, the obtained T-RGOS have shown outstanding performances. It has been found that SO_2-sensing response was improved by enhancing the density of the Sp2 domains. The treated T-RGOS at *T*= 800 °C exhibited an exceptional sensitivity response of 3.2% at a ppm level of SO_2 in ambient room temperature conditions [138]. A comparative study has highlighted the significant

influence of the GO preparation method on gas sensitivity performance. In this study, T-RGOS prepared through the heat treatment of modified Hummers' and Tour's GO were examined as gas sensors. The findings revealed that T-RGOS derived from Tour's GO exhibited a notably higher response compared to T-RGOS derived from Hummers' GO. This discrepancy can be attributed to the superior porosity of T-RGOS derived from Tour's GO in comparison to that obtained from Hummers' GO [232]. The heat treatment of GOBMs at low temperatures under atmospheric oxygen may be employed as an auspicious path to prepare T-RGOBMs with improved sensitivity [110,149]. Tegou prepared various T-RGOFs by treating GOF at various temperatures of 120, 150, 180, 200, and 300°C under an ambient atmosphere. The resulting T-RGOFs were tested as a humidity sensor and it was found that the T-RGOF obtained by annealing at 150°C had the greatest response. This is likely due to the fact that at 150°C, there is a sufficient recovery of the Sp2 structure, which improves the film's conductivity, and also preserves a quantity of OH groups compared to those treated at higher temperatures. Additionally, the T-RGOF obtained at 300°C had the lowest response due to the decrease in the inter-sheet distance [149].

9.3 *Strategies for developing T-RGOBMs for interference shielding*

Electromagnetic interferences may cause a malfunction of communication, medical, and military defense electronic equipment; more crucially, they can harm living creatures and the environment. In order to avoid this imminent problem, researchers tend to develop new materials that are capable of attenuating electromagnetic waves *i.e.* electromagnetic interference shielding materials (EISMs). EISMs have the aptitude for offsetting or reducing interferences by absorbing or reflecting electromagnetic waves. Due to their captivating characteristics including, improved electrical conductivity, enhanced thermal conductivity, expanded SSA, low density, layered structure, and AOGs content, T-RGOBMs have attracted interest as effective EISMs [233,234]. The shielding material effectiveness is normally evaluated by two factors which are the bandwidth and the intensity of adsorption [233]. Regarding the literature, a multitude of strategies has been used to develop effective T-RGOBMs toward electromagnetic shielding applications.

According to several studies, the effectiveness of the shielding materials may be increased by improving their electrical conductivity. In this view, Gonzalez et al. evaluated T-RGOAs with different degrees of reduction. the degree of reduction may be controlled by varying the temperature of heat treatment. Three T-RGOAs (T-RGOA400, T-RGOA600, and T-RGOA1000) were elaborated by treating Hydrothermally formed graphene aerogel at 400, 600, and 1000°C under the Argon-H_2 atmosphere. In the band ranging between 8 and 18 GHz, all T-RGOAs showed a high efficiency as shielding materials, transmitting only 5% of the total incident wave. Furthermore, an increase in reflected wave intensity was observed by increasing the reduction degree. The increase in the intensity of the reflected wave intensity may be attributed to the improvement of electrical conductivity by increasing the temperature of heat treatment [135].

As demonstrated by Shawi et al., the thermo-chemical modification of T-RGOBMs is a highly effective method for producing lightweight T-RGOBMs with exceptional shielding capabilities. Notably, treating chemically prepared RGOBMs with ascorbic acid as a reducing agent and subjecting them to mild heat treatment at 200°C for several hours under vacuum conditions has proven to be remarkably effective in attenuating electromagnetic waves in the X-band. This process achieves an outstanding attenuation of 94 dB with a loading capacity of 0.08 $g.cm^{-2}$. [235].

The low electrical conductivity of sheets in T-RGOA, which are not interconnected, resulted in poor shielding performance. To address this issue, Xu et al. enhanced sheet interconnection by incorporating T-RGOA, prepared by treating freeze-dried GO at 1000°C in argon, with polydimethylsiloxane as a binder. This combination resulted in a highly flexible T-RGOA/polydimethylsiloxane composite. Investigations revealed that the composite exhibited improved electrical conductivity (103 $S.m^{-1}$ with 3% loading of T-RGOA), leading to an outstanding shielding performance in the X-band with an attenuation of 54 dB [98]. Another study shows that shaping GOS into a film followed by a heat treatment to prepare T-RGOF ensures an excellent interconnection between sheets of T-RGOF, which results in a tremendous improvement in electrical conductivity [236]. Xu et al. treated GOF under a protective atmosphere at varying temperatures. T-RGOF1000 (symbolizing GOF treated at 1000°C) exhibits an astonishing electrical conductivity of 50000 $S.m^{-1}$, leading to an excellent shielding efficiency in the X-band, which is above 45 dB measured with only 50 µm thickness [237]. Another study showed that the use of thermal routes is more suitable than chemical ones for electromagnetic shielding applications. Notably, two RGOBMs were reduced by chemical and thermal approaches. Investigation in the X-band indicates that the shielding effectiveness of the T-RGOBMs attains the value of 40.2 dB, which is two-fold higher than that of the chemically prepared one. The higher electrical conductivity and the improved polarization effects of T-RGOBMs resulted in a superior value of shielding effectiveness [238].

Lightweight, highly flexible, and expanded T-RGOF may exhibit a high performance as an electromagnetic shielding material. Xi et al. prepared an expanded T-RGOF by using a two-stage thermo-chemical method by using HI in the first stage and thermal treatment at 3000°C in the second stage. The shielding effectiveness measured for the T-RGOF at a thickness of 1.40 mm. attains 135 dB in the range from 0.1 to 3 GHz. The high shielding performance is attributed to the expanded interlayer spacing [239].

T-RGOF made by a large-sized GOS may reach a high shielding effectiveness. More importantly, doping with heteroatoms may boost the shielding effectiveness. Notably, the GOF was fabricated with large-sized GOS and then reduced in three steps: chemically by using HI as a reducing agent; then, thermally at 1600°C under an argon atmosphere; and finally, thermally at 200°C under an iodine atmosphere. With a thickness of 12.5 µm, the I-DT-RGOF shows an excellent shielding effectiveness of 52.2 at 8.2 GHz. The large-sized sheets ensure a laminated structure and high electrical conductivity; moreover, iodine groups introduced into the structure, *i.e.*, tri-iodide and penta-iodide improve the carrier density of I-DT-RGOF, leading to better shielding effectiveness [240].

Due to the high thermal conductivity, T-RGOF may also act as a heat dissipation material for electronic components with a significant amount of heat generation, such as processors. Shen et al. implicated a simple method to prepare T-RGOF. First, GOF was fabricated by casting GOS suspension into a Teflon mold, and then, GOF was graphitized to T-RGOF by heat treatment at 2000 °C. The ensuing T-RGOF displays a high thermal conductivity of 1100 $Wm^{-1}K^{-1}$ and a high value of SE of 20 dB in spite of using a very thin film (8.4 µm) [241].

It is worth mentioning that the introduction of heteroatoms into T-RGOBMs enhances their physicochemical properties and, consequently, improves their performance in shielding against electromagnetic waves. In this context, S-DT-RGOBM was successfully synthesized through the heat treatment of GO at a high temperature in the presence of H_2S gas. The doping of T-RGOBMs with sulfur led to a significant increase in electrical conductivity, reaching 75 $S.cm^{-1}$. Consequently, the resulting S-DT-RGOBMs exhibited an enhanced shielding effectiveness (SE) at 100 MHz, achieving an SE of 33.2 dB, which is significantly higher than that of the undoped T-RGOBMs (15.5 dB) when measured at the same thickness (140 µm) [48].

10. Conclusion

This review presents a valuable guide for researchers and practitioners, offering insights into the safe and precise application of heat treatment for customizing the properties of GOBMs to suit specific applications. Through a thorough examination of the impact of the quality and physical form of GOBMs, as well as heat treatment conditions such as temperature, rate of heating, time, pressure, and atmosphere during preparation and annealing, we have established a consistent correlation between these factors and the resulting physicochemical properties of T-RGOBMs. Furthermore, we have delved into the thermal transformations occurring during heat treatment, investigated the mechanisms and kinetics governing thermal decomposition, assessed potential risks associated with GOBM reduction via heat treatment, and outlined strategies to ensure a secure reduction process. This review doesn't stop at the theoretical level; it also explores recent advancements in the practical application of T-RGOBMs. It provides concrete examples of heat treatment strategies applied across various fields, including supercapacitors, gas sensing, and interference shielding. With this proposed guideline, experts in the field can precisely select the optimal combination of GOBMs elaboration and thermal annealing conditions to carefully customize the physicochemical properties of the resulting T-RGOBMs for targeted applications.

As previously demonstrated, it's crucial to select the most suitable strategy for producing T-RGOBMs, as each application has specific needs for physical form and physicochemical properties. Producing T-RGOBMs begins with selecting the right method of preparation for the starting GO. The appropriate physical form must then be selected to elaborate GOBMs. Finally, suitable heat treatment conditions must be chosen to appropriately convert the GOBMs into T-RGOBMs.

Parent graphite, its granular size, oxidation, and even the purification process and sonication have a great impact on the specifications of the obtained GO, including the C/O ratio, type of AOGs, exfoliation degree, sheet size, purity, and defect density. Furthermore, there is a strong correlation between the specifications of the GO and the physicochemical properties of the resulting T-RGOBMs. For instance, to achieve high electrical and thermal conductivity in T-RGOBMs, it is recommended to prepare GO using small-sized graphite. On the other hand, if a high degree of porosity and exfoliation is desired in the T-RGOBMs, using GO with a high C/O ratio is recommended. The physical shape of the resulting GOBMs is another important factor to consider. T-RGOFs are ideal for applications requiring flexibility, electrical, and thermal conductivity. T-RGOS is suggested as a filler for improving the electrical, mechanical, thermal, and dielectric properties of materials such as polymers. T-RGOA is ideal for applications that demand porosity and lightness. Furthermore, annealing conditions greatly

impact the specifications of the resulting T-RGOBMs. These specifications, in turn, determine the physicochemical properties of the resulting T-RGOBMs. The annealing temperature, time, heating rate, pressure, and atmosphere all play important roles. Increasing the annealing temperature leads to the exclusion of more AOGs, enhancing both electrical conductivity and thermal conductivity. The rate of heating also impacts the porosity of T-RGOBMs, which can be optimized by increasing the heating rate. The annealing time serves as a useful monitor to regulate the extent of reduction in T-RGOBMs during the annealing process.

Annealing in inert, reducing, or ultra-high vacuum atmospheres allows for treatment at high temperatures (in the thousands of degrees) without damaging the structure of the T-RGOBMs, leading to high-quality T-RGOBMs with low C/O ratios and reduced defects, while annealing in ambient atmospheres can improve reactivity by introducing AOGs. Additionally, introducing heteroatoms through gas or solid precursors during annealing can result in unique and desirable properties for the resulting T-RGOBMs. Exerting pressure in GOFs during heat treatment significantly reduces the temperature required for their transformation into T-RGOFs. it may also result in T-RGOFs with fewer defects and a more compact structure, thereby enhancing their electrical and thermal conductivity and improving their transparency. It is evident that careful consideration of the preparation and annealing conditions of GOBMs can greatly impact the final properties of the T-RGOBMs, unlocking their potential for optimal performance in various applications.

Elucidating the transformations occurring in GOBMs during thermal annealing, along with understanding the underlying mechanisms and kinetics, is crucial because it provides greater control over the structure of T-RGOBMs and allows for fine-tuning their physicochemical properties for specific applications.

The explosive transformation of GOBMs to T-RGOBMs and the factors influencing this process are also worthy of investigation. This is essential for safety considerations, as it helps reduce the risk of GOBM explosions during heat treatment by employing innovative purification procedures and using chemical additives that decrease the energy release of the reduction reaction.

11.Future outlooks

Future research in the field of using heat treatment to fine-tune the properties of GOBMs should focus on the following topics:

(1) Further investigations to ensure the quality control of T-RGOBMs and the quantification of their properties for each application and establishing a strong connection between the heat-treatment conditions and the preapartion condition of GOBMs with changes in the structural and physicochemical properties of the resulting T-RGOBMs, enabling precise control over material characteristics. Additionally, further research is needed to define and optimize the key properties such as electrical conductivity, thermal conductivity, mechanical strength, and porosity that are critical and ensure an optimal performance for specific applications. This may ensure the presice quality and reprodoctibillity in the perfomance, leading to develop a standardized protocols for the industrial production of GOBMs and TR-GOBMs with optimal performance for specific application.

(2) Developing scalable and low-cost multistep approaches for mass-producing T-RGOBMs with improved performance, by harmonizing heat treatment with other enhancement strategies such as chemical reduction, joule heating, and cryogenic treatment. Chemical reduction introduces more defects into the structure of GOBMs, while joule heating ensures an extremely high degree of reduction, leading to exceptional thermal and electrical conductivity in the resulting T-RGOBMs. Cryogenic treatment enhances the porosity of the resulting T-RGOBMs. This integrated approach will ensure the production of high-quality T-RGOBMs that can be reliably used in advanced applications.

(3) Preparing non-defective and a-free-oxygen T-RGOBMs, which may be accomplished by optimizing the oxidation stage and establishing multistep thermochemical reduction approaches to properly eliminate AOGs and to consistently repair defects. This may result in T-RGOBMs with physicochemical properties close to those of pristine graphene.

(4) Further effort is required to gain a more thorough understanding of the mechanisms involved in the reactions during thermal reduction under various conditions, including the removal of AOGs and water, and the introduction of defects. This can be achieved by using advanced spectroscopic, thermal analysis, and microscopic techniques to monitor these reactions in real-time, providing detailed information on intermediate species and reaction rates. Revealing these mechanisms will ensure precise control over the structure and physicochemical properties of the resulting T-RGOBMs.

(5) Investigating the phenomenon of explosive thermal reduction of GOBMs and develop safe thermal reduction strategies to prevent potential hazards. Understanding the conditions and factors that lead to explosive

behavior is essential for ensuring the safe production of T-RGOBMs. Searching innovative strategy to mitigate explosions during thermal reduction of GOBMs.

Acknowledgments

H. AKBI is very indebted to *EcoleMilitairePolytechnique*, for the provision of Ph.D. Scholarship Granted by project number 15/2020/DRFPG/EMP.

Conflict of interest

There is no conflict of interest for this study.

References

[1] Zhong, Y.; Zhen, Z.; Zhu, H. Graphene: Fundamental research and potential applications. *FlatChem* **2017**, *4*, 20–32, https://doi.org/10.1016/j.flatc.2017.06.008.
[2] Kavitha, C. A review on reduced Graphene oxide hybrid nano composites and their prominent applications. *Mater. Today: Proc.* **2021**, *49*, 811–816, https://doi.org/10.1016/j.matpr.2021.05.343.
[3] H. Akbi, S. Rafai, A. Mekki, Reduced graphene oxide film with an ultrahigh energy density for Battery-like supercapacitor, MATERIALS CHEMISTRY (2021) 21. https://www.researchgate.net/profile/Mohamed-Kadari/publication/353333687_Proceedings_Book_ISyMC2021/links/60f56d2e16f9f3130093e897/Proceedings-Book-ISyMC2021.pdf#page=42 (accessed December 21, 2021).
[4] Akbi, H.; Yu, L.; Wang, B.; Liu, Q.; Wang, J.; Liu, J.; Song, D.; Sun, Y.; Liu, L. Effect of reducing system on capacitive behavior of reduced graphene oxide film: Application for supercapacitor. *J. Solid State Chem.* **2015**, *221*, 338–344, https://doi.org/10.1016/j.jssc.2014.10.004.
[5] Wang, Z.-L.; Xu, D.; Huang, Y.; Wu, Z.; Wang, L.-M.; Zhang, X.-B. Facile, mild and fast thermal-decomposition reduction of graphene oxide in air and its application in high-performance lithium batteries. *Chem. Commun.* **2011**, *48*, 976–978, https://doi.org/10.1039/c2cc16239c.
[6] Singh, A.; Lee, S.; Watanabe, H.; Lee, H. Graphene-Based Ultrasensitive Strain Sensors. *ACS Appl. Electron. Mater.* **2020**, *2*, 523–528, https://doi.org/10.1021/acsaelm.9b00778.
[7] Bukkitgar, S.D.; Shetti, N.P.; Reddy, K.R.; Saleh, T.A.; Aminabhavi, T.M. Ultrasonication and electrochemically-assisted synthesis of reduced graphene oxide nanosheets for electrochemical sensor applications. *FlatChem* **2020**, *23*, 100183, https://doi.org/10.1016/j.flatc.2020.100183.
[8] Struchkov, N.S.; Alexandrov, E.V.; Romashkin, A.V.; Silakov, G.O.; Rabchinskii, M.K. Uniform graphene oxide films fabrication via spray-coating for sensing application. *Full- Nanotub. Carbon Nanostructures* **2019**, *28*, 214–220, https://doi.org/10.1080/1536383x.2019.1686623.
[9] Ai, X.; Zhang, P.; Dou, Y.; Wu, Y.; Pan, T.; Chu, C.; Cui, P.; Ran, J. Graphene oxide membranes with hierarchical structures used for molecule sieving. *Sep. Purif. Technol.* **2020**, *230*, 115879, https://doi.org/10.1016/j.seppur.2019.115879.
[10] Akbi, H.; Rafai, S.; Mekki, A.; Touidjine, S.; Fertassi, M.A.; Kadri, D.E. When Copper Oxide meets graphene oxide: A core-shell structure via an intermittent spray coating route for a highly efficient ammonium perchlorate thermal decomposition. *J. Organomet. Chem.* **2021**, *957*, 122159, https://doi.org/10.1016/j.jorganchem.2021.122159.
[11] Akbi, H.; Mekki, A.; Rafai, S.; Boulkadid, M.K.; Touidjine, S.; Belgacemi, R.; Chabane, H.; Sayeh, Z.B.D. Preventing Agglomeration and Enhancing the Energetic Performance of Fine Ammonium Perchlorate through Surface Modification with Hydrophobic Reduced Graphene Oxide. *ChemistrySelect* **2024**, *9*, https://doi.org/10.1002/slct.202301795.
[12] Yang, F.; Hou, X.; Wang, L.; Li, Y.; Yu, M. Preparation of Reduced Graphene Oxide/Magnetic Metal Composites and Its Electromagnetic Wave Absorption Properties. *IOP Conf. Series: Mater. Sci. Eng.* **2020**, *729*, 012039, https://doi.org/10.1088/1757-899x/729/1/012039.
[13] Ho, C.-Y.; Liang, C.-C.; Wang, H.-W. Investigation of low thermal reduction of graphene oxide for dye-sensitized solar cell counter electrode. *Colloids Surfaces A: Physicochem. Eng. Asp.* **2015**, *481*, 222–228, https://doi.org/10.1016/j.colsurfa.2015.04.045.
[14] Singh, S.B.; De, M. Thermally exfoliated graphene oxide for hydrogen storage. *Mater. Chem. Phys.* **2019**, *239*, 122102, https://doi.org/10.1016/j.matchemphys.2019.122102.

[15] Liu, J.; Dong, J.; Zhang, T.; Peng, Q. Graphene-based nanomaterials and their potentials in advanced drug delivery and cancer therapy. *J. Control. Release* **2018**, *286*, 64–73, https://doi.org/10.1016/j.jconrel.2018.07.034.
[16] Song, N.-J.; Chen, C.-M.; Lu, C.; Liu, Z.; Kong, Q.-Q.; Cai, R. Thermally reduced graphene oxide films as flexible lateral heat spreaders. *J. Mater. Chem. A* **2014**, *2*, 16563–16568, https://doi.org/10.1039/c4ta02693d.
[17] Yuan, G.-J.; Xie, J.-F.; Li, H.-H.; Shan, B.; Zhang, X.-X.; Liu, J.; Li, L.; Tian, Y.-Z. Thermally Reduced Graphene Oxide/Carbon Nanotube Composite Films for Thermal Packaging Applications. *Materials* **2020**, *13*, 317, https://doi.org/10.3390/ma13020317.
[18] Sun, L. Structure and synthesis of graphene oxide. *Chin. J. Chem. Eng.* **2019**, *27*, 2251–2260, https://doi.org/10.1016/j.cjche.2019.05.003.
[19] Akbi, H.; Mekki, A.; Rafai, S.; Touidjine, S.; Boudina, N.; Sayeh, Z.B.D. Phenomenological description of the thermal reduction kinetics in graphene oxide films. *Mater. Chem. Phys.* **2021**, *277*, 125477, https://doi.org/10.1016/j.matchemphys.2021.125477.
[20] Jiao, L.; Chua, Z.Y.; Moon, S.K.; Song, J.; Bi, G.; Zheng, H.; Lee, B.; Koo, J. Laser-Induced Graphene on Additive Manufacturing Parts. *Nanomaterials* **2019**, *9*, 90, https://doi.org/10.3390/nano9010090.
[21] You, R.; Liu, Y.; Hao, Y.; Han, D.; Zhang, Y.; You, Z. Laser Fabrication of Graphene-Based Flexible Electronics. *Adv. Mater.* **2019**, *32*, e1901981, https://doi.org/10.1002/adma.201901981.
[22] Souleymen, R.; Wang, Z.; Qiao, C.; Naveed, M.; Cao, C. Microwave-assisted synthesis of graphene-like cobalt sulfide freestanding sheets as an efficient bifunctional electrocatalyst for overall water splitting. *J. Mater. Chem. A* **2018**, *6*, 7592–7607, https://doi.org/10.1039/c8ta01266k.
[23] Zhang, Y.; Li, K.; Liao, J.; Wei, X.; Zhang, L. Microwave-assisted synthesis of graphitic carbon nitride/CuO nanocomposites and the enhancement of catalytic activities in the thermal decomposition of ammonium perchlorate. *Appl. Surf. Sci.* **2019**, *499*, 143875, https://doi.org/10.1016/j.apsusc.2019.143875.
[24] Han, H.J.; Chen, Y.N.; Wang, Z.J. Effect of microwave irradiation on reduction of graphene oxide films. *RSC Adv.* **2015**, *5*, 92940–92946, https://doi.org/10.1039/c5ra19268d.
[25] Zhao, B.; Liu, P.; Jiang, Y.; Pan, D.; Tao, H.; Song, J.; Fang, T.; Xu, W. Supercapacitor performances of thermally reduced graphene oxide. *J. Power Sources* **2011**, *198*, 423–427, https://doi.org/10.1016/j.jpowsour.2011.09.074.
[26] Oliveira, A.E.F.; Braga, G.B.; Tarley, C.R.T.; Pereira, A.C. Thermally reduced graphene oxide: synthesis, studies and characterization. *J. Mater. Sci.* **2018**, *53*, 12005–12015, https://doi.org/10.1007/s10853-018-2473-3.
[27] Song, N.-J.; Chen, C.-M.; Lu, C.; Liu, Z.; Kong, Q.-Q.; Cai, R. Thermally reduced graphene oxide films as flexible lateral heat spreaders. *J. Mater. Chem. A* **2014**, *2*, 16563–16568, https://doi.org/10.1039/c4ta02693d.
[28] Sengupta, I.; Kumar, S.S.S.; Pal, S.K.; Chakraborty, S. Characterization of structural transformation of graphene oxide to reduced graphene oxide during thermal annealing. *J. Mater. Res.* **2020**, *35*, 1197–1204, https://doi.org/10.1557/jmr.2020.55.
[29] Akbi, H.; Rafai, S.; Mekki, A.; Touidjine, S.; Belkadi, K. Kinetic investigation of the multi-step thermal decomposition of graphene oxide paper. *J. Therm. Anal. Calorim.* **2023**, *148*, 3487–3503, https://doi.org/10.1007/s10973-023-11948-1.
[30] Jankovský, O.; Marvan, P.; Nováček, M.; Luxa, J.; Mazánek, V.; Klímová, K.; Sedmidubský, D.; Sofer, Z. Synthesis procedure and type of graphite oxide strongly influence resulting graphene properties. *Appl. Mater. Today* **2016**, *4*, 45–53, https://doi.org/10.1016/j.apmt.2016.06.001.
[31] Agarwal, V.; Zetterlund, P.B. Strategies for reduction of graphene oxide – A comprehensive review. *Chem. Eng. J.* **2020**, *405*, 127018, https://doi.org/10.1016/j.cej.2020.127018.
[32] Feng, J.; Ye, Y.; Xiao, M.; Wu, G.; Ke, Y. Synthetic routes of the reduced graphene oxide. *Chem. Pap.* **2020**, *74*, 3767–3783, https://doi.org/10.1007/s11696-020-01196-0.
[33] de Barros, N.G.; Neto, A.C.G.; Vaccioli, K.B.; Angulo, H.R.V.; Silva, L.G.d.A.e.; Toffoli, S.M.; Valera, T.S. Graphene Oxide: A Comparison of Reduction Methods. *C* **2023**, *9*, 73, https://doi.org/10.3390/c9030073.
[34] Stankovich, S.; Dikin, D.A.; Piner, R.D.; Kohlhaas, K.A.; Kleinhammes, A.; Jia, Y.; Wu, Y.; Nguyen, S.T.; Ruoff, R.S. Synthesis of graphene-based nanosheets via chemical reduction of exfoliated graphite oxide. *Carbon* **2007**, *45*, 1558–1565, https://doi.org/10.1016/j.carbon.2007.02.034.
[35] Pei, S.; Zhao, J.; Du, J.; Ren, W.; Cheng, H.-M. Direct reduction of graphene oxide films into highly conductive and flexible graphene films by hydrohalic acids. *Carbon* **2010**, *48*, 4466–4474, https://doi.org/10.1016/j.carbon.2010.08.006.
[36] Pei, S.; Cheng, H.-M. The reduction of graphene oxide. Carbon 2012, 50, 3210–3228. https://doi.org/10.1016/j.carbon.2011.11.010
[37] Chen, H.; Song, Z.; Zhao, X.; Li, X.; Lin, H. Reduction of free-standing graphene oxide papers by a hydrothermal process at the solid/gas interface. *RSC Adv.* **2012**, *3*, 2971–2978, https://doi.org/10.1039/c2ra21576d.

[38] Toh, S.Y.; Loh, K.S.; Kamarudin, S.K.; Daud, W.R.W. Graphene production via electrochemical reduction of graphene oxide: Synthesis and characterisation. *Chem. Eng. J.* **2014**, *251*, 422–434, https://doi.org/10.1016/j.cej.2014.04.004.
[39] Zhu, Y.; Murali, S.; Stoller, M.D.; Velamakanni, A.; Piner, R.D.; Ruoff, R.S. Microwave assisted exfoliation and reduction of graphite oxide for ultracapacitors. *Carbon* **2010**, *48*, 2118–2122, https://doi.org/10.1016/j.carbon.2010.02.001.
[40] Trusovas, R.; Ratautas, K.; Račiukaitis, G.; Barkauskas, J.; Stankevičienė, I.; Niaura, G.; Mažeikienė, R. Reduction of graphite oxide to graphene with laser irradiation. *Carbon* **2013**, *52*, 574–582, https://doi.org/10.1016/j.carbon.2012.10.017.
[41] Sengupta, I.; Chakraborty, S.; Talukdar, M.; Pal, S.K.; Chakraborty, S. Thermal reduction of graphene oxide: How temperature influences purity. *J. Mater. Res.* **2018**, *33*, 4113–4122, https://doi.org/10.1557/jmr.2018.338.
[42] Shang, Y.; Zhang, D.; Liu, Y.; Guo, C. Preliminary comparison of different reduction methods of graphene oxide. *Bull. Mater. Sci.* **2015**, *38*, 7–12, https://doi.org/10.1007/s12034-014-0794-7.
[43] McAllister, M.J.; Li, J.-L.; Adamson, D.H.; Schniepp, H.C.; Abdala, A.A.; Liu, .J.; Herrera-Alonso, M.; Milius, D.L.; Car, R.; Prud'Homme, R.K.; et al. Single Sheet Functionalized Graphene by Oxidation and Thermal Expansion of Graphite. *Chem. Mater.* **2007**, *19*, 4396–4404, https://doi.org/10.1021/cm0630800.
[44] Schniepp, H.C.; Li, J.-L.; McAllister, M.J.; Sai, H.; Herrera-Alonso, M.; Adamson, D.H.; Prud'Homme, R.K.; Car, R.; Saville, D.A.; Aksay, I.A. Functionalized Single Graphene Sheets Derived from Splitting Graphite Oxide. *J. Phys. Chem. B* **2006**, *110*, 8535–8539, https://doi.org/10.1021/jp060936f.
[45] S. Hun, Thermal Reduction of Graphene Oxide, in: S. Mikhailov (Ed.), Physics and Applications of Graphene - Experiments, InTech, 2011. https://doi.org/10.5772/14156.
[46] Chen, X.; Meng, D.; Wang, B.; Li, B.-W.; Li, W.; Bielawski, C.W.; Ruoff, R.S. Rapid thermal decomposition of confined graphene oxide films in air. *Carbon* **2016**, *101*, 71–76, https://doi.org/10.1016/j.carbon.2016.01.075.
[47] Wei, W.; Guan, T.; Li, C.; Shen, L.; Bao, N. Heating Rate-Controlled Thermal Exfoliation for Foldable Graphene Sponge. *Ind. Eng. Chem. Res.* **2020**, *59*, 2946–2952, https://doi.org/10.1021/acs.iecr.9b06114.
[48] Shahzad, F.; Kumar, P.; Yu, S.; Lee, S.; Kim, Y.-H.; Hong, S.M.; Koo, C.M. Sulfur-doped graphene laminates for EMI shielding applications. *J. Mater. Chem. C* **2015**, *3*, 9802–9810, https://doi.org/10.1039/c5tc02166a.
[49] Liu, R.; Gong, T.; Zhang, K.; Lee, C. Graphene oxide papers with high water adsorption capacity for air dehumidification. *Sci. Rep.* **2017**, *7*, 1–9, https://doi.org/10.1038/s41598-017-09777-y.
[50] Timofeeva, T.E.; Evseev, Z.I.; Vinokurov, P.V.; Alexandrov, G.N.; Smagulova, S.A. The Effect of Temperature Conditions During Graphene Oxide Synthesis on Humidity Dependence of Conductivity in Thermally Reduced Graphene Oxide. *J. Struct. Chem.* **2018**, *59*, 799–805, https://doi.org/10.1134/s002247661804008x.
[51] Losic, D.; Farivar, F.; Yap, P.L.; Tung, T.T.; Nine, J. New insights on energetic properties of graphene oxide (GO) materials and their safety and environmental risks. *Sci. Total. Environ.* **2022**, *848*, 157743, https://doi.org/10.1016/j.scitotenv.2022.157743.
[52] Park, J.; Cho, Y.S.; Sung, S.J.; Byeon, M.; Yang, S.J.; Park, C.R. Characteristics tuning of graphene-oxide-based-graphene to various end-uses. *Energy Storage Mater.* **2018**, *14*, 8–21, https://doi.org/10.1016/j.ensm.2018.02.013.
[53] Morimoto, N.; Kubo, T.; Nishina, Y. Tailoring the Oxygen Content of Graphite and Reduced Graphene Oxide for Specific Applications. *Sci. Rep.* **2016**, *6*, 21715, https://doi.org/10.1038/srep21715.
[54] Xu, S.; Liu, J.; Xue, Y.; Wu, T.; Zhang, Z. Appropriate conditions for preparing few-layered graphene oxide and reduced graphene oxide. *Full- Nanotub. Carbon Nanostructures* **2016**, *25*, 40–46, https://doi.org/10.1080/1536383x.2016.1247268.
[55] Staudenmaier, L. Verfahren zur Darstellung der Graphitsäure. *Eur. J. Inorg. Chem.* **1898**, *31*, 1481–1487, https://doi.org/10.1002/cber.18980310237.
[56] Collins Brodie, B. XIII. On the atomic weight of graphite. *Philos. Trans. R. Soc. Lond.* **1859**, *149*, 249–259, doi:10.1098/rstl.1859.0013.
[57] Hummers, W.S., Jr.; Offeman, R.E. Preparation of Graphitic Oxide. *J. Am. Chem. Soc.* **1958**, *80*, 1339, https://doi.org/10.1021/ja01539a017.
[58] Yu, H.; Zhang, B.; Bulin, C.; Li, R.; Xing, R. High-efficient Synthesis of Graphene Oxide Based on Improved Hummers Method. *Sci. Rep.* **2016**, *6*, 36143, https://doi.org/10.1038/srep36143.
[59] Yadav, N.; Lochab, B. A comparative study of graphene oxide: Hummers, intermediate and improved method. *FlatChem* **2019**, *13*, 40–49, https://doi.org/10.1016/j.flatc.2019.02.001.
[60] Shao, G.; Lu, Y.; Wu, F.; Yang, C.; Zeng, F.; Wu, Q. Graphene oxide: the mechanisms of oxidation and exfoliation. *J. Mater. Sci.* **2012**, *47*, 4400–4409, https://doi.org/10.1007/s10853-012-6294-5.
[61] Poh, H.L.; Šaněk, F.; Ambrosi, A.; Zhao, G.; Sofer, Z.; Pumera, M. Graphenes prepared by Staudenmaier, Hofmann and Hummers methods with consequent thermal exfoliation exhibit very different electrochemical properties. *Nanoscale* **2012**, *4*, 3515–3522, https://doi.org/10.1039/c2nr30490b.

[62] Botas, C.; Álvarez, P.; Blanco, C.; Blanco, P.; Granda, M.; Santamaría, R.; Romasanta, L.J.; Verdejo, R.; López-Manchado, M.A.; Menéndez, R. Graphene materials with different structures prepared from the same graphite by the Hummers and Brodie methods. *Carbon* **2013**, *65*, 156–164, doi:10.1016/j.carbon.2013.08.009.
[63] Botas, C.; Álvarez, P.; Blanco, C.; Santamaría, R.; Granda, M.; Ares, P.; Rodríguez-Reinoso, F.; Menéndez, R. The effect of the parent graphite on the structure of graphene oxide. *Carbon* **2011**, *50*, 275–282, https://doi.org/10.1016/j.carbon.2011.08.045.
[64] Chee, S.Y.; Poh, H.L.; Chua, C.K.; Šaněk, F.; Sofer, Z.; Pumera, M. Influence of parent graphite particle size on the electrochemistry of thermally reduced graphene oxide. *Phys. Chem. Chem. Phys.* **2012**, *14*, 12794–12799, https://doi.org/10.1039/c2cp41462g.
[65] Dao, T.D.; Jeong, H.M. Graphene prepared by thermal reduction–exfoliation of graphite oxide: Effect of raw graphite particle size on the properties of graphite oxide and graphene. *Mater. Res. Bull.* **2015**, *70*, 651–657, https://doi.org/10.1016/j.materresbull.2015.05.038.
[66] Krishnamoorthy, K.; Veerapandian, M.; Yun, K.; Kim, S.-J. The chemical and structural analysis of graphene oxide with different degrees of oxidation. *Carbon* **2013**, *53*, 38–49, https://doi.org/10.1016/j.carbon.2012.10.013.
[67] Suhaimin, N.S.; Hanifah, M.F.R.; Jusin, J.W.; Jaafar, J.; Aziz, M.; Ismail, A.F.; Othman, M.H.D.; Rahman, M.A.; Aziz, F.; Yusof, N.; et al. Tuning the oxygen functional groups in graphene oxide nanosheets by optimizing the oxidation time. *Phys. E: Low-dimensional Syst. Nanostructures* **2021**, *131*, 114727, https://doi.org/10.1016/j.physe.2021.114727.
[68] Qi, X.; Zhou, T.; Deng, S.; Zong, G.; Yao, X.; Fu, Q. Size-specified graphene oxide sheets: ultrasonication assisted preparation and characterization. *J. Mater. Sci.* **2013**, *49*, 1785–1793, https://doi.org/10.1007/s10853-013-7866-8.
[69] F., H.L.; Tan, C.P.; R.M., Z.; Z.A., N.H. Effect of sonication time and heat treatment on the structural and physical properties of chitosan/graphene oxide nanocomposite films. *Food Packag. Shelf Life* **2021**, *28*, https://doi.org/10.1016/j.fpsl.2021.100663.
[70] Bagri, A.; Mattevi, C.; Acik, M.; Chabal, Y.J.; Chhowalla, M.; Shenoy, V.B. Structural evolution during the reduction of chemically derived graphene oxide. *Nat. Chem.* **2010**, *2*, 581–587, https://doi.org/10.1038/nchem.686.
[71] Antidormi, A.; Roche, S.; Colombo, L. Impact of oxidation morphology on reduced graphene oxides upon thermal annealing. *J. Physics: Mater.* **2019**, *3*, 015011, https://doi.org/10.1088/2515-7639/ab5ef2.
[72] Zapata-Hernandez, C.; Durango-Giraldo, G.; Cacua, K.; Buitrago-Sierra, R. Influence of graphene oxide synthesis methods on the electrical conductivity of cotton/graphene oxide composites. *J. Text. Inst.* **2022**, *113*, 131–140, https://doi.org/10.1080/00405000.2020.1865507.
[73] You, S.; Luzan, S.M.; Szabó, T.; Talyzin, A.V. Effect of synthesis method on solvation and exfoliation of graphite oxide. *Carbon* **2013**, *52*, 171–180, https://doi.org/10.1016/j.carbon.2012.09.018.
[74] Storm, M.M.; Overgaard, M.; Younesi, R.; Reeler, N.E.A.; Vosch, T.; Nielsen, U.G.; Edström, K.; Norby, P. Reduced graphene oxide for Li–air batteries: The effect of oxidation time and reduction conditions for graphene oxide. *Carbon* **2015**, *85*, 233–244, https://doi.org/10.1016/j.carbon.2014.12.104.
[75] Acik, M.; Lee, G.; Mattevi, C.; Pirkle, A.; Wallace, R.M.; Chhowalla, M.; Cho, K.; Chabal, Y. The Role of Oxygen during Thermal Reduction of Graphene Oxide Studied by Infrared Absorption Spectroscopy. *J. Phys. Chem. C* **2011**, *115*, 19761–19781, https://doi.org/10.1021/jp2052618.
[76] Acik, M.; Mattevi, C.; Gong, C.; Lee, G.; Cho, K.; Chhowalla, M.; Chabal, Y.J. The Role of Intercalated Water in Multilayered Graphene Oxide. *ACS Nano* **2010**, *4*, 5861–5868, https://doi.org/10.1021/nn101844t.
[77] Feicht, P.; Eigler, S. Defects in Graphene Oxide as Structural Motifs. *Chemnanomat* **2018**, *4*, 244–252, https://doi.org/10.1002/cnma.201700357.
[78] Gong, C.; Acik, M.; Abolfath, R.M.; Chabal, Y.; Cho, K. Graphitization of Graphene Oxide with Ethanol during Thermal Reduction. *J. Phys. Chem. C* **2012**, *116*, 9969–9979, https://doi.org/10.1021/jp212584t.
[79] Araujo, P.T.; Terrones, M.; Dresselhaus, M.S. Defects and impurities in graphene-like materials. *Mater. Today* **2012**, *15*, 98–109, https://doi.org/10.1016/s1369-7021(12)70045-7.
[80] Lee, W.-J.; Kim, C.-S.; Yang, S.-Y.; Lee, D.; Kim, Y.-S. Spontaneous exfoliation of large-sized graphene oxide with low defect concentration by simple wet chemistry. *Carbon* **2021**, *182*, 214–222, https://doi.org/10.1016/j.carbon.2021.06.009.
[81] De Silva, K.K.H.; Huang, H.-H.; Joshi, R.; Yoshimura, M. Restoration of the graphitic structure by defect repair during the thermal reduction of graphene oxide. *Carbon* **2020**, *166*, 74–90, https://doi.org/10.1016/j.carbon.2020.05.015.
[82] Grimm, S.; Schweiger, M.; Eigler, S.; Zaumseil, J. High-Quality Reduced Graphene Oxide by CVD-Assisted Annealing. *J. Phys. Chem. C* **2016**, *120*, 3036–3041, https://doi.org/10.1021/acs.jpcc.5b11598.
[83] Ambrosi, A.; Chua, C.K.; Khezri, B.; Sofer, Z.; Webster, R.D.; Pumera, M. Chemically reduced graphene contains inherent metallic impurities present in parent natural and synthetic graphite. *Proc. Natl. Acad. Sci.* **2012**, *109*, 12899–12904, https://doi.org/10.1073/pnas.1205388109.

[84] Ambrosi, A.; Chee, S.Y.; Khezri, B.; Webster, R.D.; Sofer, Z.; Pumera, M. Metallic Impurities in Graphenes Prepared from Graphite Can Dramatically Influence Their Properties. *Angew. Chem. Int. Ed.* **2011**, *51*, 500–503, https://doi.org/10.1002/anie.201106917.
[85] Qiu, Y.; Guo, F.; Hurt, R.; Külaots, I. Explosive thermal reduction of graphene oxide-based materials: Mechanism and safety implications. *Carbon* **2014**, *72*, 215–223, https://doi.org/10.1016/j.carbon.2014.02.005.
[86] Kim, F.; Luo, J.; Cruz-Silva, R.; Cote, L.J.; Sohn, K.; Huang, J. Self-Propagating Domino-like Reactions in Oxidized Graphite. *Adv. Funct. Mater.* **2010**, *20*, 2867–2873, https://doi.org/10.1002/adfm.201000736.
[87] Eigler, S.; Dotzer, C.; Hof, F.; Bauer, W.; Hirsch, A. Sulfur Species in Graphene Oxide. *Chem. – A Eur. J.* **2013**, *19*, 9490–9496, https://doi.org/10.1002/chem.201300387.
[88] Shen, Y.; Boffa, V.; Corazzari, I.; Qiao, A.; Tao, H.; Yue, Y. Revealing hidden endotherm of Hummers' graphene oxide during low-temperature thermal reduction. *Carbon* **2018**, *138*, 337–347, https://doi.org/10.1016/j.carbon.2018.05.018.
[89] Akbi, H.; Rafai, S.; Mekki, A.; Touidjine, S.; Belkadi, K.; Boudina, N.; Rabah, I. Boosting the storage capacity and the rate capability of flexible graphene film via a nondestructive thermo-chemical reduction. *Diam. Relat. Mater.* **2022**, *129*, https://doi.org/10.1016/j.diamond.2022.109338.
[90] Zhang, C.; Lv, W.; Xie, X.; Tang, D.; Liu, C.; Yang, Q.-H. Towards low temperature thermal exfoliation of graphite oxide for graphene production. *Carbon* **2013**, *62*, 11–24, https://doi.org/10.1016/j.carbon.2013.05.033.
[91] Botlhoko, O.J.; Ramontja, J.; Ray, S.S. Morphological development and enhancement of thermal, mechanical, and electronic properties of thermally exfoliated graphene oxide-filled biodegradable polylactide/poly(ε-caprolactone) blend composites. *Polymer* **2018**, *139*, 188–200, https://doi.org/10.1016/j.polymer.2018.02.005.
[92] Zhang, H.-B.; Wang, J.-W.; Yan, Q.; Zheng, W.-G.; Chen, C.; Yu, Z.-Z. Vacuum-assisted synthesis of graphene from thermal exfoliation and reduction of graphite oxide. *J. Mater. Chem.* **2011**, *21*, 5392–5397, https://doi.org/10.1039/c1jm10099h.
[93] Abuoudah, C.K.; Abuibaid, A.Z.; Greish, Y.E.; Ehmann, H.M.A.; Abu-Jdayil, B.; Iqbal, M.Z. Thermally reduced graphene/polypropylene nanocomposites: Effects of processing method on thermal, mechanical, and morphological properties. *J. Polym. Res.* **2022**, *29*, 1–15, https://doi.org/10.1007/s10965-022-03100-8.
[94] Singh, V.K.; Shukla, A.; Patra, M.K.; Saini, L.; Jani, R.K.; Vadera, S.R.; Kumar, N. Microwave absorbing properties of a thermally reduced graphene oxide/nitrile butadiene rubber composite. *Carbon* **2012**, *50*, 2202–2208, https://doi.org/10.1016/j.carbon.2012.01.033.
[95] Han, Y.; Wang, T.; Gao, X.; Li, T.; Zhang, Q. Preparation of thermally reduced graphene oxide and the influence of its reduction temperature on the thermal, mechanical, flame retardant performances of PS nanocomposites. *Compos. Part A: Appl. Sci. Manuf.* **2016**, *84*, 336–343, https://doi.org/10.1016/j.compositesa.2016.02.007.
[96] He, Y.; Liu, Y.; Wu, T.; Ma, J.; Wang, X.; Gong, Q.; Kong, W.; Xing, F.; Liu, Y.; Gao, J. An environmentally friendly method for the fabrication of reduced graphene oxide foam with a super oil absorption capacity. *J. Hazard. Mater.* **2013**, *260*, 796–805, https://doi.org/10.1016/j.jhazmat.2013.06.042.
[97] Mi, X.; Huang, G.; Xie, W.; Wang, W.; Liu, Y.; Gao, J. Preparation of graphene oxide aerogel and its adsorption for Cu2+ ions. *Carbon* **2012**, *50*, 4856–4864, https://doi.org/10.1016/j.carbon.2012.06.013.
[98] Xu, F.; Chen, R.; Lin, Z.; Qin, Y.; Yuan, Y.; Li, Y.; Zhao, X.; Yang, M.; Sun, X.; Wang, S.; et al. Superflexible Interconnected Graphene Network Nanocomposites for High-Performance Electromagnetic Interference Shielding. *ACS Omega* **2018**, *3*, 3599–3607, https://doi.org/10.1021/acsomega.8b00432.
[99] Fan, Z.; Tng, D.Z.Y.; Nguyen, S.T.; Feng, J.; Lin, C.; Xiao, P.; Lu, L.; Duong, H.M. Morphology effects on electrical and thermal properties of binderless graphene aerogels. *Chem. Phys. Lett.* **2013**, *561-562*, 92–96, https://doi.org/10.1016/j.cplett.2013.01.033.
[100] Fan, Z.; Marconnet, A.; Nguyen, S.T.; Lim, C.Y.; Duong, H.M. Effects of heat treatment on the thermal properties of highly nanoporous graphene aerogels using the infrared microscopy technique. *Int. J. Heat Mass Transf.* **2014**, *76*, 122–127, https://doi.org/10.1016/j.ijheatmasstransfer.2014.04.023.
[101] Cheng, Y.; Zhou, S.; Hu, P.; Zhao, G.; Li, Y.; Zhang, X.; Han, W. Enhanced mechanical, thermal, and electric properties of graphene aerogels via supercritical ethanol drying and high-temperature thermal reduction. *Sci. Rep.* **2017**, *7*, 1–11, https://doi.org/10.1038/s41598-017-01601-x.
[102] Zhang, Y.; Huang, Y.; Chen, H.; Huang, Z.; Yang, Y.; Xiao, P.; Zhou, Y.; Chen, Y. Composition and structure control of ultralight graphene foam for high-performance microwave absorption. *Carbon* **2016**, *105*, 438–447, https://doi.org/10.1016/j.carbon.2016.04.070.
[103] Papamatthaiou, S.; Argyropoulos, D.-P.; Farmakis, F.; Masurkar, A.; Alexandrou, K.; Kymissis, I.; Georgoulas, N. The Effect of Thermal Reduction and Film Thickness on fast Response Transparent Graphene Oxide Humidity Sensors. *Procedia Eng.* **2016**, *168*, 301–304, https://doi.org/10.1016/j.proeng.2016.11.201.
[104] Dong, L.; Yang, J.; Chhowalla, M.; Loh, K.P. Synthesis and reduction of large sized graphene oxide sheets. *Chem. Soc. Rev.* **2017**, *46*, 7306–7316, https://doi.org/10.1039/c7cs00485k.

[105]Lin, X.; Shen, X.; Zheng, Q.; Yousefi, N.; Ye, L.; Mai, Y.-W.; Kim, J.-K. Fabrication of Highly-Aligned, Conductive, and Strong Graphene Papers Using Ultralarge Graphene Oxide Sheets. *ACS Nano* **2012**, *6*, 10708–10719, https://doi.org/10.1021/nn303904z.
[106]Pan, S.; Aksay, I.A. Factors Controlling the Size of Graphene Oxide Sheets Produced *via* the Graphite Oxide Route. *ACS Nano* **2011**, *5*, 4073–4083, https://doi.org/10.1021/nn200666r.
[107]Seyedin, M.Z.; Razal, J.M.; Innis, P.C.; Jalili, R.; Wallace, G.G. Achieving Outstanding Mechanical Performance in Reinforced Elastomeric Composite Fibers Using Large Sheets of Graphene Oxide. *Adv. Funct. Mater.* **2014**, *25*, 94–104, https://doi.org/10.1002/adfm.201402167.
[108]Klemeyer, L.; Park, H.; Huang, J. Geometry-Dependent Thermal Reduction of Graphene Oxide Solid. *ACS Mater. Lett.* **2021**, *3*, 511–515, https://doi.org/10.1021/acsmaterialslett.0c00423.
[109]Pan, Q.; Chung, C.-C.; He, N.; Jones, J.L.; Gao, W. Accelerated Thermal Decomposition of Graphene Oxide Films in Air via *in Situ* X-ray Diffraction Analysis. *J. Phys. Chem. C* **2016**, *120*, 14984–14990, https://doi.org/10.1021/acs.jpcc.6b05031.
[110]Le, G.T.; Manyam, J.; Opaprakasit, P.; Chanlek, N.; Grisdanurak, N.; Sreearunothai, P. Divergent mechanisms for thermal reduction of graphene oxide and their highly different ion affinities. *Diam. Relat. Mater.* **2018**, *89*, 246–256, https://doi.org/10.1016/j.diamond.2018.09.006.
[111]Singh, P.K. Impact of high temperature thermal reduction on microstructure, crystallinity and surface topography of reduced graphene oxide. *Mater. Today: Proc.* **2023**, https://doi.org/10.1016/j.matpr.2023.02.169.
[112]Menezes, I.R.; Sakai, T.; Hattori, Y.; Kaneko, K. Effect of preheating temperature on adsorption of N2 and Ar on graphene oxide. *Chem. Phys. Lett.* **2022**, *807*, https://doi.org/10.1016/j.cplett.2022.140091.
[113]Foller, T.; Daiyan, R.; Jin, X.; Leverett, J.; Kim, H.; Webster, R.; Yap, J.E.; Wen, X.; Rawal, A.; De Silva, K.K.H.; et al. Enhanced graphitic domains of unreduced graphene oxide and the interplay of hydration behaviour and catalytic activity. *Mater. Today* **2021**, *50*, 44–54, https://doi.org/10.1016/j.mattod.2021.08.003.
[114]Li, Y.; Yuan, S.; Xia, Y.; Zhao, W.; Easton, C.D.; Selomulya, C.; Zhang, X. Mild annealing reduced graphene oxide membrane for nanofiltration. *J. Membr. Sci.* **2020**, *601*, 117900, https://doi.org/10.1016/j.memsci.2020.117900.
[115]Zhao, J.; Li, Y.; Wang, Y.; Mao, J.; He, Y.; Luo, J. Mild thermal reduction of graphene oxide as a lubrication additive for friction and wear reduction. *RSC Adv.* **2017**, *7*, 1766–1770, https://doi.org/10.1039/c6ra26488c.
[116]Song, L.; Khoerunnisa, F.; Gao, W.; Dou, W.; Hayashi, T.; Kaneko, K.; Endo, M.; Ajayan, P.M. Effect of high-temperature thermal treatment on the structure and adsorption properties of reduced graphene oxide. *Carbon* **2012**, *52*, 608–612, https://doi.org/10.1016/j.carbon.2012.09.060.
[117]Zhao, Z.; Ni, S.; Su, X.; Gao, Y.; Sun, X. Thermally Reduced Graphene Oxide Membrane with Ultrahigh Rejection of Metal Ions' Separation from Water. *ACS Sustain. Chem. Eng.* **2019**, *7*, 14874–14882, https://doi.org/10.1021/acssuschemeng.9b02972.
[118]Yang, D.; Velamakanni, A.; Bozoklu, G.; Park, S.; Stoller, M.; Piner, R.D.; Stankovich, S.; Jung, I.; Field, D.A.; Ventrice, C.A., Jr.; et al. Chemical analysis of graphene oxide films after heat and chemical treatments by X-ray photoelectron and Micro-Raman spectroscopy. *Carbon* N. Y. **2009**, *47*, 145–152, https://doi.org/10.1016/j.carbon.2008.09.045.
[119]Botas, C.; Álvarez, P.; Blanco, C.; Santamaria, R.; Granda, M.; Gutiérrez, M.D.; Rodriguez-Reinoso, F.; Menéndez, R. Critical temperatures in the synthesis of graphene-like materials by thermal exfoliation–reduction of graphite oxide. *Carbon* **2013**, *52*, 476–485, https://doi.org/10.1016/j.carbon.2012.09.059.
[120]Gao, X.; Jang, J.; Nagase, S. Hydrazine and Thermal Reduction of Graphene Oxide: Reaction Mechanisms, Product Structures, and Reaction Design. *J. Phys. Chem. C* **2009**, *114*, 832–842, https://doi.org/10.1021/jp909284g.
[121]Mattevi, C.; Eda, G.; Agnoli, S.; Miller, S.; Mkhoyan, K.A.; Celik, O.; Mastrogiovanni, D.; Granozzi, G.; Garfunkel, E.; Chhowalla, M. Evolution of Electrical, Chemical, and Structural Properties of Transparent and Conducting Chemically Derived Graphene Thin Films. *Adv. Funct. Mater.* **2009**, *19*, 2577–2583, https://doi.org/10.1002/adfm.200900166.
[122]Babaev, A.A.; Zobov, M.E.; Kornilov, D.Y.; Tkachev, S.V.; Terukov, E.I.; Levitskii, V.S. Temperature Dependence of Electrical Resistance of Graphene Oxide. *High Temp.* **2019**, *57*, 198–202, https://doi.org/10.1134/s0018151x19020019.
[123]Li, M.; Gao, C.; Hu, H.; Zhao, Z. Electrical conductivity of thermally reduced graphene oxide/polymer composites with a segregated structure. *Carbon* **2013**, *65*, 371–373, https://doi.org/10.1016/j.carbon.2013.08.016.
[124]Maddumage, D.; Panamaldeniya, S.; Kimbulapitiya, K.; Jayakantha, D.; Munasinghe, M.; Pemasiri, B.; Gunawardhana, N.; Dassanayake, B. Effect of annealing temperature on electrical properties of RGO thin films deposited by Atomized Spray Pyrolysis. *Diam. Relat. Mater.* **2021**, *120*, 108712, https://doi.org/10.1016/j.diamond.2021.108712.

[125]Lipatov, A.; Guinel, M.J.-F.; Muratov, D.S.; Vanyushin, V.O.; Wilson, P.M.; Kolmakov, A.; Sinitskii, A. Low-temperature thermal reduction of graphene oxide: *In situ* correlative structural, thermal desorption, and electrical transport measurements. *Appl. Phys. Lett.* **2018**, *112*, https://doi.org/10.1063/1.4996337.
[126]Liu, S.-Q.; Zhang, K.; Yuen, M.M.; Fu, X.-Z.; Sun, R.; Wong, C.-P. Effect of reduction temperatures on the thermal and electrical conductivities of reduced graphene oxide films on the Cu foils. 2016 17th International Conference on Electronic Packaging Technology (ICEPT). LOCATION OF CONFERENCE, ChinaDATE OF CONFERENCE; pp. 310–312.
[127]Liu, S.-Q.; Zhang, K.; Yuen, M.M.; Fu, X.-Z.; Sun, R.; Wong, C.-P. Effect of reduction temperatures on the thermal and electrical conductivities of reduced graphene oxide films on the Cu foils. 2016 17th International Conference on Electronic Packaging Technology (ICEPT). LOCATION OF CONFERENCE, ChinaDATE OF CONFERENCE; pp. 310–312.
[128]Chen, C.-M.; Zhang, Q.; Yang, M.-G.; Huang, C.-H.; Yang, Y.-G.; Wang, M.-Z. Structural evolution during annealing of thermally reduced graphene nanosheets for application in supercapacitors. *Carbon* **2012**, *50*, 3572–3584, https://doi.org/10.1016/j.carbon.2012.03.029.
[129]Cao, J.; Qi, G.-Q.; Ke, K.; Luo, Y.; Yang, W.; Xie, B.-H.; Yang, M.-B. Effect of temperature and time on the exfoliation and de-oxygenation of graphite oxide by thermal reduction. *J. Mater. Sci.* **2012**, *47*, 5097–5105, https://doi.org/10.1007/s10853-012-6383-5.
[130]de Souza, C.B.; Nakagawa, M.A.; Vargas, L.R.; Hilário, R.B.; Impère, A.G.D.; Matsushima, J.T.; Quirino, S.F.; Gama, A.M.; Baldan, M.R.; Gonçalves, E.S. Evolution of dielectric properties of thermally reduced graphene oxide as a function of pyrolisis temperature. *Diam. Relat. Mater.* **2019**, *93*, 241–251, https://doi.org/10.1016/j.diamond.2019.01.015.
[131]Jun-Gang, C.; Tong-Jiang, P.; Hong-Juan, S.; Ruo-Nan, H. Influence of Thermal Reduction Temperature on the Humidity Sensitivity of Graphene Oxide. *Full- Nanotub. Carbon Nanostructures* **2014**, *23*, 418–423, https://doi.org/10.1080/1536383x.2013.833915.
[132]Fouda, A.N.; Abu Assy, M.K.; El Enany, G.; Yousf, N. Enhanced Capacitance of Thermally Reduced Hexagonal Graphene Oxide for High Performance Supercapacitor. *Full- Nanotub. Carbon Nanostructures* **2014**, *23*, 618–622, https://doi.org/10.1080/1536383x.2014.943889.
[133]Han, Y.; Wang, T.; Gao, X.; Li, T.; Zhang, Q. Preparation of thermally reduced graphene oxide and the influence of its reduction temperature on the thermal, mechanical, flame retardant performances of PS nanocomposites. *Compos. Part A: Appl. Sci. Manuf.* **2016**, *84*, 336–343, https://doi.org/10.1016/j.compositesa.2016.02.007.
[134]Kim, J.M.; Hong, W.G.; Lee, S.M.; Chang, S.J.; Jun, Y.; Kim, B.H.; Kim, H.J. Energy storage of thermally reduced graphene oxide. *Int. J. Hydrogen Energy* **2014**, *39*, 3799–3804, https://doi.org/10.1016/j.ijhydene.2013.12.144.
[135]González, M.; Baselga, J.; Pozuelo, J. Modulating the electromagnetic shielding mechanisms by thermal treatment of high porosity graphene aerogels. *Carbon* **2019**, *147*, 27–34, https://doi.org/10.1016/j.carbon.2019.02.068.
[136]Andrikopoulos, K.S.; Bounos, G.; Tasis, D.; Sygellou, L.; Drakopoulos, V.; Voyiatzis, G.A. The Effect of Thermal Reduction on the Water Vapor Permeation in Graphene Oxide Membranes. *Adv. Mater. Interfaces* **2014**, *1*, 1400250, https://doi.org/10.1002/admi.201400250.
[137]Zeng, Y.; Li, T.; Yao, Y.; Li, T.; Hu, L.; Marconnet, A. Thermally Conductive Reduced Graphene Oxide Thin Films for Extreme Temperature Sensors. *Adv. Funct. Mater.* **2019**, *29*, https://doi.org/10.1002/adfm.201901388.
[138]Kumar, R.; Kaur, A. Chemiresistive gas sensors based on thermally reduced graphene oxide for sensing sulphur dioxide at room temperature. *Diam. Relat. Mater.* **2020**, *109*, 108039, https://doi.org/10.1016/j.diamond.2020.108039.
[139]Kwon, Y.; Liu, M.; Castilho, C.; Saleeba, Z.; Hurt, R.; Külaots, I. Controlling pore structure and conductivity in graphene nanosheet films through partial thermal exfoliation. *Carbon* **2020**, *174*, 227–239, https://doi.org/10.1016/j.carbon.2020.12.050.
[140]Yang, S.J.; Kim, T.; Jung, H.; Park, C.R. The effect of heating rate on porosity production during the low temperature reduction of graphite oxide. *Carbon* **2013**, *53*, 73–80, https://doi.org/10.1016/j.carbon.2012.10.032.
[141]Verma, V.; Gurnani, L.; Das, A.; Kumari, N.; Dasgupta, T.; Mukhopadhyay, A. Reduced graphene oxides prepared via explosive and non-explosive thermal reduction: Structural evolution, functional properties and reinforcing efficacy. *Carbon* **2023**, *209*, https://doi.org/10.1016/j.carbon.2023.118007.
[142]Qiu, Y.; Moore, S.; Hurt, R.; Külaots, I. Influence of external heating rate on the structure and porosity of thermally exfoliated graphite oxide. *Carbon* **2017**, *111*, 651–657, https://doi.org/10.1016/j.carbon.2016.10.051.
[143]Ye, X.; Zhu, Y.; Jiang, H.; Wang, L.; Zhao, P.; Yue, Z.; Wan, Z.; Jia, C. A rapid heat pressing strategy to prepare fluffy reduced graphene oxide films with meso/macropores for high-performance supercapacitors. *Chem. Eng. J.* **2018**, *361*, 1437–1450, https://doi.org/10.1016/j.cej.2018.10.187.

[144]Shi, Y.; Wei, W.; Shen, L.; Bao, N. Rapid Production of Thermally Exfoliated Graphene with a Large Specific Surface Area by Introducing a Spray Predrying Process. *Ind. Eng. Chem. Res.* **2021**, *60*, 9787–9796, https://doi.org/10.1021/acs.iecr.1c01122.
[145]Jeong, H.-K.; Lee, Y.P.; Jin, M.H.; Kim, E.S.; Bae, J.J.; Lee, Y.H. Thermal stability of graphite oxide. *Chem. Phys. Lett.* **2009**, *470*, 255–258, https://doi.org/10.1016/j.cplett.2009.01.050.
[146]Akhavan, O. The effect of heat treatment on formation of graphene thin films from graphene oxide nanosheets. *Carbon* **2009**, *48*, 509–519, https://doi.org/10.1016/j.carbon.2009.09.069.
[147]Renteria, J.D.; Ramirez, S.; Malekpour, H.; Alonso, B.; Centeno, A.; Zurutuza, A.; Cocemasov, A.I.; Nika, D.L.; Balandin, A.A. Strongly Anisotropic Thermal Conductivity of Free-Standing Reduced Graphene Oxide Films Annealed at High Temperature. *Adv. Funct. Mater.* **2015**, *25*, 4664–4672, https://doi.org/10.1002/adfm.201501429.
[148]Wang, Y.; Chen, Y.; Lacey, S.D.; Xu, L.; Xie, H.; Li, T.; Danner, V.A.; Hu, L. Reduced graphene oxide film with record-high conductivity and mobility. *Mater. Today* **2017**, *21*, 186–192, https://doi.org/10.1016/j.mattod.2017.10.008.
[149]Tegou, E.; Pseiropoulos, G.; Filippidou, M.; Chatzandroulis, S. Low-temperature thermal reduction of graphene oxide films in ambient atmosphere: Infra-red spectroscopic studies and gas sensing applications. *Microelectron. Eng.* **2016**, *159*, 146–150, https://doi.org/10.1016/j.mee.2016.03.030.
[150]Assis, A.M.; da Silva, K.S.; Araújo, M.K.; Sales, D.C.; Ferreira, M.C.; de Araújo, A.C.V.; de Azevedo, W.M.; Falcão, E.H. Thermal synthesis of rGO and rGO-Co3O4 and their application as adsorbents for anionic dye removal. *Colloids Surfaces A: Physicochem. Eng. Asp.* **2020**, *599*, 124837, https://doi.org/10.1016/j.colsurfa.2020.124837.
[151]Vallés, C.; Núñez, J.D.; Benito, A.M.; Maser, W.K. Flexible conductive graphene paper obtained by direct and gentle annealing of graphene oxide paper. *Carbon* **2011**, *50*, 835–844, https://doi.org/10.1016/j.carbon.2011.09.042.
[152]Yang, H.; Cao, Y.; He, J.; Zhang, Y.; Jin, B.; Sun, J.-L.; Wang, Y.; Zhao, Z. Highly conductive free-standing reduced graphene oxide thin films for fast photoelectric devices. *Carbon* **2017**, *115*, 561–570, https://doi.org/10.1016/j.carbon.2017.01.047.
[153]Sun, H.B.; Yang, J.; Zhou, Y.Z.; Zhao, N.; Li, D. Preparation of reduced graphene oxide films by dip coating technique and their electrical conductivity. *Mater. Technol.* **2013**, *29*, 14–20, https://doi.org/10.1179/1753555712y.0000000058.
[154]Huang, S.-Y.; Zhao, B.; Zhang, K.; Yuen, M.M.F.; Xu, J.-B.; Fu, X.-Z.; Sun, R.; Wong, C.-P. Enhanced Reduction of Graphene Oxide on Recyclable Cu Foils to Fabricate Graphene Films with Superior Thermal Conductivity. *Sci. Rep.* **2015**, *5*, srep14260, https://doi.org/10.1038/srep14260.
[155]Lv, W.; Tang, D.M.; He, Y.-B.; You, C.-H.; Shi, Z.-Q.; Chen, X.-C.; Chen, C.-M.; Hou, P.-X.; Liu, C.; Yang, Q.-H. Low-Temperature Exfoliated Graphenes: Vacuum-Promoted Exfoliation and Electrochemical Energy Storage. *ACS Nano* **2009**, *3*, 3730–3736, https://doi.org/10.1021/nn900933u.
[156]Liu, Z.; Diao, Z.; Yuan, Y.; Jia, H.; Wang, L.; Fei, W. A two-step thermal treatment method to produce reduced graphene oxide with selectively increasing electrochemically active carbonyl group content for high-performance supercapacitor electrode. *Colloids Surfaces A: Physicochem. Eng. Asp.* **2021**, *620*, 126573, https://doi.org/10.1016/j.colsurfa.2021.126573.
[157]Xu, S.; Zhang, Z.; Liu, J.; Wang, Y.; Hu, J. Facile preparation of reduced graphene by optimizing oxidation condition and further reducing the exfoliated products. *J. Mater. Res.* **2016**, *32*, 383–391, https://doi.org/10.1557/jmr.2016.476.
[158]Silipigni, L.; Salvato, G.; Fazio, B.; Di Marco, G.; Proverbio, E.; Cutroneo, M.; Torrisi, A.; Torrisi, L. Temperature and environment effects on the graphene oxide reduction via electrical conductivity studies. *J. Mater. Sci. Mater. Electron.* **2020**, *31*, 11847–11854, https://doi.org/10.1007/s10854-020-03738-4.
[159]Shiravizadeh, A.G.; Yousefi, R.; Elahi, S.M.; Sebt, S.A. Effects of annealing atmosphere and rGO concentration on the optical properties and enhanced photocatalytic performance of SnSe/rGO nanocomposites. *Phys. Chem. Chem. Phys.* **2017**, *19*, 18089–18098, https://doi.org/10.1039/c7cp02995k.
[160]Lei, Y.; He, Y.; Fang, C.; Zhang, Z. Electrochemical behavior of reduced graphene oxide annealed with varying temperature and time in air/nitrogen atmosphere. *J. Mater. Sci. Mater. Electron.* **2016**, *28*, 1750–1755, https://doi.org/10.1007/s10854-016-5721-9.
[161]Kim, S.-J.; Ko, H.-S.; Jeong, G.-H.; Park, K.-H.; Yun, J.-J.; Han, E.-M. Fabrication and Characterization of Reduced Graphene Oxide Counter Electrode for Dye-Sensitized Solar Cells. *Mol. Cryst. Liq. Cryst.* **2014**, *598*, 1–5, https://doi.org/10.1080/15421406.2014.932673.
[162]Dzukarnain, M.Z.B.; Takami, T.; Imai, H.; Ogino, T. Highly conductive, monolayer and large-area reduced graphene oxide films fabricated by electrical connection at the two-dimensional boundaries between the tiled graphene oxide flakes. *Thin Solid Films* **2016**, *615*, 247–255, https://doi.org/10.1016/j.tsf.2016.07.029.

[163]Ullah, S.; Shi, Q.; Zhou, J.; Yang, X.; Ta, H.Q.; Hasan, M.; Ahmad, N.M.; Fu, L.; Bachmatiuk, A.; Rümmeli, M.H. Advances and Trends in Chemically Doped Graphene. *Adv. Mater. Interfaces* **2020**, *7*, https://doi.org/10.1002/admi.202000999.
[164]Putri, L.K.; Ong, W.-J.; Chang, W.S.; Chai, S.-P. Heteroatom doped graphene in photocatalysis: A review. *Appl. Surf. Sci.* **2015**, *358*, 2–14, https://doi.org/10.1016/j.apsusc.2015.08.177.
[165]Razmjooei, F.; Singh, K.P.; Yang, D.-S.; Cui, W.; Jang, Y.H.; Yu, J.-S. Fe-Treated Heteroatom (S/N/B/P)-Doped Graphene Electrocatalysts for Water Oxidation. *ACS Catal.* **2017**, *7*, 2381–2391, https://doi.org/10.1021/acscatal.6b03291.
[166]Lee, H.; Paeng, K.; Kim, I.S. A review of doping modulation in graphene. *Synth. Met.* **2018**, *244*, 36–47, https://doi.org/10.1016/j.synthmet.2018.07.001.
[167]Yeom, D.-Y.; Jeon, W.; Tu, N.D.K.; Yeo, S.Y.; Lee, S.-S.; Sung, B.J.; Chang, H.; Lim, J.A.; Kim, H. High-concentration boron doping of graphene nanoplatelets by simple thermal annealing and their supercapacitive properties. *Sci. Rep.* **2015**, *5*, 9817, https://doi.org/10.1038/srep09817.
[168]Poh, H.L.; Šimek, P.; Sofer, Z.; Pumera, M. Sulfur-Doped Graphene *via* Thermal Exfoliation of Graphite Oxide in H_2S, SO_2, or CS_2 Gas. *ACS Nano* **2013**, *7*, 5262–5272, https://doi.org/10.1021/nn401296b.
[169]Yang, S.; Zhi, L.; Tang, K.; Feng, X.; Maier, J.; Müllen, K. Efficient Synthesis of Heteroatom (N or S)-Doped Graphene Based on Ultrathin Graphene Oxide-Porous Silica Sheets for Oxygen Reduction Reactions. *Adv. Funct. Mater.* **2012**, *22*, 3634–3640, https://doi.org/10.1002/adfm.201200186.
[170]Li, D.; Duan, X.; Sun, H.; Kang, J.; Zhang, H.; Tade, M.O.; Wang, S. Facile synthesis of nitrogen-doped graphene via low-temperature pyrolysis: The effects of precursors and annealing ambience on metal-free catalytic oxidation. *Carbon* **2017**, *115*, 649–658, https://doi.org/10.1016/j.carbon.2017.01.058.
[171]Ren, H.; Shi, X.; Zhu, J.; Zhang, Y.; Bi, Y.; Zhang, L. Facile synthesis of N-doped graphene aerogel and its application for organic solvent adsorption. *J. Mater. Sci.* **2016**, *51*, 6419–6427, https://doi.org/10.1007/s10853-016-9939-y.
[172]Hsieh, C.-C.; Liu, W.-R. Synthesis and characterization of nitrogen-doped graphene nanosheets/copper composite film for thermal dissipation. *Carbon* **2017**, *118*, 1–7, https://doi.org/10.1016/j.carbon.2017.03.025.
[173]You, J.-M.; Ahmed, M.S.; Han, H.S.; Choe, J.E.; Üstündağ, Z.; Jeon, S. New approach of nitrogen and sulfur-doped graphene synthesis using dipyrrolemethane and their electrocatalytic activity for oxygen reduction in alkaline media. *J. Power Sources* **2015**, *275*, 73–79, https://doi.org/10.1016/j.jpowsour.2014.10.174.
[174]Agnoli, S.; Favaro, M. Doping graphene with boron: a review of synthesis methods, physicochemical characterization, and emerging applications. *J. Mater. Chem. A* **2016**, *4*, 5002–5025, https://doi.org/10.1039/c5ta10599d.
[175]Poh, H.L.; Šimek, P.; Sofer, Z.; Tomandl, I.; Pumera, M. Boron and nitrogen doping of graphene via thermal exfoliation of graphite oxide in a BF3 or NH3 atmosphere: contrasting properties. *J. Mater. Chem. A* **2013**, *1*, 13146–13153, https://doi.org/10.1039/c3ta12460f.
[176]Li, R.; Wei, Z.; Gou, X.; Xu, W. Phosphorus-doped graphene nanosheets as efficient metal-free oxygen reduction electrocatalysts. *RSC Adv.* **2013**, *3*, 9978–9984, https://doi.org/10.1039/c3ra41079j.
[177]Yin, R.; Guo, W.; Du, J.; Zhou, X.; Zheng, H.; Wu, Q.; Chang, J.; Ren, N. Heteroatoms doped graphene for catalytic ozonation of sulfamethoxazole by metal-free catalysis: Performances and mechanisms. *Chem. Eng. J.* **2017**, *317*, 632–639, https://doi.org/10.1016/j.cej.2017.01.038.
[178]Poh, H.L.; Šimek, P.; Sofer, Z.; Pumera, M. Halogenation of Graphene with Chlorine, Bromine, or Iodine by Exfoliation in a Halogen Atmosphere. *Chem. – A Eur. J.* **2013**, *19*, 2655–2662, https://doi.org/10.1002/chem.201202972.
[179]Hoyt, R.A.; Remillard, E.M.; Cubuk, E.D.; Vecitis, C.D.; Kaxiras, E. Polyiodide-Doped Graphene. *J. Phys. Chem. C* **2016**, *121*, 609–615, https://doi.org/10.1021/acs.jpcc.6b11653.
[180]Chu, K.; Wang, F.; Zhao, X.-L.; Wei, X.-P.; Wang, X.-W.; Tian, Y. One-step and low-temperature synthesis of iodine-doped graphene and its multifunctional applications for hydrogen evolution reaction and electrochemical sensing. *Electrochimica Acta* **2017**, *246*, 1155–1162, https://doi.org/10.1016/j.electacta.2017.07.001.
[181]Majee, S.; Banerjee, D.; Liu, X.; Zhang, S.-L.; Zhang, Z.-B. Efficient and thermally stable iodine doping of printed graphene nano-platelets. *Carbon* **2017**, *117*, 240–245, https://doi.org/10.1016/j.carbon.2017.02.094.
[182]Yao, Z.; Nie, H.; Yang, Z.; Zhou, X.; Liu, Z.; Huang, S. Catalyst-free synthesis of iodine-doped graphenevia a facile thermal annealing process and its use for electrocatalytic oxygen reduction in an alkaline medium. *Chem. Commun.* **2011**, *48*, 1027–1029, https://doi.org/10.1039/c2cc16192c.
[183]Matsoso, J.B.; Journet, C.; Coville, N.J.; Sofer, Z. Co-doping Graphene with B and N Heteroatoms for Application in Energy Conversion and Storage Devices. *Chemnanomat* **2022**, *8*, https://doi.org/10.1002/cnma.202200134.

[184]Ma, L.; Liu, J.; Lv, S.; Zhou, Q.; Shen, X.; Mo, S.; Tong, H. Scalable one-step synthesis of N,S co-doped graphene-enhanced hierarchical porous carbon foam for high-performance solid-state supercapacitors. *J. Mater. Chem. A* **2019**, *7*, 7591–7603, https://doi.org/10.1039/c9ta00038k.
[185]Chen, X.; Duan, X.; Oh, W.-D.; Zhang, P.-H.; Guan, C.-T.; Zhu, Y.-A.; Lim, T.-T. Insights into nitrogen and boron-co-doped graphene toward high-performance peroxymonosulfate activation: Maneuverable N-B bonding configurations and oxidation pathways. *Appl. Catal. B: Environ.* **2019**, *253*, 419–432, https://doi.org/10.1016/j.apcatb.2019.04.018.
[186]Zhan, Y.; Huang, J.; Lin, Z.; Yu, X.; Zeng, D.; Zhang, X.; Xie, F.; Zhang, W.; Chen, J.; Meng, H. Iodine/nitrogen co-doped graphene as metal free catalyst for oxygen reduction reaction. *Carbon* **2015**, *95*, 930–939, https://doi.org/10.1016/j.carbon.2015.09.024.
[187]Chen, X.; Deng, X.; Kim, N.Y.; Wang, Y.; Huang, Y.; Peng, L.; Huang, M.; Zhang, X.; Chen, X.; Luo, D.; et al. Graphitization of graphene oxide films under pressure. *Carbon* **2018**, *132*, 294–303, https://doi.org/10.1016/j.carbon.2018.02.049.
[188]Shang, Y.; Li, T.; Li, H.; Dang, A.; Zhang, L.; Yin, Y.; Xiong, C.; Zhao, T. Preparation and characterization of graphene derived from low-temperature and pressure promoted thermal reduction. *Compos. Part B: Eng.* **2016**, *99*, 106–111, https://doi.org/10.1016/j.compositesb.2016.06.030.
[189]Chen, C.-M.; Huang, J.-Q.; Zhang, Q.; Gong, W.-Z.; Yang, Q.-H.; Wang, M.-Z.; Yang, Y.-G. Annealing a graphene oxide film to produce a free standing high conductive graphene film. *Carbon* **2011**, *50*, 659–667, https://doi.org/10.1016/j.carbon.2011.09.022.
[190]Chen, X.; Li, W.; Luo, D.; Huang, M.; Wu, X.; Huang, Y.; Lee, S.H.; Chen, X.; Ruoff, R.S. Controlling the Thickness of Thermally Expanded Films of Graphene Oxide. *ACS Nano* **2016**, *11*, 665–674, https://doi.org/10.1021/acsnano.6b06954.
[191]Poh, H.L.; Šaněk, F.; Sofer, Z.; Pumera, M. High-pressure hydrogenation of graphene: towards graphane. *Nanoscale* **2012**, *4*, 7006–7011, https://doi.org/10.1039/c2nr31962d.
[192]Schmiedova, V.; Pospisil, J.; Kovalenko, A.; Ashcheulov, P.; Fekete, L.; Cubon, T.; Kotrusz, P.; Zmeskal, O.; Weiter, M. Physical Properties Investigation of Reduced Graphene Oxide Thin Films Prepared by Material Inkjet Printing. *J. Nanomater.* **2017**, *2017*, 1–8, https://doi.org/10.1155/2017/3501903.
[193]Politano, G.G.; Versace, C. Electrical and Optical Characterization of Graphene Oxide and Reduced Graphene Oxide Thin Films. *Crystals* **2022**, *12*, 1312, https://doi.org/10.3390/cryst12091312.
[194]Cao, Y.; Hu, E.; Xing, J.; Liu, L.; Gu, T.; Zheng, J.; Yu, K.; Wei, W. Optical constants of restored and etched reduced graphene oxide: a spectroscopic ellipsometry study. *Opt. Mater. Express* **2018**, *9*, 234–243, https://doi.org/10.1364/ome.9.000234.
[195]Jung, I.; Vaupel, M.; Pelton, M.; Piner, R.; Dikin, D.A.; Stankovich, S.; An, J.; Ruoff, R.S. Characterization of Thermally Reduced Graphene Oxide by Imaging Ellipsometry. *J. Phys. Chem. C* **2008**, *112*, 8499–8506, https://doi.org/10.1021/jp802173m.
[196]Guo, X.; Li, J.; Yu, Y.; Zafar, A.; Ni, Z. Thermally enhanced optical contrast of graphene oxide for thickness identification. *Nanotechnology* **2019**, *30*, 295704, https://doi.org/10.1088/1361-6528/ab1780.
[197]Kumar, P.V.; Bardhan, N.M.; Chen, G.-Y.; Li, Z.; Belcher, A.M.; Grossman, J.C. New insights into the thermal reduction of graphene oxide: Impact of oxygen clustering. *Carbon* **2016**, *100*, 90–98, https://doi.org/10.1016/j.carbon.2015.12.087.
[198]Ganguly, A.; Sharma, S.; Papakonstantinou, P.; Hamilton, J. Probing the Thermal Deoxygenation of Graphene Oxide Using High-Resolution In Situ X-ray-Based Spectroscopies. *J. Phys. Chem. C* **2011**, *115*, 17009–17019, https://doi.org/10.1021/jp203741y.
[199]Pelaez-Fernandez, M.; Bermejo, A.; Benito, A.; Maser, W.; Arenal, R. Detailed thermal reduction analyses of graphene oxide via in-situ TEM/EELS studies. *Carbon* **2021**, *178*, 477–487, https://doi.org/10.1016/j.carbon.2021.03.018.
[200]Shen, Y.; Boffa, V.; Corazzari, I.; Qiao, A.; Tao, H.; Yue, Y. Revealing hidden endotherm of Hummers' graphene oxide during low-temperature thermal reduction. *Carbon* **2018**, *138*, 337–347, https://doi.org/10.1016/j.carbon.2018.05.018.
[201]Acik, M.; Guzman, R.; Chabal, Y.J. Generation and Capture of CO2 and CO in Graphite Oxide Stacks during Thermal Reduction. *MRS Proc.* **2009**, *1205*, https://doi.org/10.1557/proc-1205-l01-05.
[202]Larciprete, R.; Fabris, S.; Sun, T.; Lacovig, P.; Baraldi, A.; Lizzit, S. Dual Path Mechanism in the Thermal Reduction of Graphene Oxide. *J. Am. Chem. Soc.* **2011**, *133*, 17315–17321, https://doi.org/10.1021/ja205168x.
[203]Acik, M.; Mattevi, C.; Gong, C.; Lee, G.; Cho, K.; Chhowalla, M.; Chabal, Y.J. The Role of Intercalated Water in Multilayered Graphene Oxide. *ACS Nano* **2010**, *4*, 5861–5868, https://doi.org/10.1021/nn101844t.
[204]Yang, Z.; Sun, Y.; Ma, F.; Lu, Y.; Zhao, T. Pyrolysis mechanisms of graphene oxide revealed by ReaxFF molecular dynamics simulation. *Appl. Surf. Sci.* **2020**, *509*, 145247, https://doi.org/10.1016/j.apsusc.2020.145247.

[205]Menezes, I.R.; Araújo, N.R.; Araújo, B.C.; Sakai, T.; Lago, R.M.; Sebastião, R.C. Shedding light on the mechanism of graphene oxide thermal decomposition: A kinetic study using isoconversional method and artificial neural network. *Thermochim. Acta* **2023**, *721*, https://doi.org/10.1016/j.tca.2023.179454.
[206]Sun, L.; Yin, K.; Li, H.; Xia, Y.; Bi, H.; Sun, J.; Liu, Z. Thermodynamic and Kinetic Analysis of Lowtemperature Thermal Reduction of Graphene Oxide. *Nano-Micro Lett.* **2011**, *3*, https://doi.org/10.5101/nml.v3i1.p51-55.
[207]Barroso-Bujans, F.; Alegría, .; Colmenero, J. Kinetic Study of the Graphite Oxide Reduction: Combined Structural and Gravimetric Experiments under Isothermal and Nonisothermal Conditions. *J. Phys. Chem. C* **2010**, *114*, 21645–21651, https://doi.org/10.1021/jp108905j.
[208]Świniarski, M.; Wróblewska, A.; Duzynska, A.; Zdrojek, M.; Judek, J. Kinetics of the thermal reduction process in graphene oxide thin films from in-situ transport measurements. *Mater. Res. Express* **2021**, *8*, 015601, https://doi.org/10.1088/2053-1591/abdc50.
[209]Akbi, H.; Mekki, A.; Rafai, S. New linear integral kinetic parameters assessment method based on an accurate approximate formula of temperature integral. *Int. J. Chem. Kinet.* **2021**, *54*, 28–41, https://doi.org/10.1002/kin.21538.
[210]Jung, I.; Field, D.A.; Clark, N.J.; Zhu, Y.; Yang, D.; Piner, R.D.; Stankovich, S.; Dikin, D.A.; Geisler, H.; Ventrice, C.A.; et al. Reduction Kinetics of Graphene Oxide Determined by Electrical Transport Measurements and Temperature Programmed Desorption. *J. Phys. Chem. C* **2009**, *113*, 18480–18486, https://doi.org/10.1021/jp904396j.
[211]Aukstakojyte, R.; Gaidukevic, J.; Barkauskas, J. Thermal reduction of graphene oxide in the presence of carbon suboxide. *J. Solid State Chem.* **2021**, *301*, 122365, https://doi.org/10.1016/j.jssc.2021.122365.
[212]Lakhe, P.; Kulhanek, D.L.; Sun, W.; Zhang, B.; Green, M.J.; Mannan, M.S. Calorimetry of explosive thermal decomposition of graphite oxide. *J. Hazard. Mater.* **2018**, *366*, 275–281, https://doi.org/10.1016/j.jhazmat.2018.11.100.
[213]Qiu, Y.; Collin, F.; Hurt, R.H.; Külaots, I. Thermochemistry and kinetics of graphite oxide exothermic decomposition for safety in large-scale storage and processing. *Carbon* **2016**, *96*, 20–28, https://doi.org/10.1016/j.carbon.2015.09.040.
[214]Li, L.; Sun, X.; Qiu, X.; Xu, J.; Li, G. Nature of Catalytic Activities of CoO Nanocrystals in Thermal Decomposition of Ammonium Perchlorate. *Inorg. Chem.* **2008**, *47*, 8839–8846, https://doi.org/10.1021/ic8008283.
[215]Krishnan, D.; Kim, F.; Luo, J.; Cruz-Silva, R.; Cote, L.J.; Jang, H.D.; Huang, J. Energetic graphene oxide: Challenges and opportunities. *Nano Today* **2012**, *7*, 137–152, https://doi.org/10.1016/j.nantod.2012.02.003.
[216]Tölle, F.J.; Gamp, K.; Mülhaupt, R. Scale-up and purification of graphite oxide as intermediate for functionalized graphene. *Carbon* **2014**, *75*, 432–442, https://doi.org/10.1016/j.carbon.2014.04.022.
[217]Bhunia, P.; Kumar, M.; De, S. Rapid and efficient removal of ionic impurities from graphene oxide through hollow fiber diafiltration. *Sep. Purif. Technol.* **2018**, *209*, 103–111, https://doi.org/10.1016/j.seppur.2018.07.025.
[218]Barkauskas, J.; Gaidukevič, J.; Niaura, G. Thermal reduction of graphite oxide in the presence of nitrogen-containing dyes. *Carbon Lett.* **2021**, *31*, 1097–1110, https://doi.org/10.1007/s42823-021-00228-3.
[219]Fouda, A.N.; Abu Assy, M.K.; El Enany, G.; Yousf, N. Enhanced Capacitance of Thermally Reduced Hexagonal Graphene Oxide for High Performance Supercapacitor. *Full- Nanotub. Carbon Nanostructures* **2014**, *23*, 618–622, https://doi.org/10.1080/1536383x.2014.943889.
[220]Luo, P.; Lin, Y. Further Thermal Reduction of Reduced Graphene Oxide Aerogel with Excellent Rate Performance for Supercapacitors. *Appl. Sci.* **2019**, *9*, 2188, https://doi.org/10.3390/app9112188.
[221]Kim, J.; Eum, J.-H.; Kang, J.; Kwon, O.; Kim, H.; Kim, D.W. Tuning the hierarchical pore structure of graphene oxide through dual thermal activation for high-performance supercapacitor. *Sci. Rep.* **2021**, *11*, 1–10, https://doi.org/10.1038/s41598-021-81759-7.
[222]Yan, J.; Liu, J.; Fan, Z.; Wei, T.; Zhang, L. High-performance supercapacitor electrodes based on highly corrugated graphene sheets. *Carbon* **2012**, *50*, 2179–2188, https://doi.org/10.1016/j.carbon.2012.01.028.
[223]Lee, J.H.; Park, N.; Kim, B.G.; Jung, D.S.; Im, K.; Hur, J.; Choi, J.W. Restacking-Inhibited 3D Reduced Graphene Oxide for High Performance Supercapacitor Electrodes. *ACS Nano* **2013**, *7*, 9366–9374, https://doi.org/10.1021/nn4040734.
[224]Wang, X.; Sun, G.; Routh, P.; Kim, D.-H.; Huang, W.; Chen, P. Heteroatom-doped graphene materials: syntheses, properties and applications. *Chem. Soc. Rev.* **2014**, *43*, 7067–7098, https://doi.org/10.1039/c4cs00141a.
[225]Ullah, S.; Shi, Q.; Zhou, J.; Yang, X.; Ta, H.Q.; Hasan, M.; Ahmad, N.M.; Fu, L.; Bachmatiuk, A.; Rümmeli, M.H. Advances and Trends in Chemically Doped Graphene. *Adv. Mater. Interfaces* **2020**, *7*, https://doi.org/10.1002/admi.202000999.
[226]Wen, Y.; Wang, B.; Huang, C.; Wang, L.; Hulicova-Jurcakova, D. Synthesis of Phosphorus-Doped Graphene and its Wide Potential Window in Aqueous Supercapacitors. *Chem. – A Eur. J.* **2014**, *21*, 80–85, https://doi.org/10.1002/chem.201404779.

[227]Gopalsamy, K.; Balamurugan, J.; Thanh, T.D.; Kim, N.H.; Lee, J.H. Fabrication of nitrogen and sulfur co-doped graphene nanoribbons with porous architecture for high-performance supercapacitors. *Chem. Eng. J.* **2017**, *312*, 180–190, https://doi.org/10.1016/j.cej.2016.11.130.
[228]Park, H.; Ahn, H.; Chung, Y.; Cho, S.B.; Yoon, Y.S.; Kim, D.-J. Transition of gas sensing behavior in non-reduced graphene oxides with thermal annealing. *Mater. Lett.* **2014**, *136*, 164–167, https://doi.org/10.1016/j.matlet.2014.07.184.
[229]Wang, J.; Kwak, Y.; Lee, I.-Y.; Maeng, S.; Kim, G.-H. Highly responsive hydrogen gas sensing by partially reduced graphite oxide thin films at room temperature. *Carbon* **2012**, *50*, 4061–4067, https://doi.org/10.1016/j.carbon.2012.04.053.
[230]Zhou, Y.; Lin, X.; Huang, Y.; Guo, Y.; Gao, C.; Xie, G.; Jiang, Y. Impact of further thermal reduction on few-layer reduced graphene oxide film and its n-p transition for gas sensing. *Sensors Actuators B: Chem.* **2016**, *235*, 241–250, https://doi.org/10.1016/j.snb.2016.05.078.
[231]Jung, W.T.; Jang, H.-S.; Jeon, J.W.; Kim, B.H. Effect of Oxygen Functional Groups in Reduced Graphene Oxide-Coated Silk Electronic Textiles for Enhancement of NO_2 Gas-Sensing Performance. *ACS Omega* **2021**, *6*, 27080–27088, https://doi.org/10.1021/acsomega.1c03658.
[232]Drewniak, S.; Procek, M.; Muzyka, R.; Pustelny, T. Comparison of Gas Sensing Properties of Reduced Graphene Oxide Obtained by Two Different Methods. *Sensors* **2020**, *20*, 3175, https://doi.org/10.3390/s20113175.
[233]Chen, H.; Ma, W.; Huang, Z.; Zhang, Y.; Huang, Y.; Chen, Y. Graphene-Based Materials toward Microwave and Terahertz Absorbing Stealth Technologies. *Adv. Opt. Mater.* **2019**, *7*, https://doi.org/10.1002/adom.201801318.
[234]Chen, Q.; Jin, L.; Zhang, Y.; Chen, H.; Liu, H.; Bai, Y. Two-step thermal treatment of electrochemical graphene oxide films for high-performance electrical heating and electromagnetic interference shielding. *Appl. Surf. Sci.* **2023**, *618*, https://doi.org/10.1016/j.apsusc.2023.156669.
[235]Sadek, R.; Sharawi, M.S.; Dubois, C.; Tantawy, H.; Chaouki, J. Superior quality chemically reduced graphene oxide for high performance EMI shielding materials. *RSC Adv.* **2022**, *12*, 22608–22622, https://doi.org/10.1039/d2ra02678c.
[236]Chen, Y.; Li, J.; Li, T.; Zhang, L.; Meng, F. Recent advances in graphene-based films for electromagnetic interference shielding: Review and future prospects. *Carbon* **2021**, *180*, 163–184, https://doi.org/10.1016/j.carbon.2021.04.091.
[237]Xu, L.; Zhang, W.; Wang, L.; Xue, J.; Hou, S. Large-scale preparation of graphene oxide film and its application for electromagnetic interference shielding. *RSC Adv.* **2021**, *11*, 33302–33308, https://doi.org/10.1039/d1ra06070h.
[238]Bi, S.; Zhang, L.; Mu, C.; Lee, H.Y.; Cheah, J.W.; Chua, E.K.; See, K.Y.; Liu, M.; Hu, X. A comparative study on electromagnetic interference shielding behaviors of chemically reduced and thermally reduced graphene aerogels. *J. Colloid Interface Sci.* **2017**, *492*, 112–118, https://doi.org/10.1016/j.jcis.2016.12.060.
[239]Xi, J.; Li, Y.; Zhou, E.; Liu, Y.; Gao, W.; Guo, Y.; Ying, J.; Chen, Z.; Chen, G.; Gao, C. Graphene aerogel films with expansion enhancement effect of high-performance electromagnetic interference shielding. *Carbon* **2018**, *135*, 44–51, https://doi.org/10.1016/j.carbon.2018.04.041.
[240]Wan, Y.-J.; Zhu, P.-L.; Yu, S.-H.; Sun, R.; Wong, C.-P.; Liao, W.-H. Graphene paper for exceptional EMI shielding performance using large-sized graphene oxide sheets and doping strategy. *Carbon* **2017**, *122*, 74–81, https://doi.org/10.1016/j.carbon.2017.06.042.
[241]Shen, B.; Zhai, W.; Zheng, W. Ultrathin Flexible Graphene Film: An Excellent Thermal Conducting Material with Efficient EMI Shielding. *Adv. Funct. Mater.* **2014**, *24*, 4542–4548, https://doi.org/10.1002/adfm.201400079.